EXTRACELLULAR VESICLES AND MICRORNA IN BIOFLUIDS, CELL CULTURE AND PRIMARY CELLS IN HEALTH AND HIV-1 AND SIV INFECTIONS

by

Dillon C. Muth, DVM

A dissertation submitted to Johns Hopkins University in conformity with the requirements for the degree of Doctor of Philosophy

Baltimore, MD

September 2018

Abstract

Extracellular vesicle (EV) research is a rapidly growing field, with renewed interest due in part to the discovery of the association of EVs with small extracellular RNAs (exRNA), in particular microRNAs. Roles of EVs and their RNA cargo in facilitating or fighting infection with viruses such as HIV-1 are likely but remain incompletely understood. To investigate one aspect through which EVs might play a role in infection, we first evaluated the EV and exRNA population of cervical-vaginal fluid in Asian macaques, initially in endometriosis and subsequently in animals with naturally suppressed SIV infections. Evaluating the miRNA cargo of EVs from infected animals relative to uninfected animals, we found that miR-186 was more abundant in the infected animals, suggesting it could be a potential restriction factor of SIV. We then used *in vitro* culture to establish the importance of EVs in HIV proliferation and maturation. We found that when EVs are removed from culture media, cell lines, either acutely or latently infected with HIV-1, experienced increased viral production. Virus produced by these cells was also more infectious than baseline. Restoration of cell-derived EVs to EV-depleted cell culture rescued virus production to normal levels. Finally, we investigated miRNA expression in different blood T-cell subsets of HIV-1 elite suppressors (ES), for comparison with those of healthy (i.e. uninfected) controls (HC) and HIV-1 chronic progressors (CP). EVs and cell-free exRNAs have also been collected from all donors. We found that several miRNA species were differentially regulated in T-cell types in ES compared with HC or CP, consistent with previous studies examining PBMCs. Interestingly, we also found that the miRNA profile of different classes of cells, i.e., Naïve, Central Memory or Effector Memory, clustered together irrespective of CD4+ or

CD8+ phenotype in HC. These data taken together demonstrate the importance of EVs and their cargo in the context of retroviral infection and set the stage for future studies to further elucidate the complex relationship between HIV-1, miRNA and EVs.

Thesis advisor: Kenneth W. Witwer, PhD, Associate Professor,
Department of Molecular and Comparative Pathobiology

Second reader: Joel N. Blankson, MD, PhD, Associate Professor,
Department of Medicine

Committee: Joel N. Blankson MD, PhD (Chair)
Amanda Brown, PhD
Andrea Cox, MD, PhD
Joseph L. Mankowski, DVM, PhD, DACVP

Acknowledgements

Of all the sections of a dissertation to write, the acknowledgements should undoubtedly be the easiest to write. Writing them elegantly, though is not. To succinctly document and highlight the contributions and importance off all the people who you have crossed paths with is next to impossible. But it's an important exercise, nevertheless, and one that I will attempt to do justice to, here.

A thesis would not exist without a thesis advisor, literally and literarily, so some words about Ken is the natural place to start. I said at the onset of graduate school that I wanted to work in a lab that would teach me to be a scientist first and a graduate student second and I don't think I could have imagined a better environment to fulfill this aspiration. Some words I've used to describe Ken over the years include: brilliant, invested, caring, rigorous, genuine, intense, accomplished, motivating. Of course, these are only a few words which do not do full justice in describing how outstanding of a mentor Ken has been. Also, I still don't really know how he manages all the responsibilities he has as well as he does. I know we have each learned something from the other and I expect our relationship to remain strong over the coming years. So, thank you for everything.

Dr. Liao, who joined our lab almost a year after I did, has been another beacon of inspiration. He is absolutely the hardest working bench scientist I have ever met and is excellent at unintentionally plucking at the strings of imposter syndrome. I genuinely appreciated all of the motivating chats and conversations we had that ran the full gamut of topics from science to sports to politics. Thank you for all you helped me with, Liao!

Bonita Powell, a research technologist in the lab has also been an excellent mentor and co-worker over the years. She arrived with strong aspirations to pursue additional training through medical school, but is still one of the most knowledgeable and friendliest technicians one could ask to have at the helm of day-to-day operations of a lab. Thanks for being willing to debate the theory of the science we were attempting and not just motivated to punch the clock.

The Retrovirus Lab is a large group and would not function without so many excellent personalities and hard-workers. On a day-to-day basis, no one has been as important as our group of lab managers and technical assistants, especially Brandon Bullock, Suzanne Queen and Erin Shirk. I've enjoyed working alongside you but also developing great personal relationships with you over my 5 years in the lab. The other Retrovirus faculty members Drs. Janice Clements, Kelly Pate, Chris Zink, Lucio Gama, and David Graham have all provided invaluable advice to me throughout my graduate career, for which I am very grateful. Finally, the numerous graduate students and postdocs in the Retrovirus lab who preceded me and follow after me should not go unmentioned: Claudia, Josh, Julia, Jeanne, Kelly, Audrey, Celina, Dionna, Daymond, thank you for being co-survivors!

It should go without saying that I have a large amount of gratitude for my committee members: Drs. Joel Blankson, Amanda Brown, Andrea Cox and Joe Mankowski, for taking the time out of their busy lives to learn about my work and provide invaluable feedback. In that vein, the work presented in Chapter IV would not have been possible without the efforts of Dr. Blankson, from experimental design consultations, to help with data analysis interpretation and for being my second reader.

Of course, a good portion of my time at Hopkins was spent in the other half of the dual-track training program, learning pathology, so I would be remiss if I didn't thank all of my patholleagues and mentors. First, to the faculty, present and past: Drs. Joseph Mankowski, Cory Brayton, Kathleen Gabrielson, Sarah Poynton, Chris Zink, David Huso, and Baktiar Karim: thank you for all of the time and effort that you put into me and making the program and resident training as excellent as it is.

This is obviously not a journey undertaken by oneself, and I would not be where I am without the huge list of fellow residents and postdocs, past and present: Drs. Katie Kelly, Gillian Shaw, Brian Simons, Simon Long, Lisa Mangus, Sarah Beck, Jennell Romero, Tasha Crawford, Nathan Pate, Jeremy Foote, Beth Ihms, Lauren Peiffer, Stephanie Myers, Katie Mulka, Adam Werts and Meghan Vermillion. This is a formidable program, and it takes a group of exceptional residents to make the experience surviveable.

Everyone should be so lucky as I was to have the group of friends and family in my corner cheering for me, even if they didn't know exactly what it was that I was doing. Peter, Tommy, Ben, David, Eric, Nick, thanks for being the friends I needed, even if not the ones I wanted (sometimes).

My parents have made almost every sacrifice imaginable to get me to the point where I am today and I am so thankful for everything they have done and for their unconditional love and support. To my Aunt Merry, thanks for being the stabilizing voice of reason when times have gotten tricky.

Of course, to my wife, Val, thanks for having a job that was so much worse than anything I was going through and keeping things in perspective. You make me be a better

version of myself and that's pretty much the best thing a life companion can do for someone. I can't wait to explore the world with you and I love you.

But, to those that know me, my acknowledgments would not be complete without a nod to the furry friends in my life: Luna (the first-born), Leo (the caricature), Loki (the lucky one), Piper (the inanimate one) and Moose (the bouncy one). You have no idea that I wrote this and cannot understand it, but I wrote it anyway.

Table of Contents

List of Tables

List of Figures

Chapter IV

I. Introduction

History and treatment of HIV-1

HIV-1, an enveloped, single-stranded RNA retrovirus, was first recognized as HTLV-III in 1983 and has developed into a global pandemic that currently remains without cure [1,2]. HIV-1 infected individuals, if left untreated, will eventually develop one of more defining conditions of acquired immune deficiency syndrome (AIDS). AIDS occurs after depletion of immune surveillance cells by HIV-1, cells which typically help to fight off common pathogens, leaving the infected individual susceptible to opportunistic infections. As of 2016, the current estimate of global infections was 36.7 million individuals living with HIV; of these 36.9 million individuals, 20.9 million were receiving antiretroviral therapy [3]. Since the peak of the pandemic in 2005, with over 2 million deaths in a single year alone, the new infection and death rates have steadily decreased. Yet, over 1 million individuals still die each year, indicating a significant remaining global impact [4]. While the development and implementation of combinatorial antiretroviral therapy (ART) has decreased morbidity and mortality rates, it does not represent a cure for HIV-1 infection, instead changing the nature of the disease to one of chronicity. Indeed, numerous non-AIDS-defining disorders associated with chronic inflammation and premature aging, such as HIV-associated neurocognitive disorders (HAND) now are prevalent in a large portion of the population whose viral loads are well suppressed [5,6]. Many of these disorders are incompletely understood and have no known therapies, which will continue to remain an issue as long as no cure for HIV-1 is developed.

A major obstacle for eradication of HIV-1 is the phenomenon of latency. Latent cells are long-lived, with integrated and quiescent HIV-1 DNA [7–10]. The best characterized latent reservoir of HIV-1 is the CD4+ T-lymphocyte, the cell preferentially infected by HIV-1 [11–13]. Importantly, when these latent cells are activated, a viral rebound is likely to result in novel infection of other cells. Just as in acutely infected cells, viral particles are formed by budding of cellular membranes of the host cell, incorporating viral nucleic acids and proteins. The released virion then undergoes a viral enzyme-driven maturation process, preparing the particle for infection of neighboring or distant cells. Importantly, the budding process relies on host cell machinery that is also used in the release of particles called extracellular vesicles (EVs), which play a role in intercellular messaging [14–17]. Could the similarities between viruses and EVs provide an avenue for development of novel therapy and potentially the eradication of HIV-1?

Extracellular vesicles and HIV-1

EVs are a heterogeneous population of mostly submicron bodies that have a double-leaflet membrane. EVs form by budding directly from the cell surface membrane (canonical “microvesicles” or “ectosomes”), while classically defined “exosomes” bud into the multivesicular body (MVB). This late endosome that releases its cargo, including exosomes, upon fusion with the plasma membrane. Considering that the retrovirion is itself a vesicle, EV studies have been ongoing in one form or another for over 80 years, with studies ranging from platelets to cartilage to antigen presentation [18–22]. Notably, a redoubled interest in the field began in 2007 with demonstration by Rataczak et al and Lötvall et al of transfer of RNA species directly associated with EVs [23,24]. It is now

known that EVs package a variety of biologically active materials, including enzymes, mRNAs, as well as both long non-coding RNAs (lncRNA) and microRNAs (miRNAs) [25–28], all of which have important biological functions, including in the immune response.

As mentioned, EVs and retroviruses have overlapping phenotypes. The diameters of HIV-1 virions and EVs are comparable, and some have likened HIV to a "Trojan exosome", evading host response by mimicking a host EV [29]. In addition, EVs express a wide range of proteins on their surfaces, including adhesion molecules and important immunological molecules such as Major Histocompatibility Complex (MHC) [30,31]. EVs can transmit genomic DNA of other viruses like Hepatitis C [32] and pegiviruses [33], and have been shown to contain important HIV molecules, like viral RNA [34] and other proteins including Gag [35] and Nef [36,37], but remain distinct from functional HIV-1 virions, as they do not appear capable of initiating a primary infection [38].

The complexity of the relationship between EVs and HIV-1 extends beyond their physical similarities to function. EVs may enhance infection by activating CD4+ T-lymphocytes, rendering them susceptible to HIV-1 infection [39,40], but can also have a protective effect, preventing HIV-1 from actively infecting other cells [41]. Just as HIV-1 strains may have different cellular or receptor tropism, EVs may play different roles against infections based on their cell origin [42,43].

EVs and the cervicovaginal compartment

EVs have been isolated from almost every bodily fluid, including semen [44], blood [45], urine [46] and saliva, among many others. In many biofluids, the EVs are

uncharacterized or poorly characterized, including those derived from the cervicovaginal compartment. This canal is a source of potential biomarkers, especially in cases of infectious disease [47], so a better understanding of its immune defense potential is warranted. This is especially true of HIV-1 and SIV infections, against which EVs have been reported to have innate defense properties [48]. One of the elements that may contribute to EV defense potency is the miRNA cargo.

miRNAs and HIV-1

microRNAs (miRNAs), first described in 1993, are ~22 nucleotide ncRNA molecules found ubitiquously in plants and animals. These small RNAs modulate expression of proteins within and between cells [49]. miRNAs function by binding to the untranslated region (3' UTR) of mRNAs, changing protein levels by degradation (complete complementarity) or translational repression (partial complementarity) of target mRNA [50]. The majority of miRNAs are transcribed by RNA Polymerase II into their first form, a long primary miRNA (pri-miRNA) [51]. The sterics of the formed molecule result in a hairpin structure, which is recognized by the Drosh-DGCR8 complex [52]. While still in the nucleus of the cell, this complex cleaves the pri-miRNA into a precursor miRNA (pre-miRNA), isolating the hairpin structure. The pre-miRNA is subsequently shuttled to the cytoplasm by the nuclear exporter protein Exportin 5 [53]. The enzyme Dicer removes the loop of the pre-miRNA, leaving a duplex comprised of the former 5' and 3' arms of the precursor. Finally, one of the complementary strands is loaded into an Argonaute protein, part of a complex called the RNA-induced Silencing Complex (RISC) [54,55].

Once loaded into the RISC complex, the complementarity of the seed sequence, located at the 5' end of the miRNA, and a target RNA sequence is the key determinant of binding capability to the target and thus the efficacy of silencing of each miRNA. While there are thousands of miRNA species, whose functions have been implicated in processes ranging from tumor suppression [56] to antiviral therapy[57].

Studies of miRNA and HIV-1 range from profile comparisons to targeting studies to functional assays evaluating potential therapies [58–60]. Previous work in our lab evaluated miRNA profiles of peripheral blood mononuclear cells (PBMCs), of HIV-1 elite suppressors (ES), people who naturally suppress HIV-1 copy numbers below a detectable threshold of 50 copies/mL of peripheral blood [61]. A more complete understanding of the ES phenomenon and their miRNA profile potentially represents a path to more effective therapy and even perhaps an avenue to eradication. The mechanism of control is assuredly multifactorial, but in-depth profiling of specific cell types involved in infection and control of infection would add another important element of understanding.

Project Overview

The goal of this project was to investigate how EVs and miRNAs are involved in SIV and HIV-1 infection, with a focus on cellular miRNA expression in human patient samples. Chapter two of this thesis reports characterization of EVs and their cargo in the cervicovaginal compartment, first looking at EV abundance in a macaque with endometriosis and then evaluating EVs and extracellular RNA in cervicovaginal lavage (CVL) from Rhesus macaques infected with SIV. The results demonstrate the importance

of vesicles in homeostasis, highlighted by a significant decrease in both the animal with endometriosis and in the animals infected with SIV. Evaluation of the miRNA cargo in the infected animals revealed an upregulation of miR-186. Additional functional *in vitro* studies with synthetic miR-186 in monocyte-derived macrophages show that miR-186 may behave as an HIV-1 restriction factor. These results underscore the importance of EVs and their cargo in viral defense and emphasize the diversity of the innate immune response and the importance anatomic location may play in facilitating immunoprotection.

Chapter three addresses the depletion of EVs from cell culture medium used for HIV-1 *in vitro* studies. While the importance of serum EVs in cell migration and growth is known, whether serum EVs play a role in HIV-1 infection *in vitro* was unclear. We report increases in HIV-1 production in certain EV-depleted conditions, along with, in some cases, cellular morphology changes and decreased cell viability. Add-back of EV-enriched ultracentrifuge pellets reduced HIV-1 production almost to baseline. Primary cells appeared to be less sensitive to EV depletion, although ACH-2 and U1 latency models also produced more HIV-1 under EV-depleted conditions. Of particular importance, virus produced under processed serum conditions was more infectious. Finally, changes in cellular metabolism and gene expression were associated with EV-depleted culture conditions. These findings indicated that EVs play a significant role in cell homeostasis and may protect against infection *in vitro*. Additional work is needed to elucidate mechanisms through which the infectivity of HIV-1 is altered by serum EV-depletion.

Chapter four covers miRNA expression in the context of HIV-1 elite suppression. Given the complexity of the ES phenotype, greater understanding of the miRNA phenotype of different T-cells that are known to play significant roles in killing HIV-1 seemed warranted. This final chapter first presents a novel pipeline for T-cell subset isolation/characterization and then presents a specialized miRNA immunophenotype for 6 subsets: CD4+ and CD8+ Naïve, Central Memory and Effector Memory cells in healthy individuals. Several patterns emerged, the most apparent being that each class of cell, i.e, Naïve, Central Memory or Effector Memory, has a unique miRNA profile and clusters with the profiles from other individuals regardless of HIV-1 infection status or CD4+ or CD8+ phenotype. The greatest expression differences in miRNA species were observed in Naïve cells, with large fold increases in expression of miR-9 and miR-21 in ES relative to healthy controls, and almost all expression differences upregulated in ES or Chronic Progressors relative to the controls. Additional notable findings included downregulation of miR-196b, -193b, -31 and -146b-3p in Chronic Progressors relative to ES, especially in CD4+ Effector Memory cells. This chapter suggests that miRNA expression is associated with innate antiviral cellular response and adds to knowledge of T-cell-specific miRNA expression.

II. Extracellular vesicles and microRNA in cervicovaginal fluid

i.

Potential role of cervicovaginal extracellular particles in diagnosis of endometriosis

The work presented in this chapter was published in BMC Veterinary Research in August 2015, Volume 11:187

Introduction

Endometriosis is a benign but debilitating disease of humans and other primates that affects the reproductive tract and has a reported incidence rate of up to 10% in females of reproductive age [62]. Generally, the term endometriosis is used to describe the condition in which endometrial cells (glands or stroma) develop ectopically, or outside of the uterine cavity [63]. Symptoms of endometriosis include chromic abdominal and pelvic pain, dysmenorrhea, as well as subfertility and likely eventual infertility [64,65]. Treatment protocols have not been standardized, but typically include surgical removal of ectopic tissue as well as removal of associated adhesions.

The current gold standard for diagnosis of the disease combines laparoscopic evaluation and biopsy. In humans, endometriosis is thought to be prevalent for an average eight to eleven years before diagnosis [66] and multiple years after the appearance of symptoms [67,68]. Earlier detection would likely make surgical treatment more effective, afford individuals affected by the disease more options for treatment, and assist in the search for factors involved in pathogenesis. Indeed, the urgent need for early diagnosis was recognized well over a half-century ago [69].

Despite a burgeoning literature on the topic, as yet there is no consensus on early, non-invasive diagnosis methods. Diagnostic markers have been sought in peritoneal, follicular, and endometrial fluid, in urine, and in blood cells and cell-free fractions (see reviews [67,68,70–72]). Employment of ultrasound, MRI [73,74] and measurement of electrical resistance of dermal-visceral zones [75] have also been studied. Recently, attention has turned to circulating miRNAs, which have been reported as biomarkers of various diseases [76]. At least three published studies [77–79] have found an association

between endometriosis and differential regulation of specific miRNAs in circulation, although caution in interpretation has been urged due to estrogen sensitivity of some miRNAs [80]. Remarkably, there is no overlap of miRNA biomarkers reported in the different studies. Indeed, one of the studies reported differential expression of miR-16, which was elsewhere used as an invariant control. The lack of concordance between circulating miRNA biomarker studies has previously been reported for conditions including breast cancer [81,82], and may be due to the high non-specific background of miRNAs that are not associated with disease or are associated with many conditions [83]. Since miRNAs are protected in biofluids by various molecular carriers [84,85], it may be possible to achieve greater discrimination by focusing on extracellular particles, such as extracellular vesicles (EVs) that may be specifically released from cells [82].

EVs are lipid bilayer vesicles [30] that carry a varied cargo including nucleic acids, proteins, metabolites, and lipids. Release of EVs is thought to have a variety of functions, including disposal of harmful cellular contents and transmission of regulatory molecules in a form of intercellular communication. While determining levels of specific EV cargoes such as miRNAs may be useful in diagnosis, an initial study might yield results with even simpler measurements such as EV particle or EV protein concentration. Indeed, such measurements have previously achieved reported success in ovarian cancer [86].

We hypothesized that a promising potential avenue for achieving early diagnosis of reproductive tract diseases including endometriosis might involve examination of total extracellular particles and EVs in cervicovaginal secretions. In this report, we examined particle concentration in total extracellular particle and EV-enriched ultracentrifuged

fractions from cervicovaginal swabs (CVS) and cervicovaginal lavage (CVL) from an individual with endometriosis. We compared these data with results obtained from reproductively normal nonhuman primates, observing apparent disease-associated differences in particle concentrations. To our knowledge, this is the first report of extracellular particle and EV-enriched particle fractions in cervicovaginal secretions from any species.

Case Presentation

A nine-year-old female rhesus macaque (*Macaca mulatta)* with a history of a previous caesarian section presented with a large, firm uterine mass on abdominal and rectal palpation at routine semi-annual physical exam. All animal studies were approved by the Johns Hopkins University Institutional Animal Care and Use Committee and conducted in accordance with the Weatherall Report, the Guide for the Care and Use of Laboratory Animals, and the USDA Animal Welfare Act. Abdominal ultrasound revealed numerous cysts near the uterus. Fine needle aspirate of one of the cysts revealed dark red-brown fluid that on cytology contained numerous degenerate red blood cells, foamy macrophages with hemosiderin, scattered neutrophils and lymphocytes as well as numerous clusters of endometrial-like cells (chocolate cyst) (Figure 1). A laparotomy was subsequently performed, which revealed extensive cyst formation localized to the ovaries; numerous adhesions extending from and between the reproductive tract and the bladder and omentum were observed. Euthanasia was elected due to poor prognosis.

Pathologic Findings

On necropsy, the animal was in good postmortem condition and good body condition (BCS 3/5). The uterus was markedly thickened and nodular with a prominent "chocolate brown" cystic structures on the serosal ventral surface. Dissection between the uterus body, uterine horns, and ovaries was not possible due to the extensive adhesions (Figure 2). One ovary was grossly discernable and exhibited multiple simple cysts as well as a cyst containing "chocolate brown" material.

Ovarian histology confirmed initial examination impressions of endometriosis: Transmurally disrupting and expanding the parenchyma of the bladder and uterus and also impacting the mesentery of the retroperitoneal space were multiple, unencapsulated, infiltrative islands of ectopic endometrial glands surrounded by densely cellular endometrial stromal tissue. The endometrial glands were lined by simple columnar epithelial cells with a moderate amount of clear to pale eosinophilic cytoplasm. The endometrial stroma was composed of spindle cells with indistinct cell borders, scant eosinophilic cytoplasm and an oval nucleus with finely stippled chromatin. Occasionally glands contained moderate numbers of macrophages, neutrophils, erythrocytes, and cellular debris. Within the retroperitoneal mesenteric adipose tissue, multifocal areas of hemorrhage, degenerate neutrophils, and necrotic debris is appreciated along with plump mature reactive fibroblasts (adhesions). The adjacent lymph node contained increased number of histiocytes, which often demonstrated erythrophagocytosis along with hemorrhage and congestion (Figure 3).

Assessment of extracellular particles in secretions

Just prior to euthanasia, CVS and CVL were collected. Samples were collected with the aid of a vaginal speculum by either gently swabbing in the endocervical area with a sterile cottom swab or by lavaging the vaginal vault with a syringe filled with 3.0 mililiters of 1X PBS, respectively. The total yield of CVL fluid was recorded. Swabs were immediately placed in two mL of 1X Dulbecco's PBS and within thirty minutes of collection were swirled in a circular fashion within the PBS and then repeatedly pressed against the side of their respective 15 mililiter conicals to ensure optimal liberation of secretions; lavage fluid was collected into a 15 mililiter conical. Normal CVL samples were pooled by species prior to analysis. Both types of samples were centrifuged at 1,000xg for 15 minutes to remove cells and large debris. Following this first spin, supernatant from each of the sample types was saved, diluted 1:10 with 1X phosphate buffered saline (PBS) and subjected to single particle tracking with a NanoSight NS-500[a] system. At least five 20-second videos were recorded of each sample at a camera setting of 14, and files were analyzed at a detection threshold of ten using NanoSight software version 2.2.

Samples subsequently underwent high-speed ultracentrifugation (110,000xg for 70 minutes at 4˚C) using a Sorvall Discovery 100SE[b] instrument and a Sorvall AH-650[b] swinging-bucket rotor (k-factor =53). After carefully pouring off supernatant, pellets were resuspended in 500 ul PBS using an optimized resuspension protocol. Both sets of samples were diluted at a ratio of 1:10 as well and observed using the same camera and detection threshold settings as were used for the pre-ultracentrifugation observation (described above).

Particle counts of samples from the endometriosis case were compared with CVL and CVS data obtained from four other individuals (two rhesus macaques and two pigtailed macaques, *Macaca nemestrina*) that had no notable reproductive tract history or pathology at necropsy, using the same protocols. Histologic examination of endometrial tissue from the 4 reproductively normal animals revealed that the animals were either in the proliferative phase (n=3) or early secretory (n=1) phase of the menstrual cycle, allowing for the best physiologic comparison with respect to the presence of endometrial cells observed in endometriosis [87–89].

Results

After removal of cells and large debris from the CVS fluid by low-speed centrifugation, on average approximately 30-fold fewer extracellular particles were found in the endometriosis sample than in samples from reproductively healthy rhesus and pigtailed macaques (Figure 4A). In corresponding CVL samples, similar but less pronounced differences were obtained (Figure 4B).

Stepped ultracentrifugation is the most widely used and accepted method for EV enrichment [90], although other particles may co-purify with EVs [90–94]. Following a standard ultracentrifugation protocol, the resulting EV-enriched particle population was approximately nine- to 13-fold more abundant in CVS samples from reproductively healthy animals than in the case of endometriosis (Figure 4C), and approximately ten- to 20-fold more abundant in corresponding CVL (Figure 4D).

Conclusions

Here, we report nanoparticle tracking analysis of extracellular particles including EVs in cervicovaginal samples associated with a verified case of an ongoing endometrial disease process. Notably, particle concentration was markedly decreased in the case of endometriosis as compared with reproductively healthy animals. Since results were obtained after the disease had taken its full course, it is unclear whether this approach could be used in diagnosis of early stage disease. In addition, we cannot be sure as to what is the precipitating factor behind this observed decrease. Perhaps due to cyclic irregularities, normal vaginal secretions are decreased. Regardless, our finding suggests that expanded studies of extracellular particles including EVs in endometriosis are warranted, and that particulate components of cervicovaginal secretions may provide a novel, minimally invasive diagnostic tool for reproductive tract disease. Carefully controlled studies are also needed to determine the possible association of menstrual cycle stage or pregnancy with abundance of cervicovaginal extracellular particles and the cellular source(s) of these particles, especially EVs. As other studies have demonstrated an increased susceptibility to infections of the reproductive tract during hormonal fluctuations, examining particle populations in concert with hormone levels would certainly provide additional insight into the functional capacity of the EVs [95,96]. Finally, investigation of the nucleic acid and protein cargo of extracellular particles and EVs in cervicovaginal secretions may identify new candidate diagnostic markers.

II.i: Figures

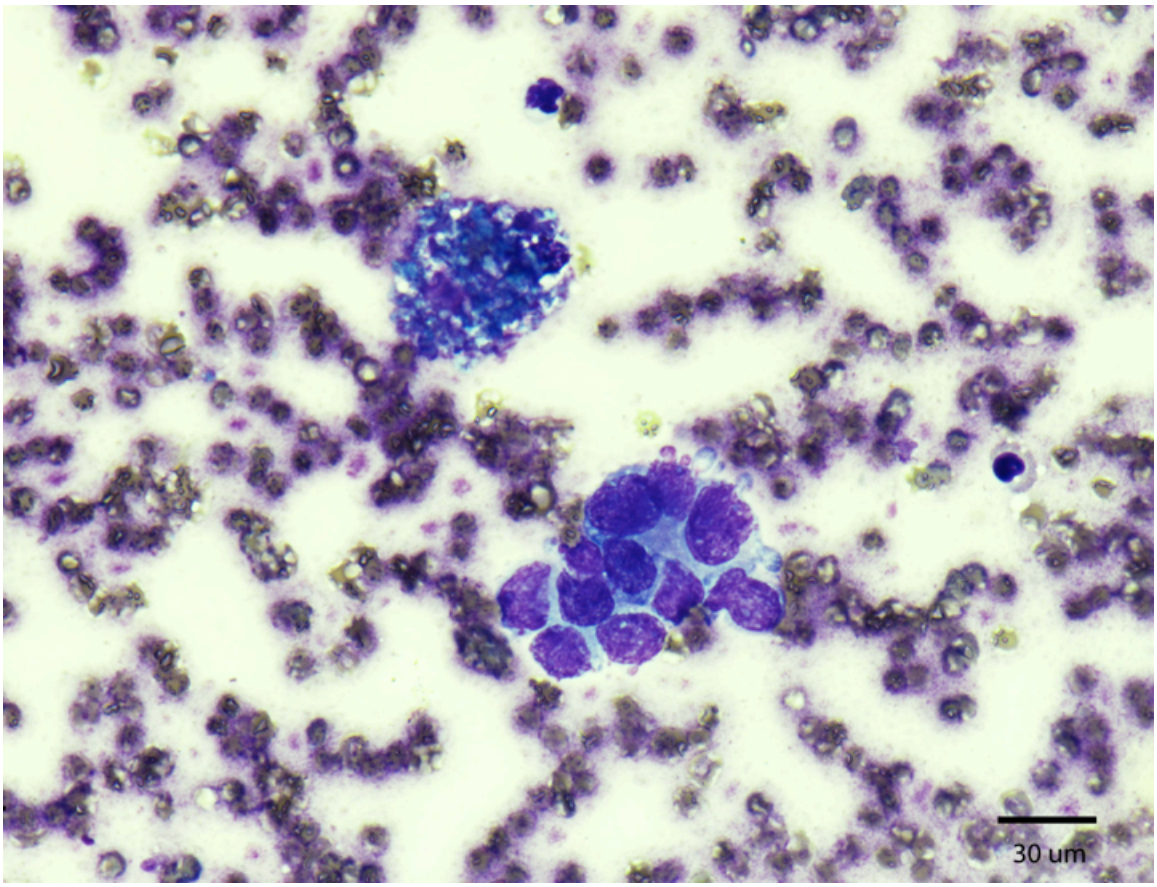

Figure 1. Cytology of fine needle aspirate obtained from abdominal mass. Characteristic hemosiderin-laden macrophages are noted along with a tight cluster of cells with dense, large nuclei and minimal cytoplasm, consistent with endometrial-like cells on a moderate background of erythrocytes. Diff-Quick stain (40X).

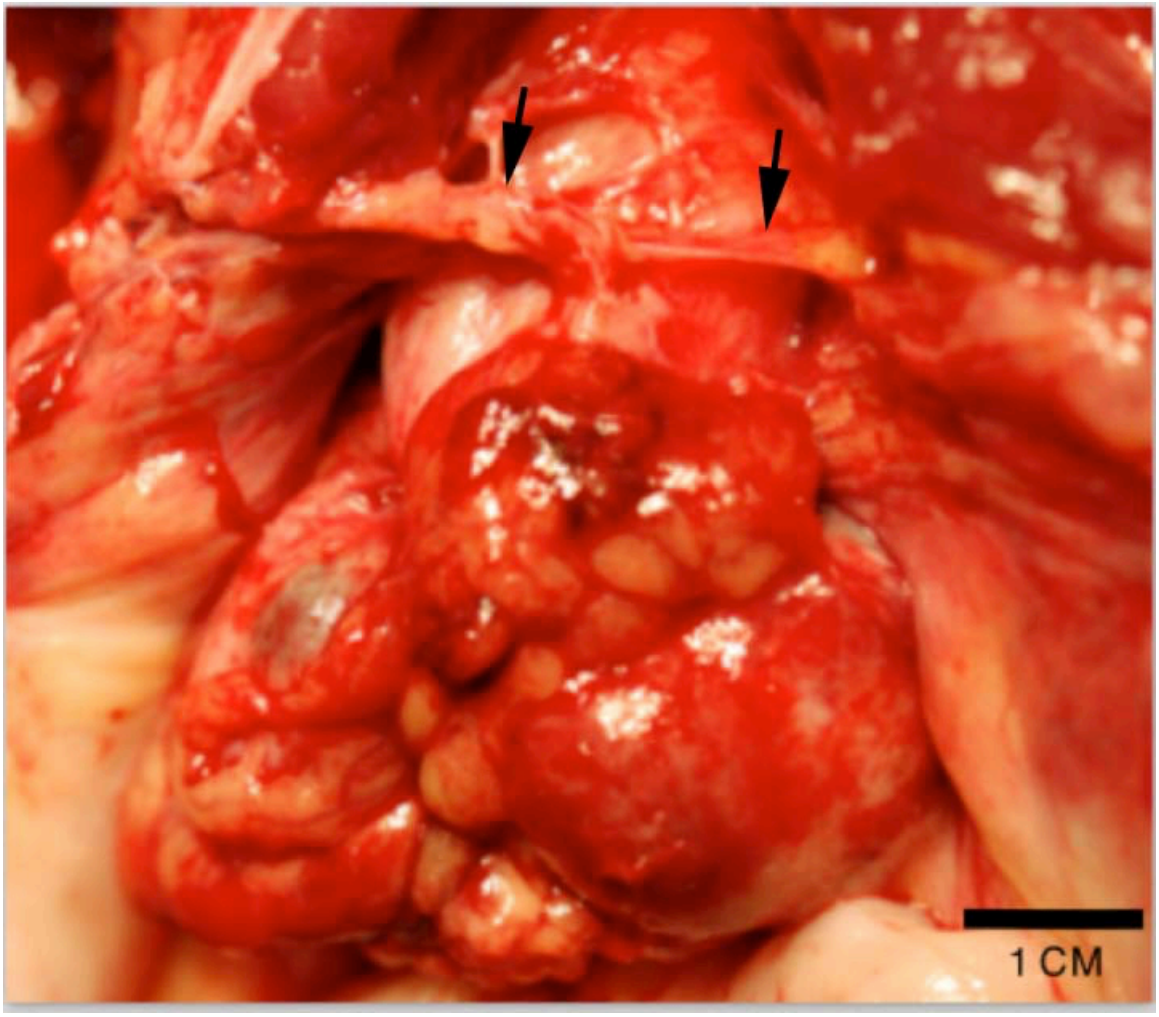

Figure 2. Abdominal Mass. Multiple, large cystic and blood-filled nodules were present in the abdominal cavity along with numerous fibrous adhesions (arrows).

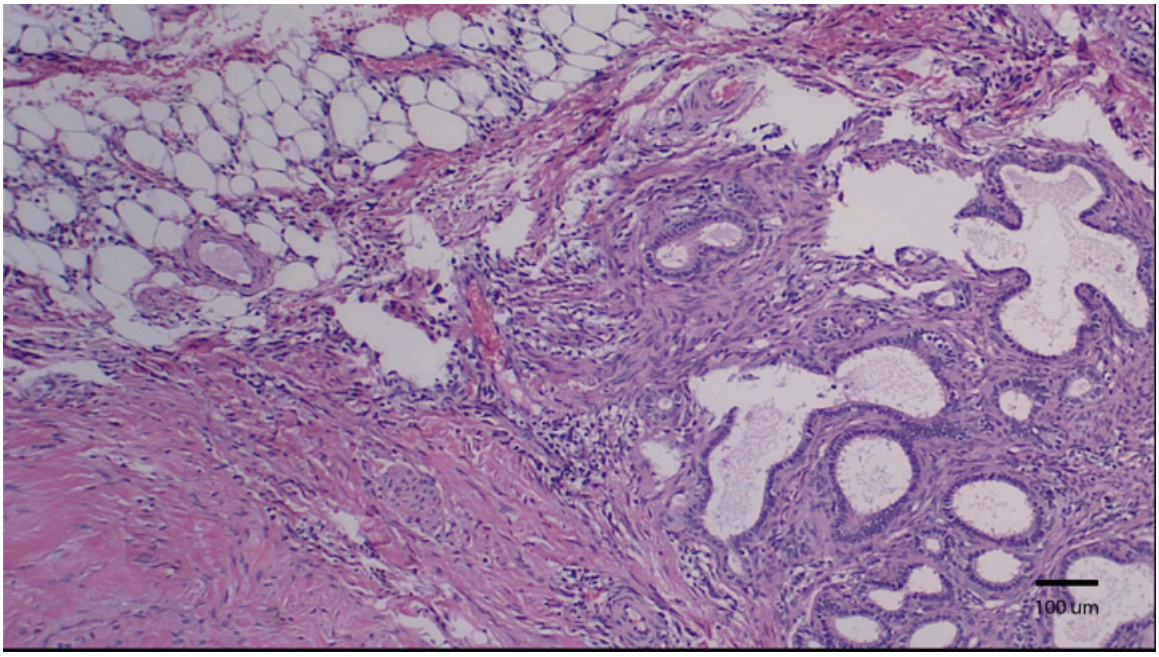

Figure 3. Abdominal Wall. Numerous poorly organized and ectacic endometrial glands were haphazardly arranged within dense connective tissue. H&E stain (10X).

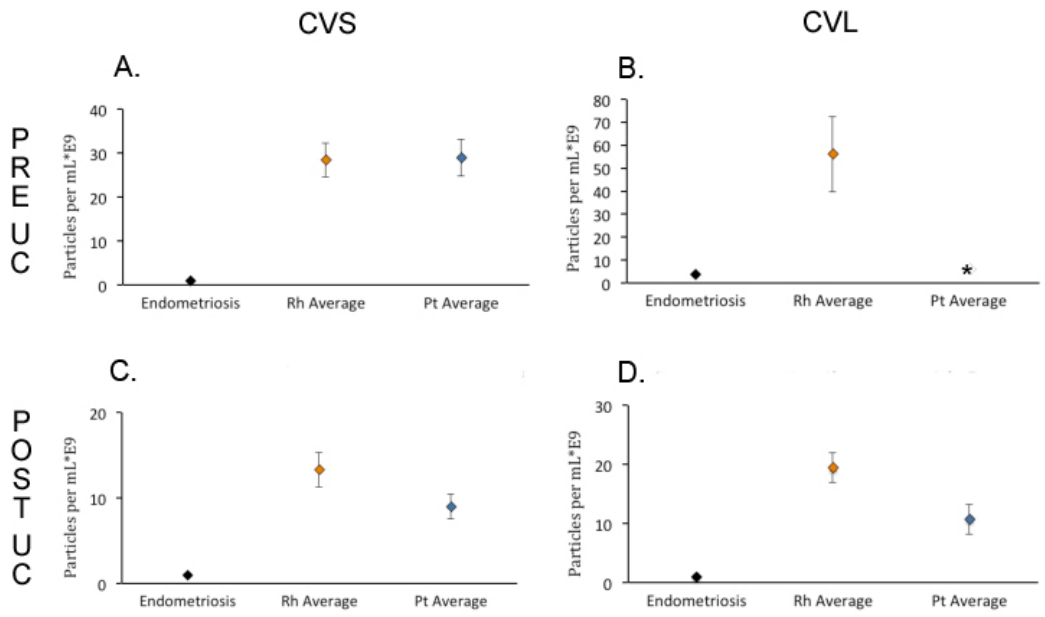

Figure 4. Pooled Data from Cervico-Vaginal Swabs and Cervico-Vaginal Lavage. NTA demonstrated a drop in particles per milliliter in pooled samples from two rhesus macaques (Rh) and two pig-tailed (Pt) macaques as compared to the number of particles observed in the animal with endometriosis. A and B compare CVS and CVL particles per milliliter at low-speed centrifugation (PRE UC) and C and D compare particles observed post-ultracentrifugation (POST UC). Asterisk in panel B: a software malfunction resulted in incomplete acquisition of data and loss of sample. Error bars for averages in CVS samples indicate standard deviation of readings across multiple animals and deviation between readings for the case endometriosis and CVL pooled samples.

ii

miRNA profiling of primate cervicovaginal lavage and extracellular vesicles reveals miR-186-5p as a potential retroviral restriction factor in macrophages

The work presented in this chapter was first released on biorxiv in February 2018

Introduction

The cervicovaginal canal is a potential source of biological markers in forensics investigations [97–100] and reproductive tract cancers [101] and infections [47]. Cervicovaginal secretions may be collected by swab, tampon, or other methods, or secretion components may be liberated by a buffered wash solution and collected as cervicovaginal lavage (CVL). Beyond utility as biomarkers, constituents of cervicovaginal secretions including proteins [102] and certain microbes [103] may have protective roles, for example in wound healing and against HIV-1 infection [104–111]. Secreted components may also change quantitatively or qualitatively during the menstrual cycle [112].

Compared with secreted proteins and the microbiome, several components of cervicovaginal fluids are less well understood, including extracellular RNAs (exRNAs) and their carriers, such as extracellular vesicles (EVs) and ribonucleoprotein complexes (exRNPs). EVs are potential regulators of cell behavior in paracrine and endocrine fashion due to their reported abilities to transfer proteins, nucleic acids, sugars, and lipids between cells [113]. EVs comprise a wide array of double-leaflet membrane extracellular particles, including exosomes and microvesicles [114], and range in diameter from 30 nm to well over one micron (large oncosomes) [115]. EV macromolecular composition tends to reflect, but is not necessarily identical to, that of the cell of origin [116]. EVs have been isolated from most cells, as well as biological fluids [113,117], including cervicovaginal secretions of humans [48] and rhesus macaques [118].

microRNAs (miRNAs) are one of the most studied classes of exRNA. These noncoding RNAs average 22 nucleotides in length and, in some cases, fine-tune the expression of

target transcripts [119,120]. Released from cells by several routes, miRNAs are among the most frequently examined biomarker candidates in biofluids and are reported to be transmitted via EVs. miRNAs are found not only in EVs, but also in free Argonaute-containing protein complexes; the latter may outnumber the former, at least in blood [85,121]. miRNAs are also highly conserved [120], and abundant species typically have 100% identity in humans and nonhuman primates [122]. (For this reason, we will refer to hsa- (Homo sapiens) and mml- (*Macaca mulatta*) miRNAs without the species designation unless otherwise warranted by sequence disparity.) While miRNAs have been profiled in cervicovaginal secretions and menstrual blood, mostly in the forensics setting [100,123,124], their associations with EV and exRNP fractions require further study. A recent publication reported that EVs from healthy vaginal secretions inhibited HIV-1 infection [48]. Another report found that CVL EVs (styled "exosomes") were present at higher concentrations in cervical cancer, and that two miRNAs were also upregulated [101]. Our laboratory described a reduction of CVL EVs in a severe endometriosis case compared with reproductively healthy primates [118]. However, our study, along with others, was limited by the absence of molecular profiling of EV cargo [118].

Here, we performed targeted miRNA profiling of EV-enriched and -depleted fractions of CVL and vaginal secretions collected from healthy and retrovirus-infected rhesus macaques. We queried how CVL EVs and miRNAs are affected by the menstrual cycle, an important potential confounder of biomarker studies. Similarly, we assessed possible associations with simian immunodeficiency virus (SIV) infection. We report an association of miR-186 levels with SIV infection and find that this miRNA also appears

to act in an antiretroviral fashion in HIV infection of macrophages. These studies provide baseline information for easily accessed CVL markers including EVs and miRNAs that may become useful tools in the clinic.

Methods

Sample Collection

CVL and whole blood samples were collected weekly for five weeks from two uninfected (control) and four SIVmac251-infected (infected) rhesus macaques (*Macaca mulatta*) as previously described [118]. All macaques were negative for simian T-cell leukemia virus and simian type D retrovirus and were inoculated intravenously. Animals were sedated with ketamine at a dose of 7-10 mg/kg prior to all procedures. CVL was performed by washing the cervicovaginal cavity with 3 mL of phosphate buffered saline (PBS, Thermo Fisher Scientific, Waltham, MA, USA) directed into the cervicovaginal canal and re-aspirated using the same syringe. Materials and procedures for sample collection are depicted in Figure 8. Volumes of CVL yield across collection dates were documented in Table 1. Whole blood (3 mL) was collected by venipuncture into syringes containing acid citrate dextrose solution (ACD) (Sigma Aldrich, St. Louis, MO, USA).

Study Approvals

All animal studies were approved by the Johns Hopkins University Institutional Animal Care and Use Committee (IACUC) and conducted in accordance with the Weatherall Report, the Guide for the Care and Use of Laboratory Animals, and the USDA Animal Welfare Act.

Sample Processing

Sample processing began within a maximum of 60 minutes of collection and utilized serial centrifugation steps to enrich EVs as described previously [125], based on a standard EV isolation protocol [126]. Specifically, fluids were centrifuged: (1) 1,000 × *g* for 15mins at 4°C in a tabletop centrifuge; (2) 10,000 × *g* for 20 mins at 4°C; and (3) 110,000 × *g* for 2 hours at 4°C with a Sorvall Discovery SE ultracentrifuge (Thermo Fisher Scientific) with an AH-650 rotor (k factor: 53.0) (Figure 8B). Following each centrifugation step, most supernatant was removed, taking care not to disturb the pellet. After each step, supernatant was set aside for nanoparticle tracking analysis (NTA; 200 µL), and RNA isolation (200 µL) following the second and third steps. The pellet was resuspended in 400 µL of PBS after each centrifugation step. After the final step, the remaining ultracentrifuged supernatant was concentrated to approximately 220 µL using Amicon Ultra-2 10 kDa molecular weight cutoff filters (Merck KGaA, Darmstadt, Germany). 200 µL of the concentrate was used for RNA isolation and the remainder was retained for NTA. All samples reserved for RNA isolation were mixed with 62.6 µL of RNA isolation buffer (Exiqon, Vedbaek, Denmark) containing three micrograms of glycogen and 5 pg of synthetic cel-miR-39 as previously described [127]. Processed samples were analyzed immediately or frozen at -80°C until further use.

For plasma, whole blood was centrifuged at 800 × *g* for 10 mins at 25°C. Supernatant was centrifuged twice at 2,500 × *g* for 10 mins at 25°C. The resulting platelet-poor plasma was aliquoted and frozen at -80°C.

Hormone Analysis

Levels of progesterone (P4) and estradiol-17b (E2) were measured in plasma samples shipped overnight on dry ice to the Endocrine Technology and Support Core Lab at the Oregon National Primate Research Center, Oregon Health and Science University.

Nanoparticle Tracking Analysis

Extracellular particle concentration was determined using a NanoSight NS500 NTA system (Malvern, Worcestershire, UK). Cervicovaginal lavage samples were diluted as needed and specified in Table 2 to ensure optimal NTA analysis. At least five 20-second videos were recorded for each sample at a camera setting of 12. Data were analyzed at a detection threshold of two using NanoSight software version 3.0.

Western Blot

Western blot was used to detect the presence of EV protein markers and the absence of calnexin (endoplasmic reticulum marker) in CVL and enriched CVL EVs. Because of low quantities, both CVL and enriched EVs were pooled as indicated in Table 2. 20 µL of pooled samples were lysed with 5 µL 1:1 mixture of RIPA buffer (Cell Signaling Technology, Danvers, MA. Cat #: 9806S) and protease inhibitor (Santa Cruz Biotechnology, Dallas, TX. Cat #: sc29131). 8 µL of Laemmli 4X sample buffer (BioRad, Hercules, CA. Cat #:161-0747 Lot #: 64077737) was added per sample, and 30 µL of each was loaded into a Criterion TGX 10% gel (BioRad, Hercules, CA. Cat #: 5671034 Lot #: 64115589) after 5 mins of 95ºC incubation. The gel was electrophoresed by application of 100V for 100 mins. The proteins were then transferred to a PVDF membrane (BioRad, Hercules, CA), which was blocked with 5% milk (BioRad, Hercules,

CA. Cat #: 1706404. Lot #: 64047053) in PBS+0.1%Tween®20 (Sigma-Aldrich, St. Louis, MO Cat #: 274348 Lot #: MKBF5463V) for 1 hour. The membrane was subsequently incubated with mouse anti-human CD63 (BD Biosciences, San Jose, CA Cat #: 556019 Lot #: 6355939) and mouse monoclonal IgG_2b CD81 (Santa Cruz Biotechnology, Dallas, TX Cat #: 166029 Lot #: L1015) primary antibodies, at a concentration of 0.5 μg/mL for 1 h. After washing the membrane, it was incubated with a goat anti-mouse IgG-HRP secondary antibody (Santa Cruz Biotechnology, Dallas, TX Cat #: sc-2005 Lot #: B1616) at a 1:10,000 dilution for 1 h. The membrane was then incubated with a 1:1 mixture of SuperSignal West Pico Stable Peroxide solution and Luminol Enhancer solution (Thermo Scientific, Rockford, IL Cat #: 34080 Lot #: SD246944) for 5 min. The membrane was visualized on chemiluminescence film (Denville Scientific, Holliston, MA Cat #: E3018 Lot #:79608091) for up to 150 seconds. The second blot was done in a reducing environment using 10mM DTT (Promega, Madison, WI Cat #: P1171 Lot #: 0000198991). Same procedures were followed with rabbit anti-human TSG101 (Cat #: ab125011 Lot #:GR180132-14), rabbit anti-syntenin (Abcam, Cambridge, MA Cat #: ab133267 Lot #: GR89146-10), and rabbit anti-calnexin (Abcam, Cambridge, MA Cat #: ab22595 Lot #:GR243392-3) primary antibodies. Subsequent incubation with goat anti-rabbit IgG-HRP secondary antibody (Abcam, Cambridge, MA Cat #: sc-2204 Lot #: B2216). All antibodies were used at the same concentration as the first blot. Film was exposed to the membrane for up to 8 mins for visualization.

Electron Microscopy

Gold grids were floated on 2% paraformaldehyde-fixed CVL–derived samples for two minutes, then negatively stained with uranyl acetate for 22 seconds. Grids were observed with a Hitachi 7600 transmission electron microscope in the Johns Hopkins Institute for Basic Biomedical Sciences Microscope Facility.

Total RNA Isolation and Quality Control

RNA isolation work flow is shown in Figure 8C. RNA lysis buffer was added into each sample as described above prior to freezing (-80 °C). Total RNA was isolated from thawed samples using the miRCURY RNA Isolation Kit-Biofluids (Exiqon) per manufacturer's protocol with minor modifications as previously described (10). Total RNA was eluted with 50 µL RNase-free water and stored at -80°C. As quality control, expression levels of several small RNAs including snRNA U6, miR-16-5p, miR-223-3p, and the spiked-in synthetic cel-miR-39 were assessed by TaqMan miRNA assays (Applied Biosystems/ Life Technologies, Carlsbad, California, USA) [128].

miRNA Profiling by TaqMan Low-Density Array

A custom 48-feature TaqMan low-density array (TLDA) (11) was ordered from Thermo Fisher, with features chosen based on results of a human CVL pilot study (G. Hancock and K.W. Witwer, unpublished data). Stem-loop primer reverse transcription and pre-amplification steps were conducted using the manufacturer's reagents as previously described [129] but with 14 cycles of pre-amplification. Real time quantitative PCR was performed with a QuantStudio 12K instrument (Johns Hopkins University DNA Analysis Facility). Data were collected using SDS software and Cq values

extracted with Expression Suite v1.0.4 (Thermo Fisher Scientific, Waltham, MA USA). Raw Cq values were adjusted by a factor determined from the geometric mean of 10 relatively invariant miRNAs. The selection process for these invariant miRNAs was to 1) rank miRNAs by coefficient of variation; 2) remove miRNAs with high average Cq (>30), non-miRNAs, and those with low amplification score; 3) select the lowest-CV member of miRNA families (e.g., the 17/92 clusters); and 4) pick the top 10 remaining candidates by CV: let-7b-5p, -miR-21-5p , -27a-3p, -28-3p, -29a-3p, -30b-5p, -92a-3p, -197-3p, -200c-3p, and -320a-3p.

Individual RT-qPCR Assays

Individual TaqMan miRNA qPCR assays were performed as previously described [129] for miRs-19a-3p (Thermo Fisher Assay ID #000395), -186-5p (Thermo Fisher Assay ID #002285), -451a-5p (Thermo Fisher Assay ID #001105) , -200c-3p (Thermo Fisher Assay ID #002300), -222-3p (Thermo Fisher Assay ID #002276), -193b-3p (Thermo Fisher Assay ID #002367), -181a-5p (Thermo Fisher Assay ID #000480), and -125b-5p (Thermo Fisher Assay ID #00449). We also measured miR-375-3p (Thermo Fisher Assay ID #00564), which was not included on the array. Data were adjusted to Cqs of miR-16-5p and miR-19a-3p, but conclusions were robust to different normalization methods.

Blood Cell Isolation and Monocyte-Derived Macrophage Culture

Total PBMCs were obtained from freshly drawn blood from human donors under a Johns Hopkins University School of Medicine IRB-approved protocol (JHU IRB #CR00011400). Blood was mixed with 10% Acid Citrate Dextrose (ACD) (Sigma

Aldrich, St. Louis, MO Cat #: C3821 Lot #: SLBQ6570V) with gentle mixing by inversion. Within 15 minutes of draw, blood was diluted with equal volume of PBS+ 2% FBS, gently layered onto room temperature Ficoll (Biosciences AB, Uppsala, Sweden Cat #:17-1440-03 Lot #: 10253776) in Sepmate-50 tubes (STEMCELL Technologies, Vancouver, BC, Canada Cat #: 15450 Lot #: 06102016) and centrifuged for 10 minutes at 1200 × *g*. Plasma and PBMC fractions were removed, washed in PBS+ 2% FBS, and pelleted at 300 × *g* for 8 minutes. Pellets from 5 tubes were combined by resuspension in 10 mL RBC lysis buffer (4.15 g NH_4Cl, 0.5 g $KHCO_3$, 0.15 g EDTA in 450 mL H_2O; pH adjusted to 7.2–7.3; volume adjusted to 500 mL and filter-sterilized); total volume was brought to 40 mL with RBC lysis buffer. After incubation at 37 °C for 5 mins, the suspension was centrifuged at 400 × *g* for 6 mins at room temperature. The cell pellet was resuspended in Macrophage Differentiation Medium with 20% FBS (MDM20) to a final concentration of 2×10^6 cells/mL. PBMCs were plated at 4×10^6 cells per well in 12-well plates and cultured in MDM20 for 7 days. One half of the total volume of medium was replaced on day 3. On day 7, cells were washed 3 times with PBS to remove non-adherent cells. The medium was replaced with Macrophage Differentiation Medium with 10% serum (MDM10) and cultured overnight prior to transfection.

miRNA Mimic Transfection

Differentiated macrophages were transfected with 50 nM miRNA-186-5p using Lipofectamine 2000 (Invitrogen/Life Technologies, Carlsbad, CA Cat #: 11668-019 Lot #:1467572) diluted in OptiMEM Reduced Serum Medium (Gibco, Grand Island, NY Cat #: 31985-070 Lot #: 1762285). Controls included mock transfections and transfection of

50 nM siRNA oligo labeled with Alexa Fluor 555 (Invitrogen, Fredrick, MD Cat #: 14750-100 Lot #: 1863892). Plates were incubated for 6 hours at 37 °C. After incubation, successful transfection was confirmed by examining uptake of labeled siRNA with an Eclipse TE200 inverted microscope (Nikon Instruments, Melville, NY). Transfection medium was removed. The plates were washed with PBS and refed with 2 mL fresh MDM10 medium.

HIV Infection

HIV-1 BaL stocks were generated from infected PM1 T-lymphocytic cells and stored at −80 °C. 24 hours after mimic or mock transfections, macrophages were infected with HIV BaL and incubated overnight (stock, 80 μg p24/mL, diluted to 200 ng p24/mL). At days 3, 6, and 9 post-infection, 500 μL supernatant was collected for p24 release assays and cells were lysed with 600 μL mirVana lysis buffer for subsequent RNA isolation and analysis.

HIV p24 Antigen ELISA

Supernatant samples were lysed with Triton-X at a final concentration of 1%. The DuPont HIV-1 p24 Core Profile ELISA kit (Perkin Elmer, Waltham, MA Cat #: NEK050B001KT Lot #: 990-17041) was used per manufacturer's instructions to measure p24 concentration based on the provided standard.

Total RNA Isolation

Total RNA was isolated using the mirVana miRNA Isolation Kit per manufacturer's protocol (Ambion, Vilnius, Lithuania Cat #: AM1560 Lot #: 1211082). Note that this procedure yields total RNA, not just small RNAs. After elution with 100 µL RNase-free water, nucleic acid concentration was measured using a NanoDrop 1000 spectrophotometer (Thermo Fisher Scientific, Wilmington, DE). RNA isolates were stored at -80 °C.

HIV Gag RNA RT-qPCR

Real-time one-step reverse transcription quantitative PCR was performed with the QuantiTect Virus Kit (Qiagen, Foster City, CA Cat #:211011 Lot #: 154030803). Each 25 µl reaction mixture contained 15 µl of master mix containing HIV-1 RNA standard, 100 µM of FAM dye and IBFQ quencher labeled Gag probe (5' ATT ATC AGA AGG AGC CAC CCC ACA AGA 3'), 600 nM each of Gag1 forward primer (5'TCA GCC CAG AAG TAA TAC CCA TGT 3') and Gag2 reverse primer (5' CAC TGT GTT TAG CAT GGT GTT T 3'), nuclease-free water, and QuantiTect Virus RT mix, and 10 µL serial-diluted standard or template RNA. No-template control and no reverse transcriptase controls were included. Linear standard curve was generated by plotting the log copy number versus the quantification cycle (C_q) value. Log-transformed Gag copy number was calculated based on the standard curve.

Macrophage Viability Assessment by MTT Cell Proliferation Assay

5 mg 3-(4,5-Dimethylthiazol-2-yl)-2,5- diphenyltetrazolium bromide (MTT) (Vybrant MTT cell proliferation assay kit, Invitrogen, Eugene, OR Cat #: V13154 Lot #: 1897699) was dissolved in 1mL of PBS and incubated in the dark for 20 mins. Dissolved MTT was then diluted in 12 mL of phenol red-free MDM10 medium. Macrophages in 12 well plates were washed with 2 mL PBS. 1 mL of MTT/MDM10 medium was added to each well and incubated at 37 °C for 45 mins. 12 mL of 0.01N hydrochloric acid was added to dissolve SDS, and 1 mL acidified SDS solution was added to each well and mixed thoroughly until all formazan crystals were dissolved. Formazan quantification was performed using an iMark microplate absorbance reader (BioRad, Hercules, CA) with a 570 nm test wavelength. Data were expressed as mean absorbance value (OD) of duplicate samples plus standard error of the mean.

Data analysis

Data processing and analysis were conducted using tools from Microsoft Excel (geometric mean normalization), Apple Numbers, GraphPad Prism, the MultiExperiment Viewer, and R/BioConductor packages including pheatmap (http://CRAN.R-project.org/package=pheatmap; quantile normalization, Euclidean distance, self-organizing maps, self-organizing tree algorithms, k-means clustering). Figures and tables were prepared using R Studio, Microsoft Excel and Word, Apple Numbers and Keynote, GraphPad Prism, and Adobe Photoshop.

Data Availability and Rigor and Reproducibility

Array data have been deposited with the Gene Expression Omnibus (GEO) [130] as GSE107856. Data in other formats are available upon request. To the extent that sample quantities would allow, the MISEV2014 recommendations for EV studies were followed [93,131], and the EV experiments have been registered with the EV-TRACK knowledgebase [132] with preliminary EV-TRACK code XL5296IL.

Results

Abnormal menstrual cycle of SIV-infected macaques and ovulation-associated changes in CVL EV-enriched particles

Plasma and CVL were collected from two control and four SIV-infected macaques over the course of five weeks (Figure 8). Abnormal cycling was observed for infected subjects (K. Mulka, et al, manuscript in preparation). By nanoparticle tracking analysis, CVL EV concentration increased during ovulation (Figure 1A). Transmission electron microscopy was performed for representative fractions of CVL, revealing bacteria and large particles in the 10,000 × *g* pellet (Figure 1B). The 100,000 x g pellet included apparent EVs up to 200 nm in diameter (Figure 1C). EV markers (shown: CD63 and CD81) were confirmed by Western blot in samples from control and infected subjects (Figure 1D). Calnexin was found only in tissue samples (Figure 1E). Interestingly, neither TSG101 nor syntenin (considered to be luminal EV proteins) could be detected in the EV-enriched fractions of CVL (Figure 1E), potentially indicating a predominance of surface-released EVs over endosomal-origin exosomes in these preparations.

TLDA reveals an extracellular miRNA profile of the cervicovaginal compartment

Based upon preliminary findings from a study of human CVL (Hancock and Witwer, unpublished data), we designed a custom TaqMan low-density array (TLDA) to measure 47 miRNAs expected to be present in CVL, along with the snRNA U6. CVL from all subjects and at all time points was fractionated by stepped centrifugation to yield

a 10,000 x g pellet (10K pellet), a 100,000 x g pellet (UC pellet), and 100,000 x g supernatant (UC supernatant). Total RNA from all fractions was profiled by TLDA. Raw (Figure 2A), quantile normalized (Figure 2B), and geometric mean-adjusted Cq values (Figure 2C) were subjected to unsupervised hierarchical clustering. This clustering did not reveal broad miRNA profile differences associated with sample collection time, menstruation, or SIV infection.

Distribution of miRNAs across CVL fractions

Across the three examined CVL fractions (p10, p100, S100), the ten most abundant miRNAs (lowest Cq values) were miRs-223-3p, -203a-3p, -24-3p, -150-5p, -146a-5p, -21-5p, -222-3p, -92a-3p, -17-5p, and -16-5p. The average normalized Cq value for each miRNA was greater (i.e., lower abundance) in the p100 than the s100 fraction (Figure 3A and inset), and indeed in p10 and p100 combined (Figure 3B), suggesting that most miRNA in CVL, as in various other body fluids, is found outside the EV-enriched fractions. Considering all fractions, the differences between the EV-enriched and EV-depleted fractions were significant even after Bonferroni correction for all features except U6, miR-191-5p, and miR-451a-5p. On average, the s100 fraction contained 86.5% of the total miRNA from these three fractions. In the p10 fraction, the average miRNA was detected at 10.5% its level in the s100 fraction (SD=5.7%). miR-34a-5p had the lowest (5.9%) and miR-28-3p the highest (33.7%) abundance compared with s100. In the p100 fraction, miRNAs were on average 5.6% (SD=2.4%) as abundant as in s100. The least represented in p100 was miR-27a-3p (2.3%), and the best represented was again miR-28-

3p (13.4%). miRNA rank was significantly correlated across fractions, despite minor differences in order (Figure 3C).

qPCR validation

Individual stem loop RT/hydrolysis probe qPCR assays were used to verify TLDA results for miRs-19a-3p, -186-5p, -451a-5p, -200c-3p, -222-3p, -193b-3p, -181a-5p, and -125b-5p. miR-375-3p (not included on the array), was also measured because of a reported association with goblet cells (12). Results of qPCR assays, adjusted by miR-16-5p for each sample, are shown in Figure 4A. Figure 4B compares miRNA ranks (1-11) by TLDA and individual qPCR, which are generally in concordance. Note that expression of red blood cell miRNA miR-451a-5p was low, suggesting minimal contamination from blood for most samples.

miRNA association with retroviral infection status

An association of miRNA abundance with infection status could yield novel biomarkers as well as clues to roles of miRNA in modulating infection. However, the small number of subjects in our study was a challenge. Nevertheless, by considering all subjects and time points together for both infected and uninfected subjects, microarray data suggested a slightly reduced abundance of miRs-186-5p, -222-3p, and -200c-3p in infected samples, while qPCR revealed differential abundance of miRs-186-5p, -375-3p, and -125b-5p. (Figure 5). miR-186-5p was thus identified by both techniques as potentially associated with retroviral infection.

miR-186-5p inhibits HIV p24 release by monocyte-derived macrophages.

To assess a possible influence of miR-186-5p ("miR-186") on retroviral replication, we introduced miR-186 mimic or control RNAs into monocyte-derived macrophages 24 hours before infection or not with HIV. At days 3, 6, and 9 post-infection (dpi), we measured HIV release (capsid p24 protein in culture supernatant) and transcription (cellular Gag mRNA copy number). By p24 release, robust infection was observed by 3 dpi, and p24 counts increased by two-fold or more by 9 dpi (Figure 6A) for multiple replicate experiments with cells from three donors. Compared with infected, untreated controls, mock-transfected cells (not shown), and cells transfected with a negative control RNA (labeled with a fluorophore to assess transfection efficiency), miR-186 transfection was associated with a significant decline of released p24 at all time points (ANOVA with Bonferroni correction) (Figure 6B-D). The negative control condition showed a suppressive trend that reached nominal significance at 9 dpi. However, miR-186-associated suppression was significantly greater at all time points.

No consistent effect of miR-186 on HIV RNA abundance

Using a gag qPCR/standard curve, we quantitated full-length HIV-1 transcript in cells from three donors. In cells from only one of three donors were fewer HIV-1 copies associated with miR-186 mimic transfection (Figure 7). Overall, there was no statistically significant difference in HIV RNA between the conditions.

Discussion

Cervicovaginal lavage and CVL EVs and exRNPs, like EVs in the uterus [133,134], may offer information about the health of the reproductive tract as well as clues about factors that facilitate or block transmission of infectious agents. Proteomic analyses of human [135] and rhesus macaque [47] CVL have suggested a core proteome and a highly variable proteome that responds to changes in pregnancy status, menstruation, infection, and other stressors. However, exRNA and extracellular vesicle profiles are less understood in this compartment. Thus, the major finding of this study is further characterization of CVL fluid of primates, including extracellular vesicle and miRNA profiles. EVs could be liberated from vaginal secretions by lavage, and these EVs could be concentrated using a standard stepped centrifugation procedure, with enrichment of positive (membrane-associated) markers and apparent absence of a cellular negative control. Furthermore, both EV-replete and EV-depleted fractions of CVL contained abundant miRNA.

As reported for other biological fluids [85,136], miRNA concentration was highest in the EV-depleted CVL fractions, not in EV-enriched ultracentrifuged pellets, consistent with packaging of most extracellular miRNA into exRNPs; the function, if any, of extracellular miRNAs in the cervicovaginal tract of healthy individuals remains to be determined. We observed minimal differences in extracellular miRNA profiles between SIV-infected and uninfected subjects or, most surprisingly, during the course of the menstrual cycle, suggesting a certain stability of extracellular miRNA in the compartment. Correlation of miRNA concentrations in EV-depleted and -replete fractions was also apparent. Based on relative abundance, miRNAs in EVs and exRNPs of CVL

are likely derived from epithelial cells (including goblet cells), and cells of the immune system (as suggested, e.g., by myeloid-enriched miR-223 and lymphocyte-enriched miR-150) [137]. Of the most abundant miRNAs we identified, many have been ascribed tumor-suppressive roles in various types of cancer (14–19). Also, miR-223 and miR-150 have been described as "anti-HIV" miRNAs [60] among a variety of reported antiretroviral sRNAs, both host and viral [144–149]. Given their relative abundance in the vaginal tract, a common site for HIV infection, these miRNAs may contribute to antiviral defenses.

Along these lines, a second major finding of this study is a possible role for miR-186 in anti-retroviral defense. In contrast with an early report of direct binding of host miRNAs to retroviral transcripts and subsequent suppression [60], it now appears that this mechanism of suppression is relatively uncommon [150], and that anti-HIV miRNAs may exert effects through control of host genes instead [e.g., [151]]. Our data also support the conclusion that reduction of HIV RNA levels is not the main mechanism for miR-186-mediated suppression of HIV release.

We would like to emphasize several weaknesses of the study and opportunity for future research:

1) We used stepped ultracentrifugation without density gradients because of the small sample volumes available. Although stepped ultracentrifugation remains a widely used method for EV enrichment [126,152], subsequent gradients or alternative isolation methods could be attempted with larger volume samples to increase purity in future. Possibly, our study overestimates the abundance of

miRNAs in CVL EVs, and differential packaging into EVs and exRNPs is masked by contamination of our EV preps with exRNPs.

2) Our qPCR array approach and focus on miRNAs leaves room for additional work. While we are confident that our array captured most of the abundant miRNAs in CVL, sequencing short and longer RNAs could reveal additional markers.

3) The small number of subjects and the absence of obvious menstrual cycle in infected subjects precludes strong conclusions about EV or miRNA associations with either infection or the menstrual cycle. For example, we did not observe the expected increase in miR-451a or other red blood cell-specific miRNAs during menstruation. However, since only two animals showed evidence of cycling, experiments with more subjects and larger sample volumes are needed.

4) Our previous criticisms of miRNA functional studies [153] also apply to our work here. Additional work is needed to prove that miR-186 can regulate retroviral release at endogenous levels, that it is present in active RNPs [154], its interactions with host targets, and a mechanism for viral suppression. Finally, it is possible, but must be demonstrated, that miR-186 acts in a paracrine fashion via EV or exRNP shuttles.

5) We have investigated the effects of miR-186 only in monocyte-derived macrophages. We chose to begin with this cell type because of the abundance of miR-223 and the known role of macrophages in the epithelium. Other cell types should also be investigated.

Overall, the results presented here support further development of CVL and its constituents as a window into the health of the cervicovaginal compartment.

II.ii Figures:

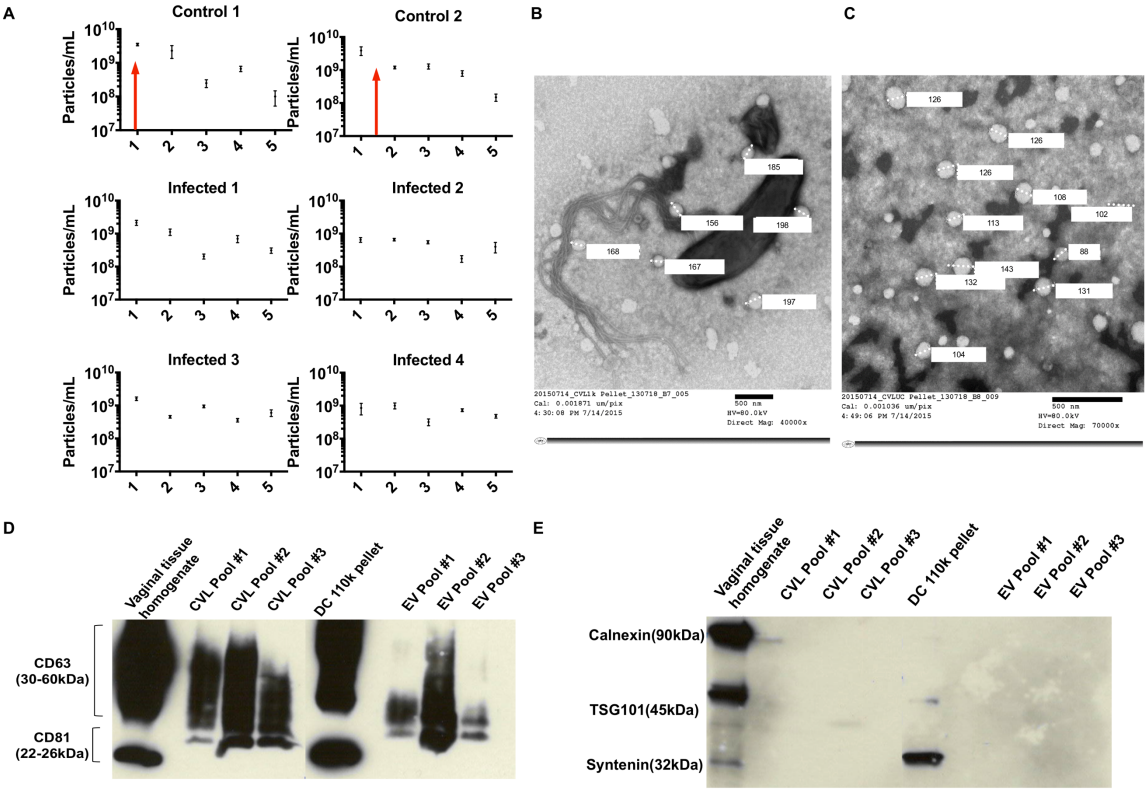

Figure 1. EVs are found in cervicovaginal lavage. A) Particle concentrations of CVL 100,000 × *g* ultracentrifuge (UC) pellets (blue) monitored weekly over five weeks for two SIV-negative ("control") and four SIV-infected subjects. Red arrows indicate estimatedtime of ovulation of animal. **B and C)** Transmission electron micrographs of CVL 10,000 × *g* pellet **(B)** and 100,000× *g* pellet **(C)** confirm presence of bacteria and EVs (B) and EV-like particles (C). Western blot: enrichment of CD63 and CD81 markers **(D)** and absence of ER marker calnexin **(E)** in pooled 10,000 and 10,000 × *g* pellet fractions. Vaginal tissue homogenate and dendritic cell 100,000 × *g* pellet controls were also positive for CD63 and CD81. EV luminal markers syntenin and TSG101 were present in cellular but not putative EV samples. In subfigure D, two blots are shown, with the separation occurring between CVL Pool#3 and DC 110k pellet.

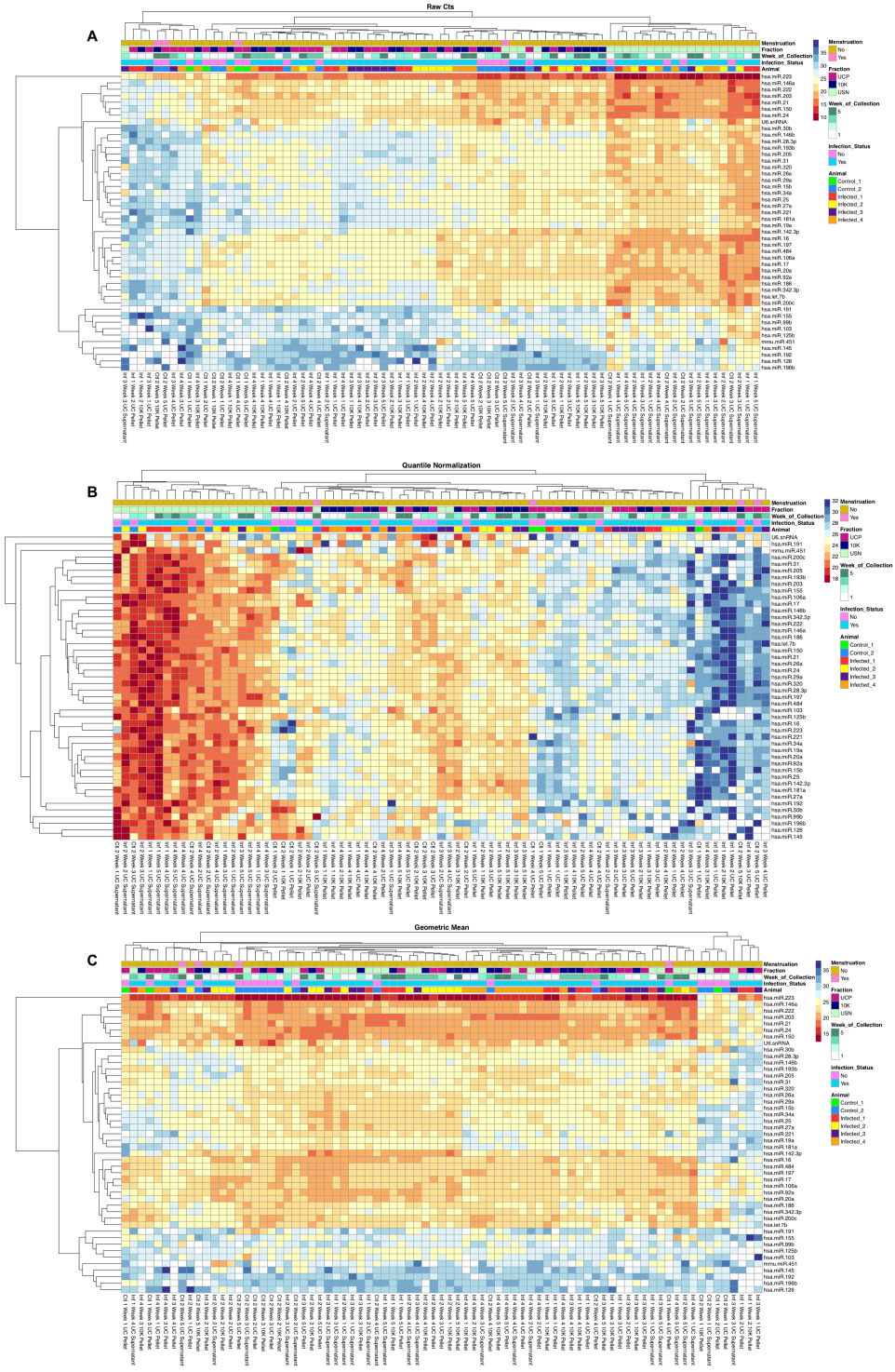

Figure 2. miRNA profile of CVL fractions. Targeted miRNA profiles were determined by custom TaqMan low-density array (TLDA). Hierarchical clustering of samples and features (Pearson correlation, average linkage) of data: raw **(A)** or normalized by **(B)** quantiles or **(C)** a geometric mean approach as described in the methods. Abundance scale: red (high) to low (blue).

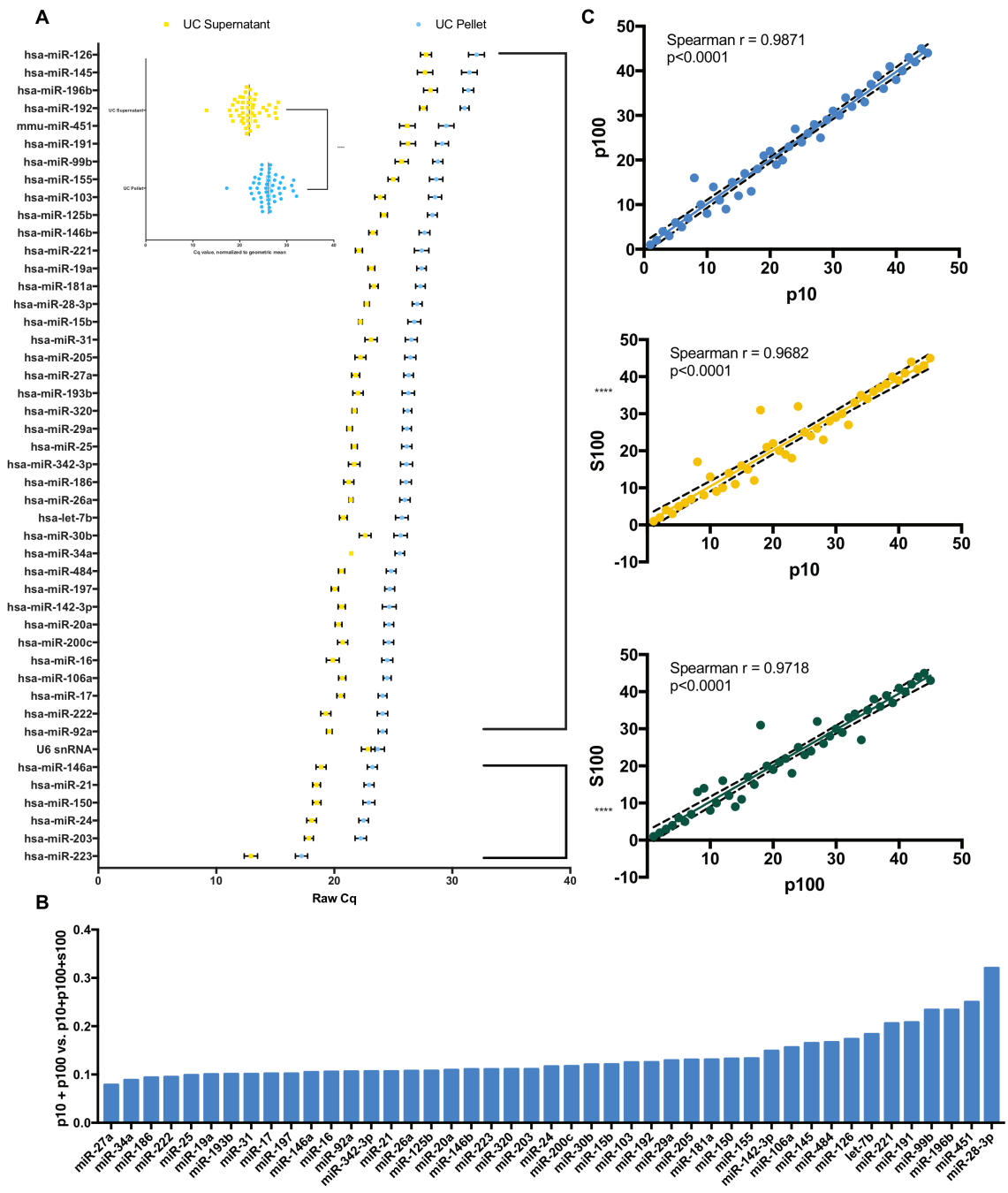

Figure 3. Relative abundance of miRNAs in centrifuged CVL fractions. A) Abundant miRNAs in descending order based on Cq values normalized to the geometric mean for each sample. Inset: average of all miRNAs in UC pellet and UC supernatant. Error bars: SEM. B) miRNAs in each fraction (10,000× g pellet=p10, 110,000 × g pellet=p100, 110,000× g supernatant=S100) are significantly correlated (p<0.0001, Spearman). C) miRNA expression in EV-enriched fractions (p10, p100) as a percentage of total estimated expression (p10+p100+S100 by Cq) in ascending order, from miR-27a-3p (7.9%) to miR-28-3p (32.0%).

A

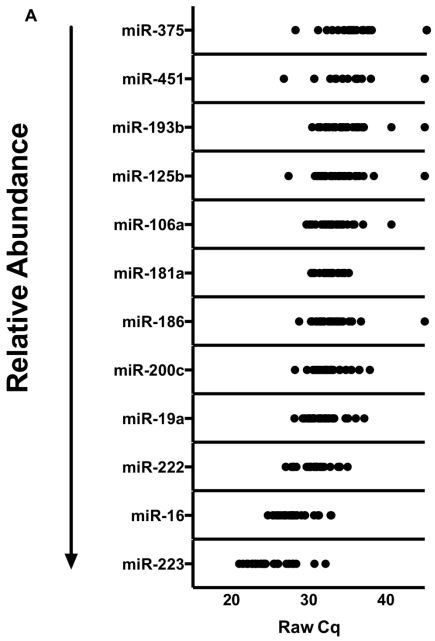

B

Relative Abundance Rank by qPCR	miRNA	Rank of Relative Abundance by TLDA
1	hsa-miR-223-3p	**1**
2	hsa-miR-16-5p	**3**
3	hsa-miR-222-3p	**2**
4	hsa-miR-19a-3p	**9**
5	hsa-miR-200c-3p	**4**
6	hsa-miR-186-5p	**6**
7	hsa-miR-181a-5p	**8**
8	hsa-miR-106a-5p	**5**
9	hsa-miR-125b-5p	**10**
10	hsa-miR-193b-3p	**7**
11	hsa-miR-451a-5p	**11**

Figure 4. miRNA qPCR validation. A) Stem-loop reverse transcription/qPCR validation of UC p100 samples, all subjects and time points (individual dots). B) Ranks of abundant miRNAs based on qPCR and TLDA Cq data.

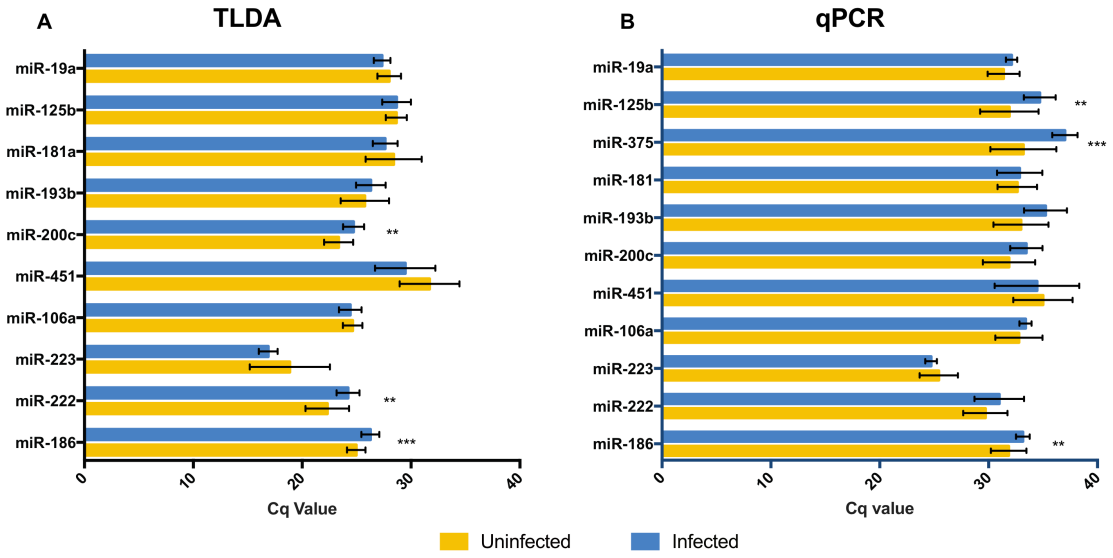

Figure 5. miR-186-5p downregulation: SIV. A) By TLDA, miRs-186, -222, and -200c were significantly less abundant in the CVL p100 fraction of infected subjects, ** $p < 0.01$, *** $p<0.001$. **B)** By qPCR, miRs-186, -375, and -125b were significantly less abundant, ** $p < 0.01$, *** $p<0.001$.

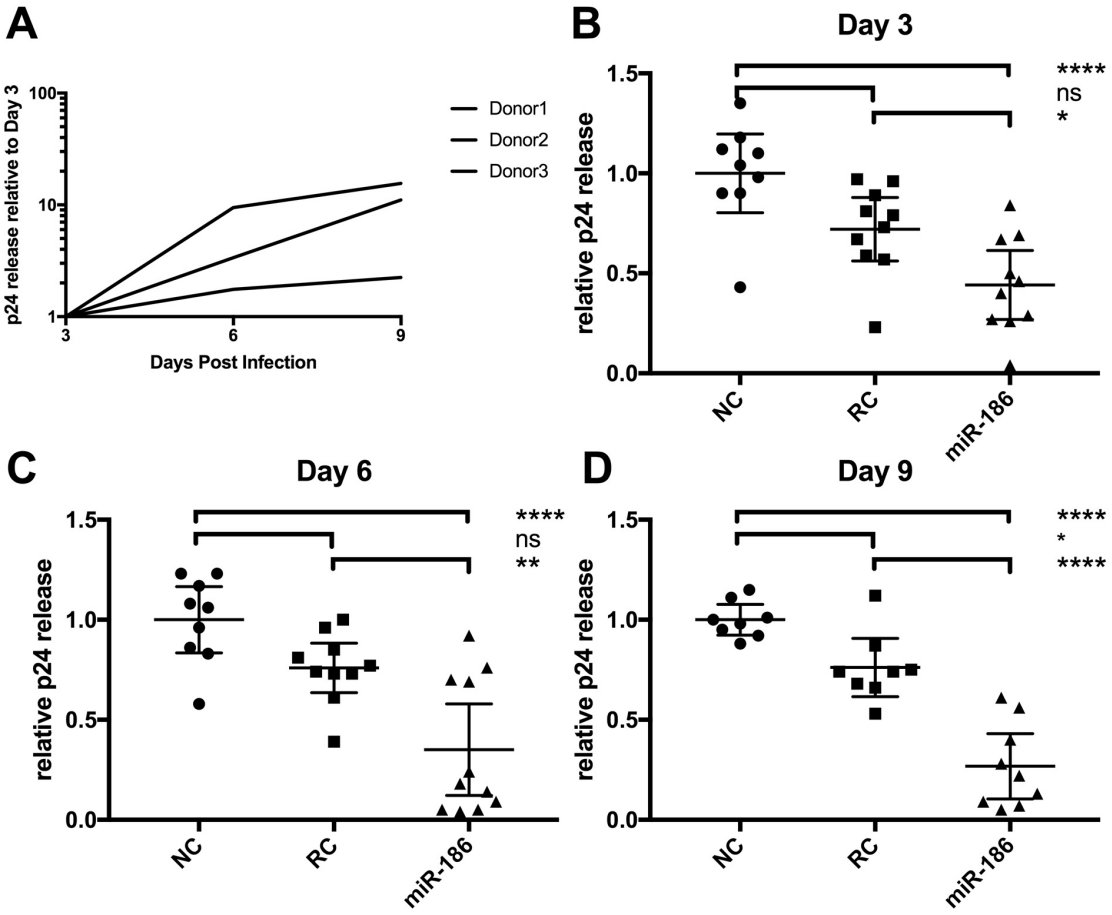

Figure 6. miRNA-186-5p inhibits p24 release. Monocyte-derived macrophages from human donors were infected with HIV-1 BaL. A) p24 production increased >2 fold for all donors from 3 to 9 days post-infection (dpi), infected but otherwise untreated cells. B-D) Transfection of miR-186 mimic was associated with a decrease of p24 release compared with untransfected controls (NC) and control RNA mimic-transfected controls (RC); ns=not significant, * $p<0.05$, ** $p<0.01$, **** $p<0.0001$ (ANOVA followed by Bonferroni correction for multiple tests). Results were obtained from 8 to 11 replicate experiments with cells from 3 human donors.

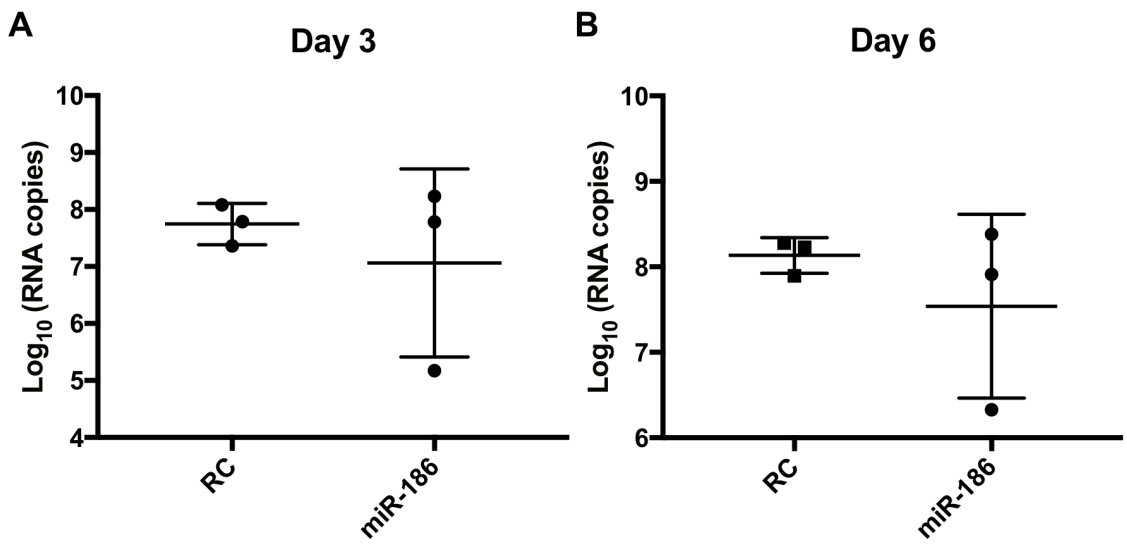

Figure 7. miRNA-186-5p mimic transfection inconsistently suppresses HIV-1 gag mRNA production. Apparent downregulation of gag mRNA (qPCR assay with standard curve) was observed in miR-186-transfected monocyte-derived macrophages from only 1 of 3 donors compared with control RNA-transfected cells (RC). Overall, results were insignificant by t-test, $p>0.1$, with multiple replicates of cells from 3 human donors.

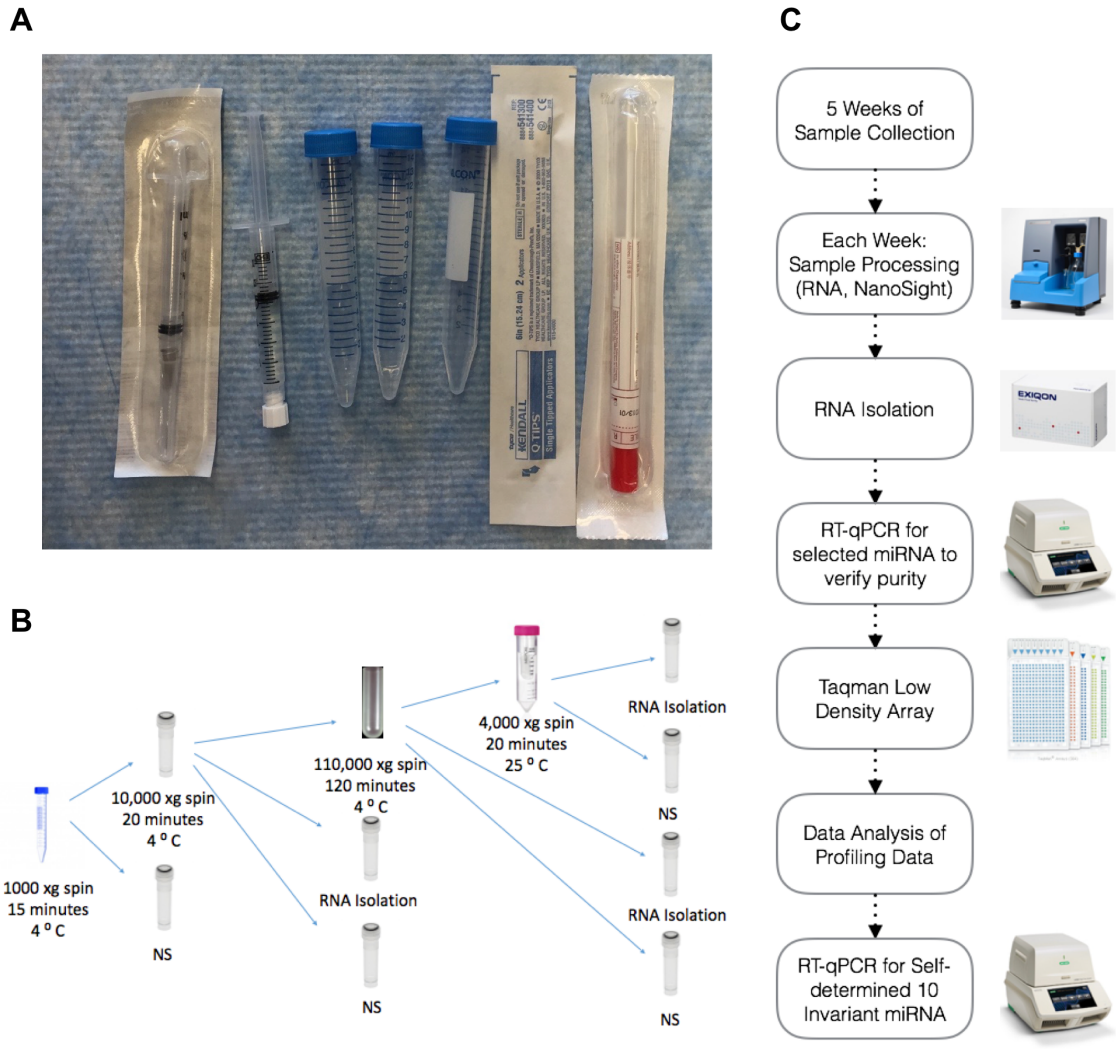

Figure 8. Specimen Collection and Sample Processing Workflow. A) Materials used to collect blood, cervicovaginal lavage (CVL) and vaginal swab (VS—not discussed here) samples. CVL was collected with a syringe containing 3 mL of PBS. PBS was injected into the vaginal cavity and then withdrawn into the same syringe. VS samples were obtained serially using two cotton applicators to swab the vaginal canal. Each swab was placed in 2mL of 1× PBS and the swab material was removed from the cotton by swirling in PBS and then pressing to the side of the conical. B) Stepped ultracentrifugation to enrich for extracellular vesicles (EVs). C) Workflow including miRNA profiling by TaqMan low-density array. 10 miRNAs were verified by qPCR.

Subject	Week 1	Week 2	Week 3	Week 4	Week 5
Control 1	1 mL	2 mL	1 mL	1 mL	1 mL
Control 2	3 mL	0.7 mL	2 mL	0.5 mL	1.25 mL
Infected 1	1 mL	0.2 mL	0.5 mL	0.3 mL	1.5 mL
Infected 2	1.5 mL	1.5 mL	2 mL	0.8 mL	1.75 mL
Infected 3	0.5 mL	0.6 mL	2.8 mL	0.8 mL	2 mL
Infected 4	0.8 mL	0.3 mL	0.6 mL	0.3 mL	1.5 mL

Table 1. Recovered Volumes: CVL

	Time point	Subject					
		Control 1	Control 2	Infected 1	Infected 2	Infected 3	Infected 4
CVL (UC Supernatant)	Week 1	1:25	1:50	1:25	1:25	1:25	1:25
	Week 2	1:100	1:5	1:25	1:10	1:5	1:5
	Week 3	1:10	1:5	1:5	1:5	1:10	1:10
	Week 4	1:10	1:5	1:10	1:5	1:10	1:10
	Week 5	1:5	1:10	1:10	1:10	1:5	1:5
CVL (UC Pellet)	Week 1	Neat	1:5	1:5	1:5	1:5	1:5
	Week 2	1:10	1:10	1:5	1:5	1:5	1:5
	Week 3	1:5	1:5	1:5	1:5	1:5	1:5
	Week 4	1:5	1:5	1:5	1:5	1:5	1:5
	Week 5	1:5	1:5	1:5	1:5	1:5	1:5

Abbreviations: CVL = cervicovaginal lavage; UC = ultracentrifugation

Table 2. NTA Dilution factors, CVL

III

Serum extracellular vesicle depletion processes affect release and infectivity of HIV-1 in culture

The work presented in this chapter was published in Scientific Reports in May 2017, volume 7:2558

Introduction

Extracellular vesicles (EVs) are a diverse group of bilayer-membraned particles that include so-called "exosomes" (canonically defined as budding into multivesicular bodies (MVBs) and being released upon MVB fusion with the plasma membrane) and "microvesicles" (often described as blebbing directly from the plasma membrane) [113,155]. The mode diameter of EVs in circulation approximates that of retroviral particles [155], and EVs and retroviruses share many common features [29]. Indeed, HIV has been called a "Trojan exosome," eluding the host immune responses in part by masquerading as an EV [29].

The relationship between EVs and HIV-1 infection is an area of active study, with some contrasting findings. While several other viruses can replicate via viral genomes packaged into host EVs [156,157], HIV-1 does not appear to be capable of transmitting infection through this route [38]. However, EVs produced by HIV-1-infected cells contain fragments of viral RNA [158] and viral proteins such as Nef [159] and Gag [35] (although another study did not find Nef to be associated with EVs [160]). HIV infection may alter the number and size of EVs as well as the host microRNA and proteins contained in EVs, which in turn may have implications for immune activation and HIV-1 pathogenesis [41,161–163]. In the setting of HIV-1 infection, EVs containing viral or host components may contribute to or exacerbate other conditions, such as HIV-1- or opiate-mediated neuron damage [164,165]. Whether specific EVs enhance or oppose HIV infection remains unclear and likely is context-dependent. EVs from HIV-infected cells can facilitate infection by several different mechanisms: by forming aggregates that include and deliver HIV-1 virions [166]; by activating CD4+ T lymphocytes, rendering

them permissive for HIV-1 infection [39,40,167]; and by activating latent HIV-1 infection [168]. On the other hand, EVs from CD4+ T-cells can act as decoys to prevent infection of cells [41], while EVs derived from human semen appear to inhibit HIV-1 replication and transmission [169,170].

We previously showed that many cell types grow more slowly in media prepared with serum that had been ultracentrifuged to remove EVs [171]. Serum EV depletion has been observed to alter cell migration [172], and macrophages become more proinflammatory when grown without serum EVs [173]. In general, we observed a slight but significant decline in replication and viability in EV-depleted conditions [171]. The magnitude of these effects was variable, and, notably, an astrocyte cell line (U87) did not appear to be affected. Adding isolated EVs back to the EV-depleted medium rescued cell growth, suggesting that the reduction in cell growth was in fact due to the depletion of EVs (although a role for EV-associated or otherwise co-purifying factors cannot be ruled out). We also found that the majority of the EVs that were internalized by cells, in a protein-dependent fashion, were targeted to lysosomes [171]. The identity of any specific growth-promoting factors contained in the EVs, such as RNA, proteins, or lipids, remains unknown, as does the extent to which these putative factors are involved in nutrition, signaling, and/or information exchange.

Prompted by these findings, we sought to determine whether serum EVs might affect HIV-1 replication in vitro. We used serum depleted of EVs by two methods and examined the effects of media prepared with these sera on the growth and behavior of cells that are susceptible to or infected with HIV-1. We also assessed the influence of EV depletion on virus production and infectivity. Finally, possible cellular explanations for

these results were probed via RNA, miRNA and Gene Ontology analysis. We conclude that two separate serum EV depletion protocols have a profound effect on HIV-1 replication and infection, and that EVs and/or closely associated or co-depleted factors tend to exert a virus-suppressive effect.

Methods

EV Depletion

For "TF-UC-EVD" FBS or "UC-EVD" FBS, either Thermo Fisher whole FBS or other commercially available FBS was diluted 1:4 [126] with Dulbecco's PBS or base culture medium and was centrifuged in a Beckman ultracentrifugation tube at 110,000 x g for 18 hours at 4˚C (*AH-629 rotor, k factor=242).* Supernatant was gently removed from the top down by pipette, avoiding disturbing the bottom of the tube, and used for preparation of EV-depleted media, which was then filtered through a 0.22 μm filter (Millex no. SLG5033SS). "TF-EVD" medium was prepared similarly, but with Thermo Fisher Gibco™ Exosome-Depleted FBS (ThermoFisher, USA, Catalog # A2720801), depleted by the manufacturer using a proprietary method. "EVR" refers to EV replete medium.

Single particle tracking analysis

Extracellular particle concentration was measured using a NanoSight NS300 (Malvern, Worcestershire, UK) equipped with a 532 nm laser or a NanoSight NS500 with a 405 nm laser. At least five 20 second videos were recorded of each sample at a camera setting of 10, and files were analyzed at a detection threshold of five using NanoSight NTA software version 3.1.

Western Blot

Samples were lysed with RIPA buffer (ThermoFisher, #89900). Protein concentration was determined by bicinchonic acid assay. 100 ug of protein from each sample was loaded onto a Criterion 10% Tris-HCL gel (BioRad, Hercules, CA, cat #3451018) and electrophoresed. The proteins were then transferred to a PVDF membrane (BioRad, cat# 1620174) and blocked with 5% powdered milk (BioRad, cat #1706404) in Dulbecco's PBS (ThermoFisher, cat# 14190250) +0.1%Tween®20 (Sigma-Aldrich, St. Louis, MO, cat # P9416) for 1 h. The membrane was subsequently incubated with mouse-anti-human CD63 primary antibody (BD, cat #556019), at a 1:1000 dilution for 1 hour, and mouse-anti-human CD81 (Santa Cruz Biotechnology, cat# sc-166029), at a 1:1000 dilution for 1 hour. After washing the membrane, it was incubated with a goat-anti-mouse IgG-HRP secondary antibody (Santa Cruz Technology, cat #sc-2005) at a 1:10,000 dilution for 1 h. The membrane was then incubated with a 1:1 mixture of SuperSignal West Pico Stable Peroxide solution (ThermoFisher, cat# 34080) and Luminol Enhancer solution (ThermoFisher, cat# 34080) for 5 min. The membrane was visualized on Amersham Hyperfilm^{TM} ECL chemiluminescence film (GE Life Sciences, PA, cat # 28906839).

Cell culture

Cell lines

H9 and PM1 (both T-lymphocytic); chronically HIV-1-infected T-lymphocytic (ACH-2) and promonocytic (U1) cells; and TZM-bl and HEK-293T cells were obtained

from AIDS Reagent and ATCC. Cells were grown in complete RPMI medium (R10) prepared with EVR, UC-EVD, or TF-EVD FBS as well as 1 mM L-glutamine (ThermoFisher, MA, USA; Cat # 25030081), and 1 mg/mL Pen-Strep (ThermoFisher, MA, USA; Cat # 15140148) and 10 mM HEPES (ThermoFisher, MA, USA; Cat # 15630080).

Primary cells

Blood was obtained from healthy human donors under a university-approved protocol (JHU IRB # CR00011400). Within 15 minutes of draw, blood was diluted approximately 2:5 in PBS/5 mM ethylenediaminetetraacetic acid (EDTA)/2% EV-depleted FBS, loaded over room temperature Ficoll (GE Healthcare Biosciences, MA, USA; Cat # 17-1440-03) in SepMate^{TM} 50 mL tubes (StemCell, Vancouver, Canada; Cat # 85450), and centrifuged at 1200 x g for 10 minutes. The plasma/PBMC fraction was centrifuged at 300 x g for 8 minutes, and incubated in red blood cell lysis buffer (4.15 g NH_4CL, 0.5 g $KHCO_3$, 0.15 g EDTA in 450 mL H_2O, adjusted pH 7.2-7.3, brought to 500 mL and filter-sterlized) at 37˚C for 10 minutes. For monocyte-derived macrophages (MDM), PBMC were pelleted at 400 x g for 6 minutes, resuspended in cell culture media, and plated at 10^7 cells per well in 6-well plates. Differentiation proceeded for seven days in the presence of macrophage colony stimulating factor (M-CSF) (R&D Systems, MN, USA; cat # 216-MC) as described previously [174].

CD4+ T-cells were isolated from PBMCs via EasySep^{TM} Human Naïve CD4+ T cell Isolation Kit (Vancouver, CA; Cat # 19155) (2). Purity was determined by flow

cytometry on a BD Fortessa using a CD4+ antibody (Becton Dickinson, NJ, USA; Cat #562658). Interleukin-2 was added as a baseline stimulant at a concentration of 10 U/mL (Thermo Fisher, MA, USA #PHC0026). Cells were activated 24 hours after isolation with phytohemagglutinin (PHA) at a concentration of 5 ug/mL, diluted in culture medium (Sigma-Aldrich, MO, USA; Cat # 693839-1G).

HIV-1 infection

HIV-1 Rf and BAL stocks were generated from chronically infected H9 and PM1 strains, respectively, and stored at -80˚C. For H9 and PM1 cultures, HIV.Rf and HIV.BAL were added at a concentration of 500 ng/mL (p24) and incubated at 37˚C for 4-6 hours. Cells were then rinsed with PBS and spun twice at 400 x g for 5 minutes each. For primary macrophage cultures, HIV.BAL was added at a concentration of 200-250 ng/mL (p24) and incubated overnight at 37˚C before rinsing twice with PBS.

Cell Viability

Cell viability was assessed using the Muse™ Cell Analyzer and the Muse™ Count and Viability Kit according to manufacturer's instructions (EMD Millipore, Billerica, MA, USA; Cat # MCH100102) or the WST-1 cell viability assay (Roche, IN, USA; Cat # 5015944001). The plates were mixed on an Orbital Shaker on setting 2 (Bellco, NJ, USA; Cat # 7744-20220) at room temperature for 30 min and absorbance was measured at 630 nm using an iMark™ Microplate Absorbance Reader (Bio-rad, CA, US). MTT cell viability assay (Thermo Fisher MA, USA; cat # V-13154) was performed by incubating culture plates with MTT reagent for four hours at 37˚C, adding SDS lysis

buffer, and incubating for four hours to overnight at 37˚C. Absorbance was measured at 570 nm with a plate reader as above.

HIV-1 P24 Assay

200 µl of cleared cell culture supernatant from all evaluated samples was set aside for p24 assays (Perkin Elmer, Holland, via ThermoFisher Cat # 50-905-0509) at appropriate dilutions and following the manufacturer's protocol. p24 levels were determined based on the manufacturer's p24 standard. All results represent at least three separate experiments.

Luciferase Assay

Luciferase expression in TZM-bl, which contain a luciferase gene under the control of a retroviral LTR, was monitored following overnight exposure of cells to H9/HIV.Rf- or PM1/HIV.BAL-containing-media from infected cells. The luciferase assay was done according to the manufacturer's protocol using the Luciferase Assay System (Cat # E1500; Promega, WI, USA) and was read on a Fluoroskan Ascent FL luminometer (ThermoFisher, MA, USA).

Flow Cytometry

Cells were removed from plates with gentle pipetting, washed with 1 x PBS, and stained for 20 minutes at room temperature in the dark. All antibodies were from BD (CD4, ApC-Cy7 : Cat # 341095; CD18, FITC: Cat # 555923; CD106, PE: Cat # 555647; CD54, PE-Cy7: Cat # 559771; CD195, APC: 556903). Samples were washed with 2 ml

of 1x PBS once, spun at 400 x g for 5 minutes, and resuspended in 300 µl of PBS to remove excess antibodies. Using a BD LSRFortessa, PBMCs were gated on lymphocytes by forward and side scatter profiles. Data were analyzed using FlowJo software v10.1 (FlowJo, OR, USA).

EV add-back

Pellets from ultracentrifuged FBS were re-suspended and added at $1/200^{th}$ and $1/50^{th}$ of the re-suspension volume to separate wells containing EVR, UC-EVD or TF-EVD-serum-containing media. These pellets were co-added with virus stock at the time of infection.

RNA Isolation and Gene Expression Analysis

HEK293T cells (5×10^5) were grown on a 10 cm dish for 24 hours. Medium was replaced with fresh media containing EVR or UC-EVD serum. Following 48 hours of growth, RNA was extracted using Trizol (Trizol Reagent, Invitrogen) according to manufacturer's instructions. RNA integrity was assessed by Agilent Bioanalyzer RNA 6000 Chip (Agilent, Santa Clara, CA), and 500 ng total RNA labeled according to the manufacturer's instructions (Illumina TotalPrep RNA kit). Biotinylated aRNA (750 ng) was hybridized to Illumina Human HT12v4 bead arrays overnight, rinsed and incubated with streptavidin-conjugated Cy3. Arrays were scanned at a resolution of 0.54 microns (Illumina iScan), and intensities were extracted from the scanned images using Illumina GenomeStudio software V2011.1. Data were normalized by Z-Score transformation and analyzed with DIANE 6.0, a spreadsheet-based microarray analysis program. Z-

normalized data were analyzed with principal component analysis (PCA). Z-Scores for paired treatment groups were compared using the Z-Ratio statistic to determine gene expression changes within each comparison. Expression changes for individual genes were considered significant if they met four criteria: Z-Ratio above 1.5 or below -1.5; false detection rate (FDR) < 0.30; a P-value statistic for Z-Score replicability below 0.05; and mean background-corrected signal intensity greater than zero. Gene set analysis was performed using the open-source DAVID Functional Annotation.

miRNA qPCR array

Total RNA was harvested from ACH-2, U1, and MDM grown under the different conditions using the miRvana total RNA isolation protocol as previously described [61]. A custom TaqMan low density array was ordered from Thermo Fisher, containing qPCR assays for 47 common miRNAs and the snRNA U6. Reverse transcription (100 ng starting material for each condition), pre-amplification, TLDA card processing were done using Thermo Fisher/Life Technologies reagents per manufacturer's protocol and as previously described [129]. Data were extracted and processed as previously described [129], except that normalization was performed to the geometric mean of ten miRNAs detected in all samples (miRs-24, 17, 30b, 106a, 142-3p, 92a, 146a, 342-3p, 21, and 16). Hierarchical clustering (Pearson, average linkage) and visualization was done with MultiExperiment Viewer (MeV) [175].

Seahorse Respiration assays

Macrophages were plated in a Seahorse 96-well plate and were differentiated for seven days (see above) in EVR and EVD media. Cells were washed three times with media that did not contain sodium bicarbonate. Following one hour of incubation in a 37 degree incubator, mitochondrial activity was assessed using the Seahorse XF96 Analyzer (Seahorse Bioscience) [176] according to the manufacturer's instructions. Briefly, oxygen consumption rate (OCR) was measured following sequential addition of 2 μM oligomycin, 1 μM FCCP, and 5 μM rotenone/antimycin A.

Data availability

Gene expression data and miRNA microarray data have been deposited with the Gene Expression Omnibus (GEO) under accessions GSE89067and GSE88838, respectively, part of the SuperSeries GSE89068 and BioProject PRJNA350212. Any additional data are available upon request.

Results

EV depletion and effects on cell line viability and proliferation

FBS was processed by dilution and overnight ultracentrifugation ("UC-EVD") as previously described [126] or by a proprietary commercial process (ThermoFisher or "TF-EVD"). These sera and unmanipulated FBS ("replete," EVR) were used to make cell culture media as described in Methods. Relative abundance of particles in replete or depleted conditions was assessed by NanoSight nanoparticle tracking analysis (Figure 1A), revealing decreased particle concentration of approximately 60-70%, with the greatest particle decline in the TF-EVD condition. However, we would like to make two important points. First, the apparent efficacy of ultracentrifugation-based particle depletion varies in our hands by lot of serum, ultracentrifuge run, and nanoparticle tracking instrument/protocol, ranging from approximately 50-80%, while the TF-EVD process efficacy ranged from about 65-95% (Figure 2). Second, as the terminology indicates, single particle tracking does not distinguish EVs from other particles. In contrast, Western blot for EV markers CD63 and CD81 reveals that, while these markers are barely detected in unprocessed FBS, they are highly enriched in ultracentrifuge pellets, demonstrating EV depletion (Figure 1B). Similar results were obtained for TSG101 and CD9, but the ER marker calnexin, golgi marker GM130 and nucleus marker nucleoporin were not detected in the pelleted fraction (Figure 3). We conclude that both ultracentrifugation and the TF-EVD process significantly but variably deplete particles including EVs from FBS, and that the TF-EVD process appears to be more effective than ultracentrifugation.

Two T lymphocytic cell lines, H9 and PM1, were cultured in EVR, UC-EVD and TF-EVD media to assess the effect of EV-depleted serum on cell viability and growth. For all three conditions, WST-1 assay demonstrated small but significant ($p<0.0001$, 2-way ANOVA with multiple comparisons) differences in cell proliferation at Days 2, 3, 4 post initial culture conditions (Figure 1C, D) consistent with previous reports (23). Similar results were obtained by measurement of cytotoxicity by means of an LDH assay (Figure 4). However, primary CD4+ T-cells and macrophages displayed minimal differences in metabolic activity when grown in TF-EVD media compared to replete conditions, as measured by MTT assay (Figure 1 E, F).

Cells maintained in EV-depleted cell culture media exhibit increased HIV-1 production

T-lymphocytic H9 and PM1 cell lines cultured for seven days under the three conditions were infected with HIV-1.Rf and HIV-1.BAL respectively. Morphologic and behavior differences were observed in the TF-EVD condition when compared with the EV replete condition. Specifically, cells in TF-EVD medium tended to cluster and form syncytia (Figure 5D, H) more frequently than cells in EVR medium (5C, G). Minimal morphologic differences between the two media types were seen in control, uninfected H9 and PM1 cells (Figure 5A,B and E, F). Cells in UC-EVD medium were of intermediate phenotype that varied considerably by production lot of UC-EVD FBS, consistent with the variable and less efficient particle depletion by UC that we observed. Unexpectedly, HIV-1 release, as measured by p24 ELISA, was significantly increased in the TF-EVD condition in both H9 and PM1 cells (Figure 3A, B). Increased HIV-1

production was also observed from CD4+ T-cells and MDM infected with HIV-1.Rf and HIV-1.BAL strains, respectively (Figure 6C, 3D, 7).

EV add-back restores HIV-1 production to baseline levels in cells cultured in TF-EVD media

To confirm that depleted material enriched in EVs contributes to the observed effects, resuspended EV-enriched UC pellets were added back to TF-EVD culture conditions. Irrespective of dose down to a 20% add-back, virus production was restored to levels significantly below the TF-EVD conditions (for example, HIV-1.Rf-infected H9 cells, Figure 6E). That virus production was not restored completely to baseline may be consistent with reports that UC-pelleted EVs may tend to aggregate and lose functionality [177–179].

EV-depleted cell culture conditions reverse HIV-1 latency

ACH2 and U1 cells—models of HIV-1 latency in T-cells and monocytes, respectively—were cultured in replete medium and TF-EVD medium conditions. Significant differences in p24 production were observed in the TF-EVD condition as compared with the replete medium condition for both U1 and ACH2 cells in three experiments (Figure 8A, B)). Cell density was correspondingly reduced after day one in both cell types (TF-EVD medium, Figure 8C, D). Of potential interest, the U1 cells were the most sensitive to depleted conditions of any cell type we studied. Nevertheless, the minority of live cells appeared to continue releasing relatively large quantities of p24. We do not think this p24 detection is simply the result of release from dead cells, as analysis

of the cell lysate in PM1, U1 and ACH2 cell lines was lower or on par with the p24 expression in the supernatant (Figures 9, 10E,F).

Heightened infectivity of viruses produced under depleted cell culture conditions

HIV-1 produced under depleted conditions was collected from H9 and PM1 cells and placed in p24-normalized amounts onto TZM-bl reporter cells, which encode a luciferase gene under the control of the HIV-1 LTR. Virus from TF-EVD conditions produced significant increases in luciferase expression that were at least two-fold higher when compared with virus produced under EVR source serum conditions for many tested concentrations of virus (Figure 11A-D, 12). Similarly, when virus grown in replete conditions was added to TZM-bl cells raised in either TF-EVD Source-based media or TF-EVD media, significant differences in luciferase expression were appreciated at higher concentrations of viral input for both HIV-1.BAL and HIV-1.RF (Figure 11E, F).

Assessing functional differences of cell lines raised in EVD conditions

To gather evidence for cellular changes that might possibly explain the observed responses to EV depletion, we performed several tests, including flow cytometry, respiration assays, miRNA qPCR array, and gene array.

Flow cytometry: cell surface proteins

The cell clumping observed in H9 cell cultures under EVD conditions prompted us to examine expression of several adhesion molecules and HIV-1 receptors by flow cytometry. Indeed, among other differences, VCAM-1 (CD106) and CCR5 expression

were found to be increased on H9 and PM1 cells cultured in EV-depleted conditions (Figure 13A, B).

Respiration assay

We next used the Seahorse Respiration assay to test respiration under EV-depleted conditions (Figure 13C). There was a significant, multiple-fold decrease in basal and maximal respiration, as well as compromised ATP production in mitochondria of MDM grown with EV-depleted media (Figure 13D). This reduction in mitochondrial respiration is in agreement with our previous and current observations of reduced cell growth.

miRNA qPCR array

Certain cellular microRNAs (miRNAs) have been reported to control retroviral replication [60,145], while exogenous RNAs in cell culture medium are said to be taken up by cells [180]. We hypothesized that miRNA levels in cultured cells might be augmented by serum EV miRNAs, and that EV depletion might also indirectly affect miRNA expression. Either circumstance could result in reduced abundance of anti-HIV miRNAs, explaining an increase in HIV-1 production. However, results from miRNA profiling by a custom TaqMan low density array (TLDA) revealed no consistent changes in miRNAs across three cell types maintained in the different types of media. Unbiased hierarchical clustering showed cell type-specific miRNA expression patterns, but no indication of consistent differences associated with EVD conditions (Figure 14A). A total of five miRNAs appeared to be less abundant by 2-fold or more in one cell type under

EV-depleted conditions (one in MDM, three in U1, one in ACH2), but no miRNA was 2-fold downregulated in more than one cell type, as one would expect if serum were an important and consistent source of miRNAs (Figure 14B). Importantly, previously reported anti-HIV miRNAs, including miRs-28-3p, -29a, -125b, -150, and -223, were not consistently diminished under EVD conditions. Similarly, there were no consistently upregulated miRNAs during EV depletion.

Gene expression and lipidomics

Gene array analysis was performed with cells grown in EVR and EVD conditions. Gene ontology analysis of genes that were at least 2.5-fold more abundant in cells grown with EVD media revealed a significant increase in transcripts associated with lipid synthesis pathways, and especially sterol biosynthesis pathways (Table 1). It was previously reported that EVs contain a high proportion of cholesterol, sphingomyelin and ceramide; therefore, the increase in their biosynthesis may be a compensation response to loss of exogenous sources.

Discussion

We show here the significant impact of serum EV depletion protocols on virus production by HIV-1 susceptible cells. Additionally, HIV-1 latency models undergo a degree of viral activation under EVD conditions. Effects of EV depletion were less pronounced in primary cells, but we did observe an impact on HIV-1 production by primary macrophages. Altogether, our findings suggest that EVs can inhibit HIV-1 infectivity and release from leukocytes, and point to alterations in cellular lipids as a possible underlying mechanism.

Greater HIV production could be achieved through higher rates of infection (i.e., involving viral life cycle steps from cell binding through integration). The finding that certain cell adhesion molecules, including HIV-1 receptors and co-receptors, are upregulated on cells in EVD conditions might be consistent with more efficient infection. It could also explain the greater aggregation and syncytium formation we found in H9 cell culture. However, the observation that latency models are also affected by EVD conditions suggests that infection is not the sole explanation for our findings. Additionally, our EV add-back experiments—in which EV-enriched ultracentrifuge pellets were re-introduced into the proprietarily-depleted medium simultaneously with virus exposure—suggest that any cellular responses to the absence of EVs would have been reversed rapidly, perhaps too rapidly to invoke receptor involvement. Alternatively, virion interactions with EVs or lipids that were added back could have inhibited infection (although this seems inconsistent with previous findings [181]. It is also apparent that circulating or EV-bound miRNA are not changing due to the depletion process and thus are not a likely explanation for the observed cellular responses.

Gene ontology data, however, suggest another mechanism whereby virus production could be increased: in the relative absence of EVs, lipids involved in EV (and thus virion) biogenesis are upregulated. This may occur as the cell strives to achieve a homeostasis of membrane components, which must be sensed in some fashion. According to this hypothesis, normal interactions with diverse, non-self EVs or other lipid particles such as those found in serum preps could be viewed as a "security blanket" or a constant source of nutrition. In EV depletion, the cell might release its own EVs but be unable to make up for the presence of foreign entities. This is highly feasible, as culture media tend to contain much lower amounts of EVs than unprocessed serum. The observed surface upregulation of adhesion receptors is also consistent with this idea, bringing cells into closer contact with other membranes (cellular or EV). Notably, the sterol upregulation scenario would imply that the upregulation of HIV release is non-specific, or specific only to the extent that virions bud from sterol-rich membrane microdomains. To delve further into these possibilities, more information is needed on how cells sense the presence of EVs: through molecules of or on the EV surface, the cell surface, or both. One might also anticipate experiments to investigate the contribution of EVs from different cellular sources, which could explain the reviewed the differing findings in the literature reviewed previously.

Our latency model results are perhaps most exciting, suggesting that EV depletion could inform new strategies in HIV-1 eradication therapy. Depleting bulk EVs from plasma in vivo to increase HIV-1 production from latent cells in an eradication effort—in an approach analogous to leukapheresis—would be a difficult task. Even if such depletion were feasible, the same would likely be impossible in tissue. However, it might

be possible through pharmacologic means to block cells from sensing the presence of EVs. Clearly, more knowledge about the system is needed to assess and develop this possibility.

As a final note, we would like to draw attention to an important caveat of this study. Although we concentrate here, in our language and experiments, on the effects of EVs, we hope that we have adequately conveyed that other interpretations are possible. The most accurate description of our results might be that putative EV depletion processes are associate with the observed effects. By extension, one might assume that EVs are involved, and this seems a reasonable assumption, given that we observed EV depletion by ultracentrifugation and by the commercial process, and the reversal of our findings during EV add-back. However, we cannot rule out that ultracentrifugation and other EV depletion protocols also deplete other components of serum. A recent publication from the Buzás lab found extensive low density lipoprotein contamination of EV preparations, and that LDL particles decorate EVs after co-incubation [182]. It is possible that LDL, other lipoprotein particles, and protein aggregates contribute to the phenomena we report here. We hope that others will join us in pursuing the many potentially informative studies that these findings might prompt.

III Figures:

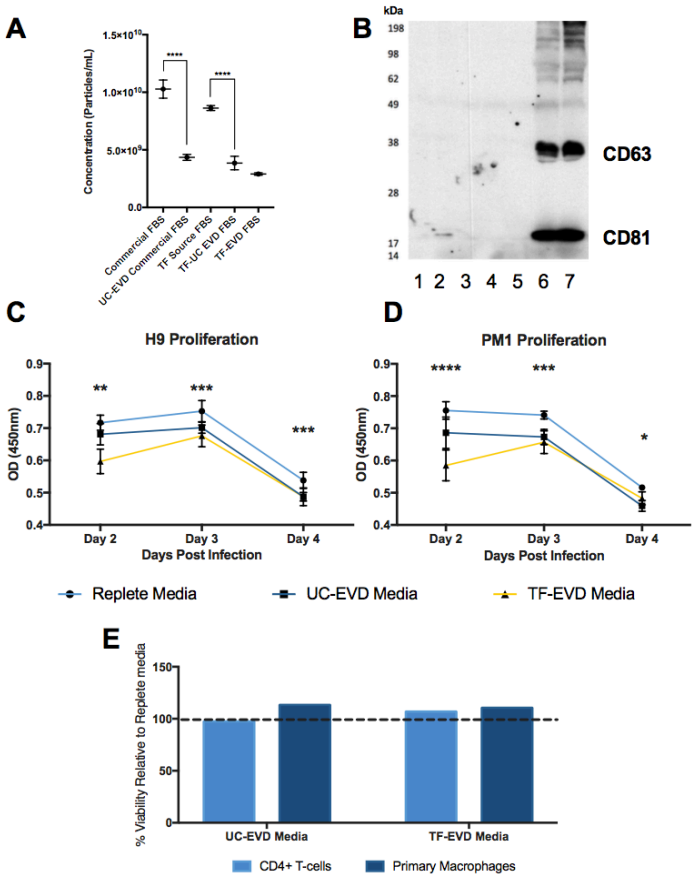

Figure 1. EVD conditions affect cell culture proliferation. A) NTA of 25% FBS, 25% TF "source" FBS, UC-EVD of 25% commercial FBS, UC-EVD of 25% TF-Source FBS, and TF-EVD FBS and shows depletion of approximately 60% of particles by UC for both FBS types and the greatest depletion in TF-EVD FBS when compared with TF source FBS. Error bars represent standard deviation of 4 independent readings. **** $p<0.005$, one-way ANOVA with Tukey's multiple comparison test. B) Western Blot analysis of 25% TF source FBS (1), 25% Commerical FBS (2), TF-EVD FBS (3), UC-EVD of 25% TF-Source FBS (4), UC-EVD 25% commercial FBS (5), and the UC pellet of TF Source FBS (6) and commercial FBS (7) , and shows significant extraction of particles containing CD63 (MW ~ 30-65 kDa) and CD81 (MW ~22-25 kDa). All lanes were loaded with 100ug of protein. C) For H9 cells, WST-1 assay optical density was greatest at all time points for the replete media conditions. D) PM1 cells: results similar to H9 cells. *=p<.005, difference between Replete and UC-EVD only; ** = $p<0.005$, differences between EVR and UC-EVD, UC-EVD and TF-EVD only; *** = p<.005, differences between EVR and UC-EVD and EVR and TF-EVD media; **** = p<.005, all types of media different from each other; Two-way ANOVA with multiple comparisons, six biological replicates measured E) No significant differences in cell viability observed in CD4+ T-cells or monocyte-derived macrophages cultured in UC-EVD and TF-EVD media compared to replete medium (n=3 biological replicates for each condition).

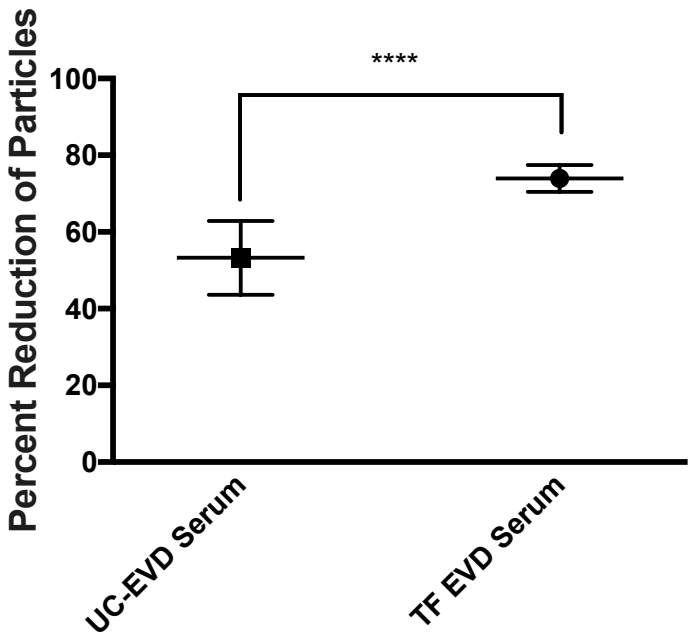

Figure 2. UC-EVD serum (n=23) has an overall lesser and wider range of particle reduction than the observed in TF-EVD serum (n=5) by NTA assessment. A range of 70-77% reduction is observed for TF-EVD method compared to a range of 41-62% in UC-EVD prepared serum. ****=p<.0001, unpaired t-test

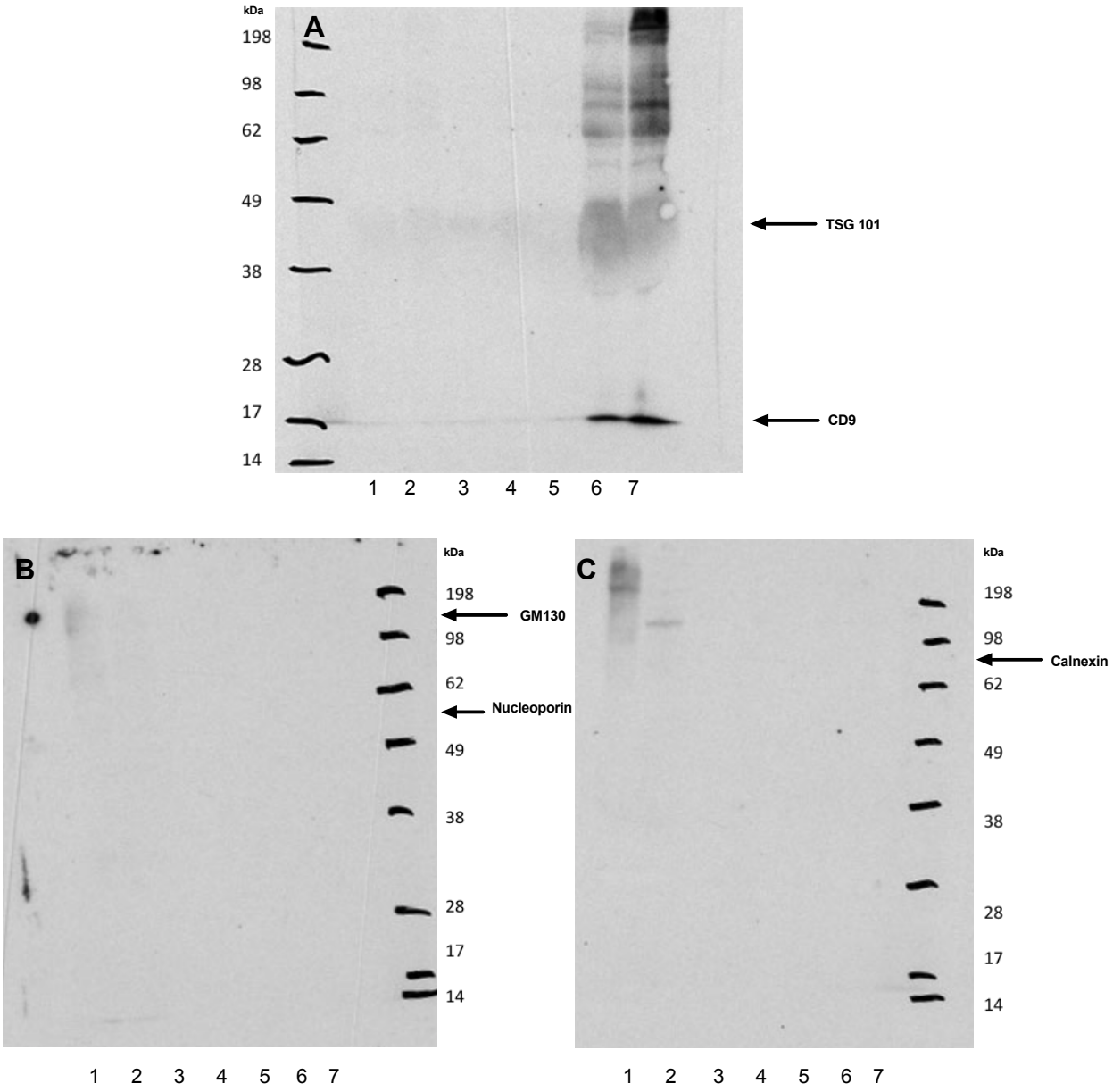

Figure 3. Western Blot Verification. A) Western Blot for TSG101 (~49kDa) and CD9(~24kDa) shows high presence of markers in UC pellets of both TF-Source FBS and in-house FBS (lanes 6, 7) compared to the source and depleted FBS (Lanes 1-5), indicating significant removal of EVs. UC pellets (lanes 1, 2) examined for GM130 (~130kDa), Nucleoporin (~53kDa) and calnexin (~80kDa) (B, C) demonstrated no presence of protein, indicating no significant cellular contamination from FBS source material. These proteins were also not observed in the FBS itself (lanes 5-7) or the UC-EVD media (lanes 3,4). All lanes were loaded with 100ug of protein.

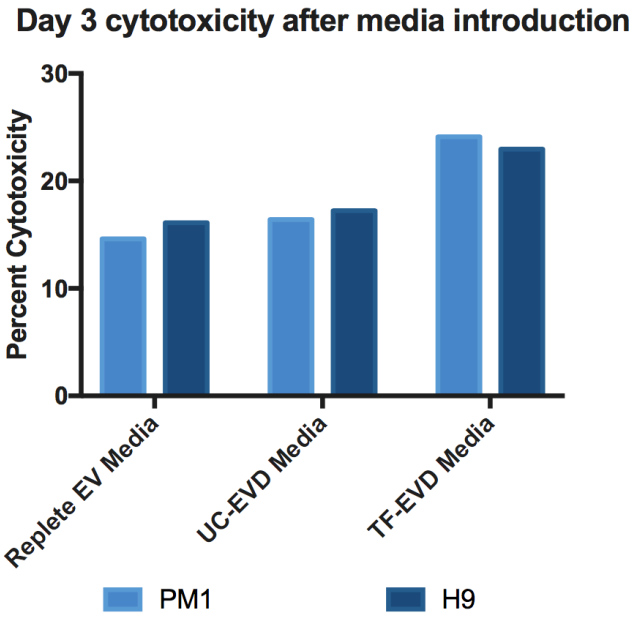

Figure 4. Cell Viability Data. LDH assay of uninfected H9 and PM1 cells grown in replete, UC-EVD and TF-EVD conditions after 3 days of incubation shows small increases in cell cytotoxicity for cells grown in TF-EVD conditions.

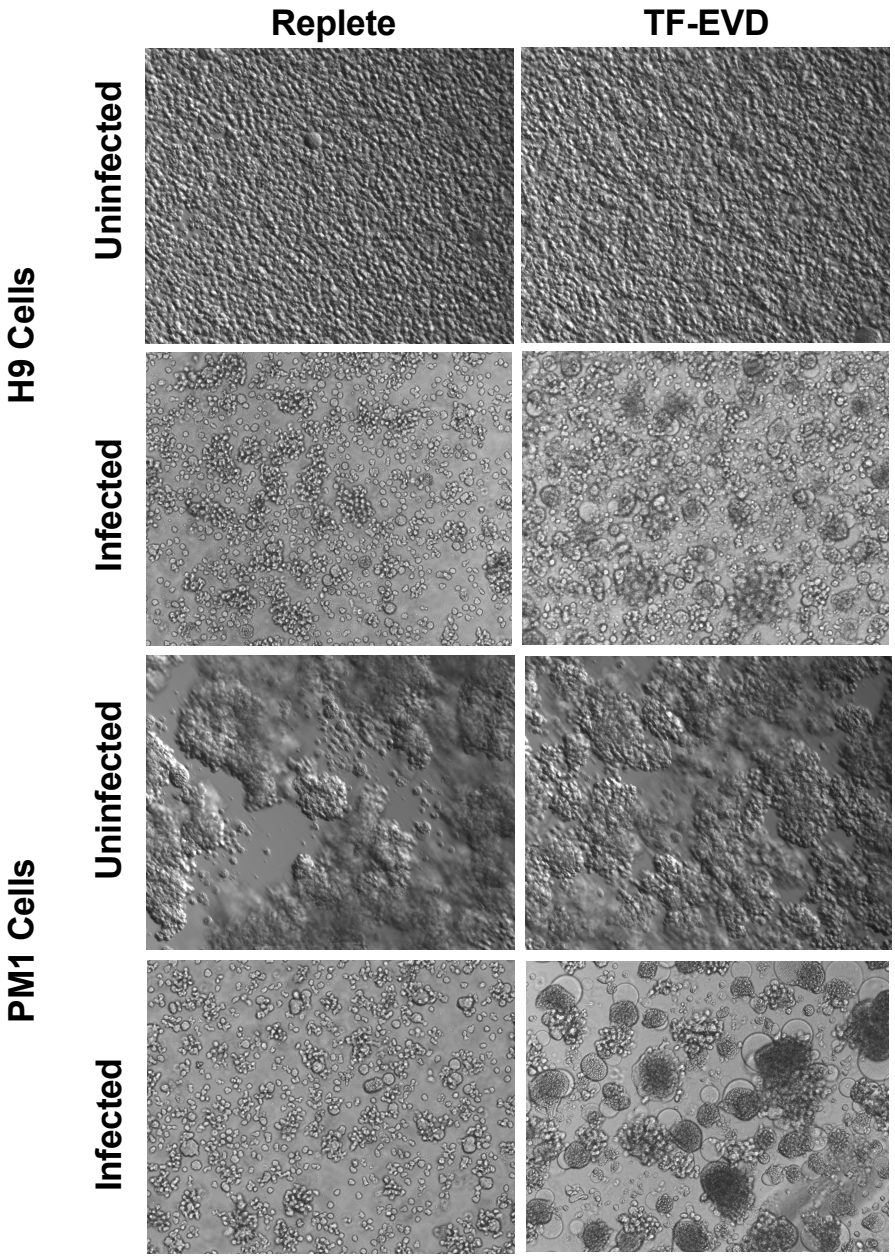

Figure 5. EVD serum affects cell morphology of cells infected with HIV-1. Marked aggregation and syncytium formation was observed in extended culture of HIV-1 infected H9 T-cell line under EVD conditions compared with EVR conditions and with uninfected controls grown in both replete and depleted conditions Extended culture of uninfected PM1 cells in replete and depleted media shows no differences in cell morphology, while similar phenotype changes as observed in H9 cells are noted between repleteand depleted media conditions in HIV-1 infected PM1 cells.

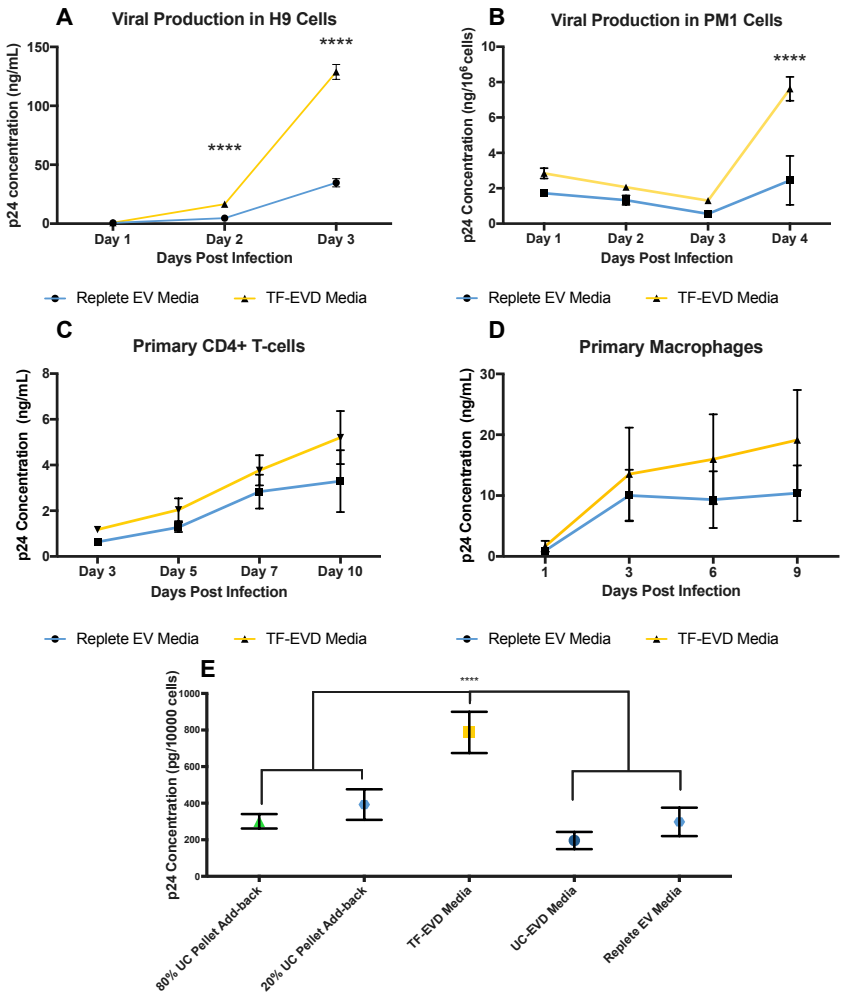

Figure 6. EVD serum increases p24 production in multiple cell types, while add-back of UC-derived pellet rescuses cells A) HIV-1.Rf production in H9 cells is increased significantly in TF-EVD conditions by day 4. ****=p<.0001, 2 sample t-test with Holm-Sidak correction of three biological repeats B) By Day 4 post infection, HIV.BAL production in PM1 cells grown in TF-EVD conditions is significantly higher when compared with EVR medium. ****: p<.0001; 2 sample t-test, Holm-Sidak multiple comparison correction. Representative experiment of at least 3 biological replicates of CD4+ T-cells infected with HIV-1.Rf (C) and three independent experiments of at least 3 biological replicates of monocyte-derived macrophages (MDM) infected with HIV-1.BAL (D) show a modest increase in virus production when grown in TF-EVD medium. E) Addition of previously removed EVs to TF-EVD medium reduces p24 production back to near the EVR medium baseline in H9 cells. EVs isolated from stock FBS were added back to TF-EVD medium at 80% and 20% of their original concentrations. Supernatant was collected 1, 2, and 3 days post HIV-1.Rf infection. Measurements of virus release by p24 concentration at day 3 showed a pronounced difference between TF-EVD conditions and all others, ****=p<0.001, one-way ANOVA, Tukey's multiple comparison test of 3 biological repeats in one independent experiment.

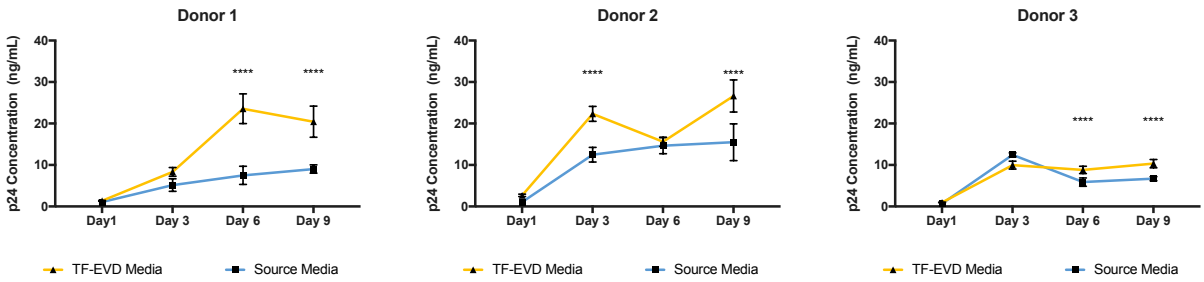

Figure 7. Individual experiments from Figure 3D, showing donor-donor variability of p24 production. All experiments contain at least 5 biological replicates. For all graphs, ****=p>.0001, two-way ANOVA with Sidak's multiple comparison test.

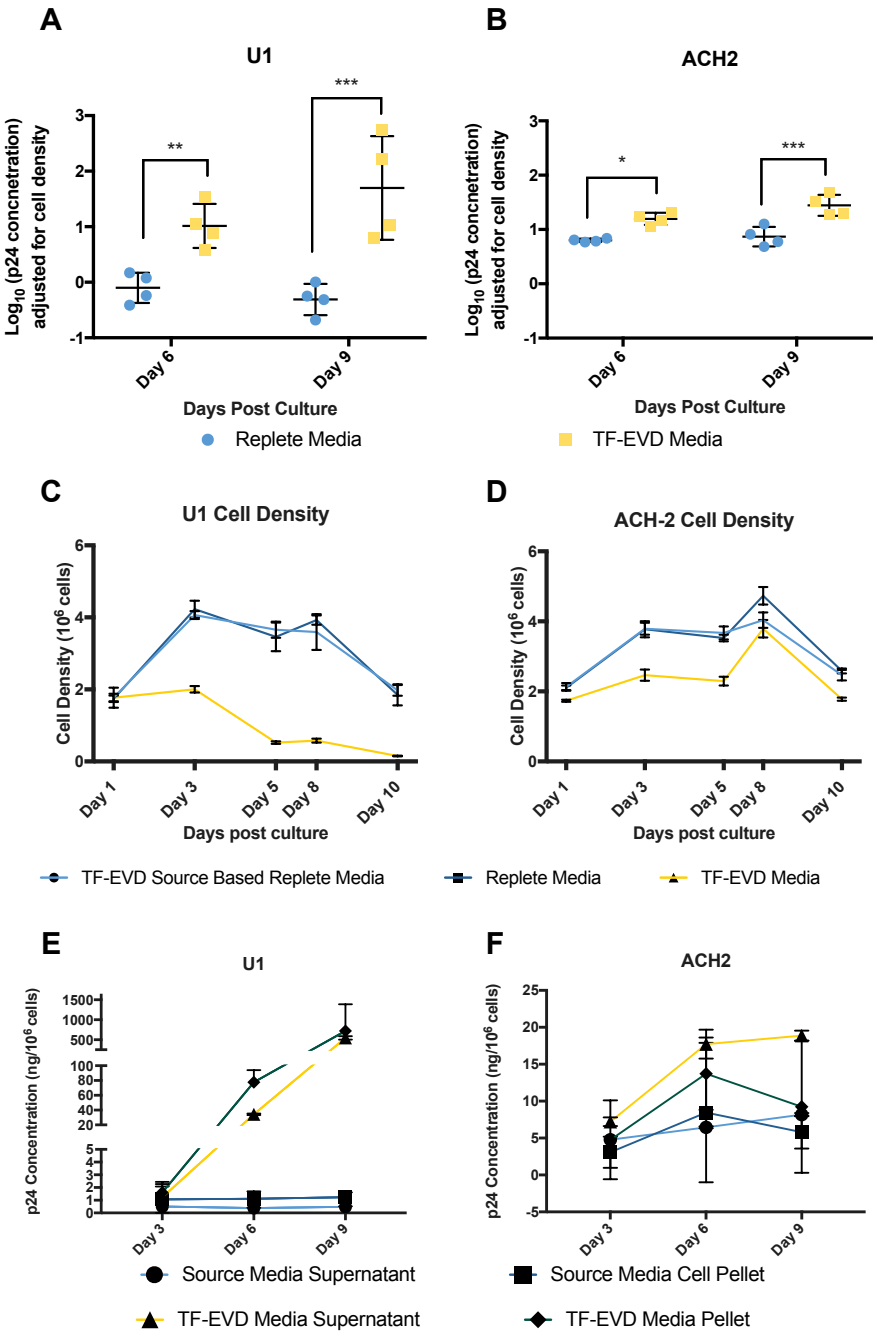

Figure 8. EVD serum reverses latency in two latency model cell lines. A,B) Four independent experiments confirm higher p24 production in both ACH2 and U1 cells grown in TF-EVD conditions compared to replete conditions. *=p<.05, **=p<.005, ***=p<.0005, two-way ANOVA with Sidak's multiple comparisons test. C, D) Representative cell density data for U1 and ACH-2 cells from a single experiment. E) Representative data from a single experiment shows supernatant and pellet from U1 cells pellet has a much higher p24 production in TF-EVD conditions when compared to replete conditions, with a lesser contrast observed in ACH2 cells (F).

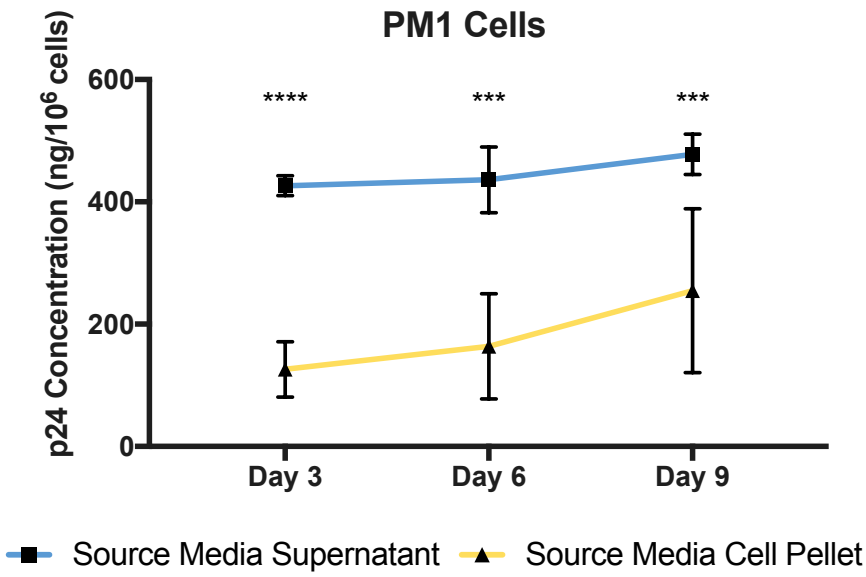

Figure 9. p24 concentration in supernatant is significantly higher than cell lysate in infected PM1 cells grown in replete conditions. ****=p<0.001, **=p<.01, 2-way ANOVA with Sidak's multiple comparison test of a single independent experiment with three biological repeats.

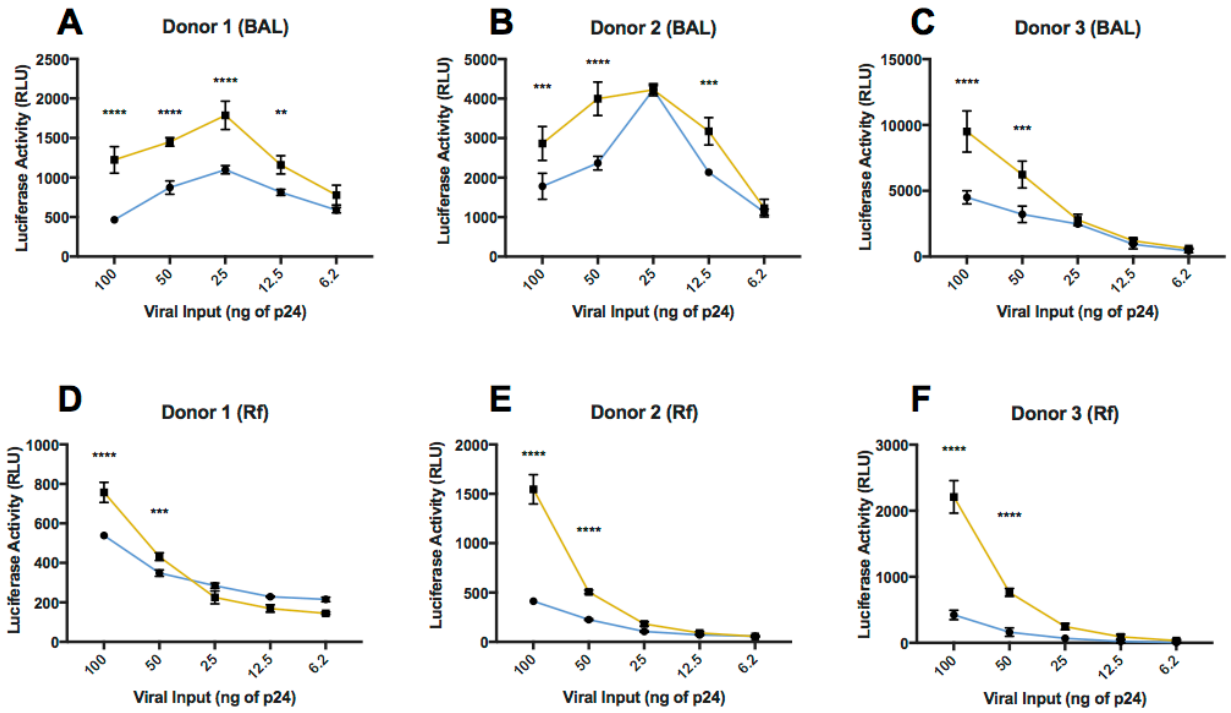

Figure 10. Three independent experiments demonstrating decrease in luciferase expression. Experiments contain at least 3 biological replicates and demonstrate that luciferase expression in TZM/BL cells infected either with HIV.BAL (A-C) or HIV.RF (D-F) harvested from cells cultured with TF-EVD serum show variance in RLU from experiment to experiment, but show constant increase in relative infectivity of virus used for all experiments with 100ng and 50 ng of p24 input. Other inputs show a similar trend but are not significant across all experiments. ****=p<0.001, ***=p<.005, **=p<.01, *=p<.05, 2-way ANOVA with Sidak's multiple comparison test.

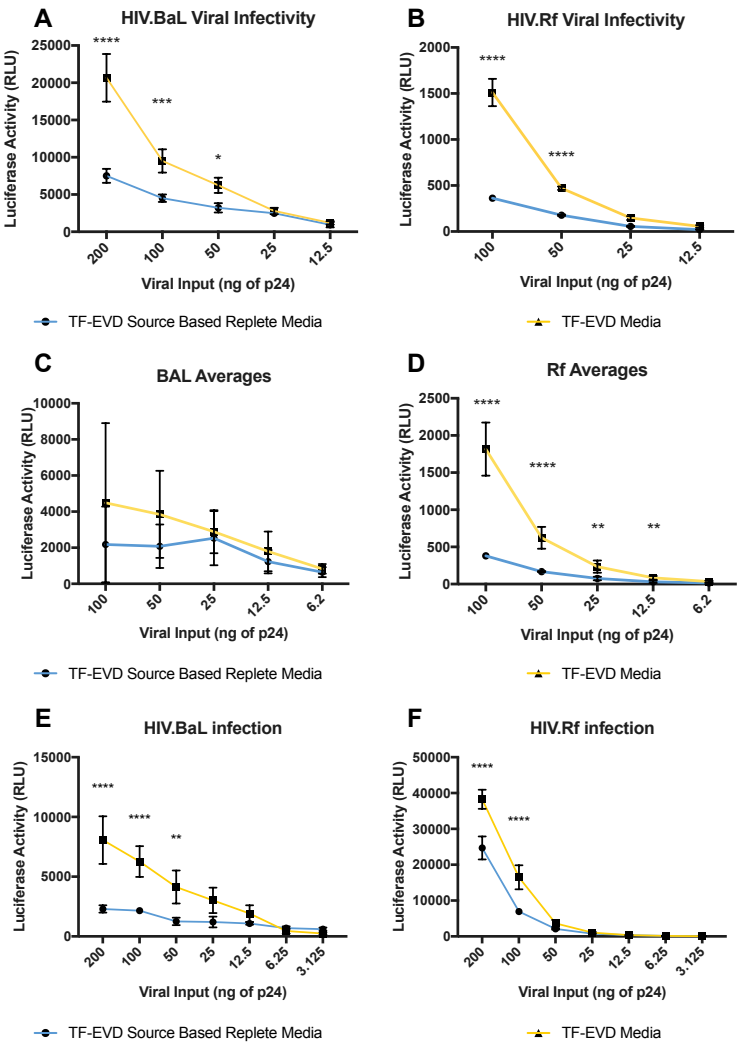

Figure 11. EVD serum affects virus infectivity. A, B) Representative experiments demonstrating that EV-depleted media produce virus with comparatively greater infectivity. HIV-1.BAL-infected PM1 Cells (A) or HIV-1.Rf-infected H9 cells (B) were cultured in EVR or TF-EVD medium conditions. Virus was collected at 7 days post infection and pelleted at 100,000xg for 2 hours. Pellet was diluted at 4 concentrations (shown on x-axis) in PBS and used to inoculate TZM/BL cells containing luciferase under the control of HIV LTR. After overnight incubation, an increase in luciferase activity was observed in the cells cultured with virus originating from TF-EVD medium compared with EVR medium at all concentrations. ****=p<0.0001, ***=p<.005, two-way ANOVA with Sidak's multiple comparison test of three biological repeats. C,D) show the average, including the individual experiments shown in A and B, for three independent experiments of at least 4 biological replicates for both HIV-BAL and HIV-RF. ****=p<0.0001, **=p<.01, two-way ANOVA with Sidak's multiple comparison test. E,F) HIV-1.BAL and RF harvested from cells grown in replete media and subsequently added to TZM/BL cells grown in either condition demonstrates the same phenomenon. ****=p<0.0001, **=p<.01, two-way ANOVA with Sidak's multiple comparison test of three biological repeats.

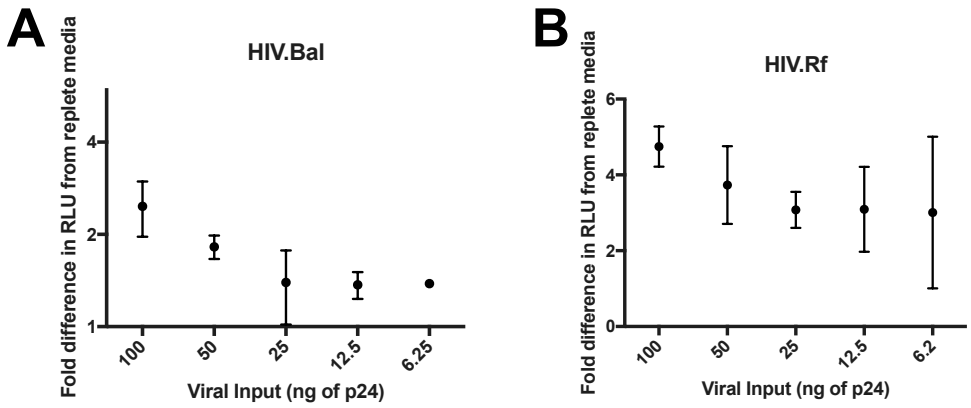

Figure 12. Increased infectivity of virus produced under EVD conditions from PM1 (A) and H9 cells (B), as assessed by TZM-BL luciferase reporter cells. Infectivity is at least 2 fold hiigher for HIV-1.Rf at all viral inputs except 6.25 ng/p24 when averaged across all experiments. Shown are averages of three independent experiments.

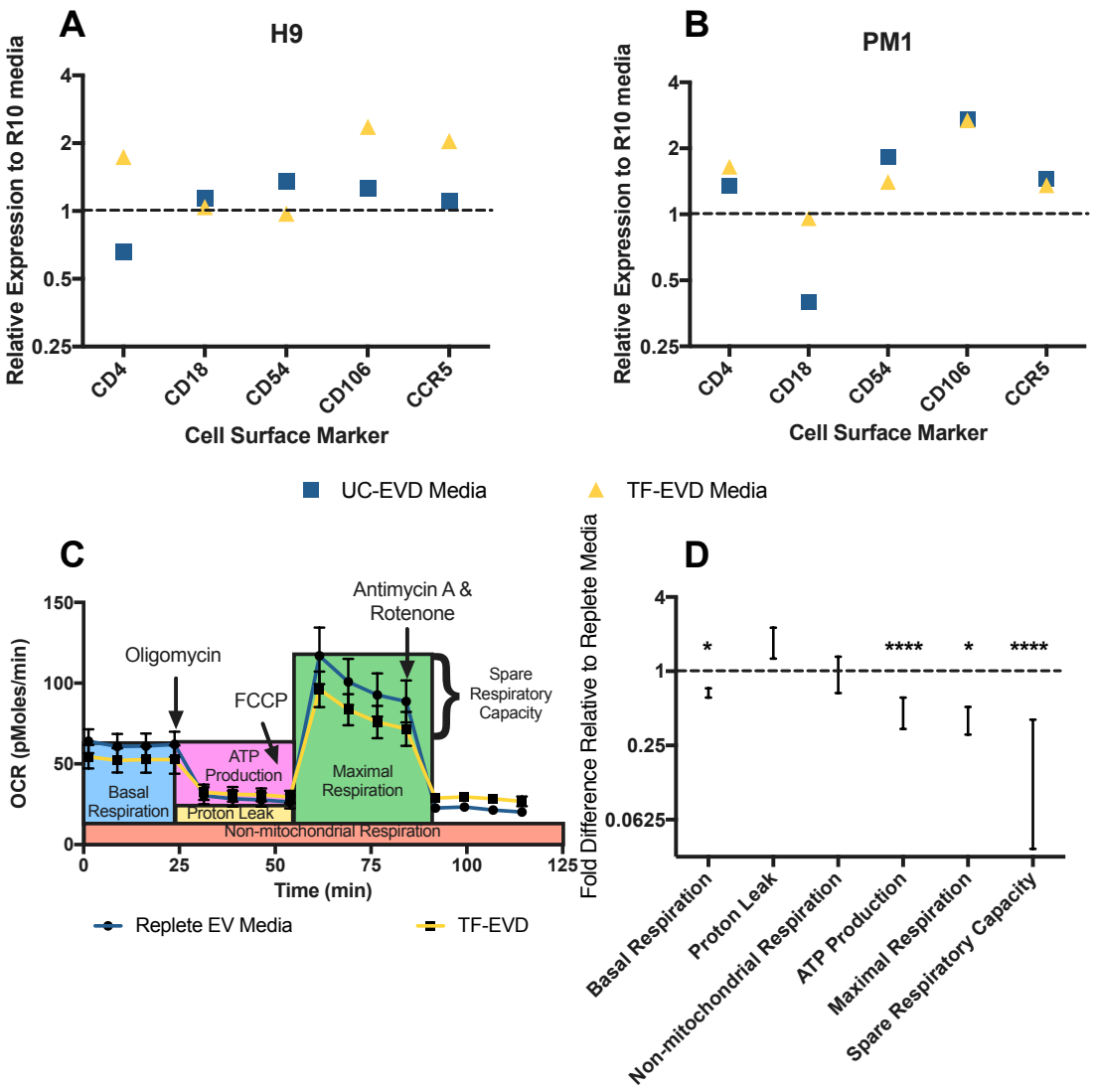

Figure 13. EVD conditions alter cell surface markers and respiration. A) H9 cells and B) PM1 cells displayed increased expression of selected surface/adhesion proteins by flow cytometry when cultured in UC-EVD or TF-EVD medium for 7 days; 1=expression on cells cultured in EVR. C,D) Seahorse Respiration Assay of mitochondria of monocyte-derived macrophages grown in TF-EVD had significantly reduced basal and maximal respiration, as well as compromised ATP production and spare respiratory capacity. ****=p<0.001, *=p<.05, 2-way ANOVA with multiple comparison, Sidak test. Annotations in C) are adapted from the product materials (Agilent Technologies). 1 (Dotted Line in D) denotes values for replete media for the same experiment

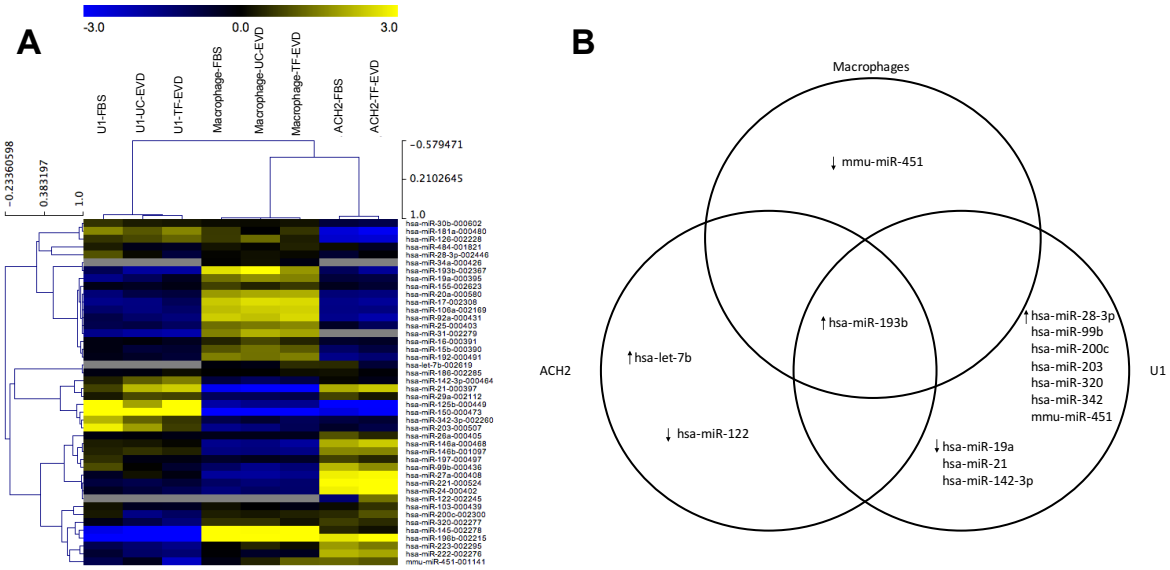

Figure 14. Little evidence for miRNA uptake from serum or serum-induced changes in miRNA expression. A) Unbiased hierarchical clustering demonstrates cell type-dependent miRNA expression, but no indication of differences associated with TF-EVD medium conditions. B) A total of five miRNAs appeared to be less abundant in TF-EVD conditions by two-fold or more in just one of the cell types, with no consistent findings between cell types. miR-193b was between 1.5- and two-fold upregulated in all three cell types.

Term	Count	%	Benjamini-Hochberg
Steroid biosynthesis	8	1.4	4.1E-09
Sterol biosynthesis	6	1	8.3E-07
Endoplasmic reticulum	15	2.5	8.2E-07
Lipid synthesis	8	1.4	6.6E-07
Cholesterol biosynthesis	5	0.8	8.9E-06
Lipid metabolism	6	1	2.4E-03
Nucleosome core	4	0.7	9.5E-03
Steroid metabolism	4	0.7	9.6E-03

Table 1. Gene Ontology Analysis reveals increased transcripts associated with lipid synthesis in EV-starved cells.

SREBF1
LDLR
CYP1A1
DHCR7
INSIG1
HMGCS1
HSD17B6
IDI1
FDFT1
HERPUD1
SGK1
SCD
LSS
LPIN1
ABCG1
RTN3
FOS
PTRF
SQLE
SDCBP
ACSL4
HIST2H2AA3
HIST1H2AC
HIST1H2BD
HIST1H2BJ
HIST1H3H

Table 2. List of genes with increased transcript levels from Table 1.

IV

MicroRNA in T-cell Subsets in HIV-1 Elite Suppression

Introduction

The initial stages of HIV-1 infection are characterized by unchecked viral replication, followed by a decrease in plasma viral levels due to the host immune response. Eventually, if left untreated, viral levels will rebound above this set point. Most people living with HIV are chronic progressors (CP), who will gradually lose immune function and succumb to secondary infections if untreated. In a minority of individuals, however, known as elite suppressors (ES), a viral set point is established below the limit of detection of standard clinical assays (<50 copies of HIV-1 RNA/mL of blood) and maintained for extended periods of time [183,184].

While there have been significant advances in understanding how this viral control is achieved, the precise mechanisms have not been fully elucidated. For example, protection has been correlated to different elements involving HLA corresponding to MHC class I. Some ES have a CCR5 delta-32 gene deletion or have the HLA-B57 allele; the modification of the former conveys resistance to attachment of HIV-1, while the increased expression of the latter enhances cytotoxic T-lymphocyte response [185–190] . Others have single-nucleotide polymorphisms in genes like MX-2, which encodes for a protein whose expression levels are increased by interferon-α and blocks HIV-1 nuclear import [191,192]. These genetic elements are not the sole drivers of elite suppression, however. One category of molecule that remains incompletely understood in HIV-1 latency and elite suppression is small RNA, including miRNA.

miRNAs modulate and reflect numerous cellular functions in immune response and host-pathogen interactions [193–195]. Most cells release miRNAs into the extracellular space, contained within protein complexes that protect the RNA species

from degradation [23] and in some cases also packaged into extracellular vesicles (EVs). Their stability has led to consideration of miRNAs as possible biomarkers and therapies alike [196–199]. anti-miR-122 therapies have now entered the clinic for Hepatitis C virus therapies. Could similar strides be made in HIV-1 disease?

Multiple studies indicate that miRNAs may modulate HIV-1 latency and contribute to protection in ES. Some studies focus on specific miRNAs in cell lines or primary cells infected with HIV-1 [59,200–205]. Huang, et al. reported that miR-28, -125b, -150, -223 and -382 targeted the 3' LTR of HIV-1 in CD4+ T-cells, suggesting a role in HIV-1 latency [60]. Houzet, et al. demonstrated that miR-92a, -133b, -138, -149, and -326 decreased HIV-infection by targeting HIV-1 RNA [206]. HIV-1-produced sRNA may contribute to infection [207,208]. Differential miRNA expression has also been reported in ES and in HIV-1 infection in PBMCs, CD4+ T-cells, CD8+ T-lymphocytes, plasma, monocytes [209–214]. Our lab reported significant differential miRNA expression between PBMC of ES and HIV-1 untreated viremic individuals, including the first identification of miR-31 as a possible restriction factor for HIV-1 [215].

Despite evidence that miRNAs affect HIV-1 infection, to date, there have been no studies of miRNAs in specific T-cell subsets, comparing ES to CP and healthy control (HC) individuals. In this study, we profiled CD4+ and CD8+ Naïve, Central Memory and Effector Memory for a few reasons. First, specific subtypes of immune cells may contain unique patterns of miRNAs and certain miRNAs may contribute to cellular identity and functional development [213,216]. Second, memory T-cells are preferentially infected by HIV-1. Memory cells from ES individuals are quantitatively and qualitatively different

from those found in CP and healthy donors [183]. Third, levels of CD8+ activation are higher in anti-retroviral-treated (ART) CPs than ES individuals, even when viral loads in both are similarly undetectable [217]. Finally, cells derived from ES patients are known to resist cell death through pathways involving factors FOXO3a, STAT5 and Wnt, which include well-characterized miRNA co-regulators including miR-29, miR-21, miR-155, and miR-28 [215,217–220]. Importantly, this work allows us to follow up and specifically identify subsets responsible for the changes seen in our work in PBMCs.

Here, we provide the first miRNA profile comparing T-lymphocyte subsets between healthy donors and ES patients, utilizing a novel, combinatorial isolation strategy to obtain the different subsets from whole blood. In addition, we show specific miRNAs that not only distinguish ES from CP and healthy controls, but also that many of these expression differences are unique to a class of T-lymphocyte. Several of these miRNA species that are differentially expressed in this study, confirming findings from previous studies, including our own.

Materials and Methods

Donors

Eighteen total and sixteen unique control (biological duplicates collected at different time points of two individuals were also obtained), eight elite suppressor (ES), ten chronic progressor (CP) and three viremic controller (VC) donors contributed blood to this study. Controls were healthy, HIV-1-negative donors. The ESs consistently maintain a viral load below the limit of detection (50 copies/mL) and had a median CD4+ T-cell count of 694 cells/μL (range 447-1453 cells/μL) at the time of donation All blood was obtained from patients and healthy donors (HDs) after they provided written and informed consent and was handled as recommended by the Institutional Review Board of the Johns Hopkins University (JHU IRB #CR00011400, NA_00093758). A full readout of donor characteristics, including sex, age, BMI and ART regimen (where applicable) can be found in Table 1.

PBMC isolation and plasma separation

Blood was collected into 60 mL syringes pre-loaded with 6 mL anticoagulant Acid Citrate Dextrose (ACD) (Sigma Aldrich, St. Louis, MO. Cat #: C382, multiple lots), or six 8.5 mL vacutainers pre-coated with ACD (BD, 366645). Whole blood was centrifuged within 30 minutes of draw at 1300 x g for 15 minutes at room temperature to pellet cells. Supernatant was subsequently centrifuged twice at 2500 x g for 15 minutes each at room temperature to produce platelet-poor plasma (PPP), which was aliquoted and frozen at -80˚C until later use.

Cell pellets were re-suspended and diluted 1:1 with 2% fetal bovine serum (FBS) (Atlanta Biologicals) in Dulbecco's phosphate buffered saline (DPBS) without Ca2+ or Mg2+ (Gibco) and added to a Ficoll-Hypaque (GE) gradient in SepMate™-50 tubes (STEMCELL Technologies, Vancouver, BC, Canada Cat #: 15450) and centrifuged for 10 minutes at 1200 × g at room temperature. Plasma and PBMC fractions were removed, washed in PBS+ 2% FBS, and pelleted at 300 × g for 8 minutes. Pellets from 5 tubes were combined by resuspension in 10 mL RBC lysis buffer (4.15 g NHCl, 0.5 g KHCO, 0.15 g EDTA in 450mL H_2O; pH adjusted to 7.2–7.3; volume adjusted to 500 mL and filter-sterilized); total volume was brought to 40 mL with RBC lysis buffer. After incubation at 37 °C for 5 mins, the suspension was centrifuged at 400 × g for 6 mins at room temperature. An aliquot of PBMC was used for flow cytometric characterization for downstream separation of cells. The remaining PBMC were set aside for T-cell subset isolation.

T-cell subset isolation

Whichever cell subset was observed to have lowest population percentage at the time of collection, as measured by flow cytometric evaluation of whole PBMC, was treated as the "experiment-limiting population." In all cases, this was the CD8+CD45RA-CCR7+ cell population (CD8+ Central Memory). Population percentage (of total lymphocytes) of each cell type was entered into a spreadsheet and a calculation to obtain the largest number of the rate limiting cell type was performed, based on total PBMC yield, and percentage of lymphocytes that were the experiment-limiting cell type. This calculation informed the proper ratio to use when aliquoting all PBMC at the appropriate

concentrations for initial immunomagnetic separation. An example spreadsheet is shown in Figure 1. Initially, PBMC were isolated into CD4+ and CD8+ categories by using EasySep™ Human CD4+ or CD8+ T Cell Isolation Kits (StemCell, Catalog #17952 and #17953). Success of isolation and determination for inclusion in the study was assessed by positive staining for CD4+ or CD8+ (depending on isolation) with a positive rate of greater than 90% on all gated singlet lymphocytes measured on a LSRFortessa (BD).

CD4+ and CD8+ cells were subsequently aliquoted into different tubes and stained with either CD45RA and CCR7 antibodies or with CD45RO antibodies per manufacturer's recommendations. Cells were incubated for 15 minutes with antibodies and then washed and re-pelleted, and finally re-suspended in a volume of 250 µL. Each sample was then sorted on an Aria II (BD), with the negatively staining fractions being collected (i.e., CD45RO- for collection of the Naïve population, and CD45RA-, CCR7+ and CCR7- fractions for collection of central memory and effector memory populations, respectively. The schematic for this strategy is outlined in Figure 1B. Total counts of cells sorted were recorded. Cell fractions were pelleted, lysed with 600 µL mirVana RNA lysis buffer (Ambion, Austin, Texas, USA), and frozen at -80°C until RNA purification.

The following antibodies were used for all staining of PBMC surface markers: PE mouse anti-human CD197 (Clone: 150503, Cat # 560765), FITC mouse anti-human CD45RA (Clone: HI100, Cat # 561882), PerCP-Cy5.5 mouse anti-human CD45RO (Clone: UCHL1, Cat # 560607), APC-H7 mouse anti-human CD8 (Clone: SK1, Cat # 560179), BV605 mouse anti-human CD4 (Clone: RPA-T4, Cat # 562658). All antibodies were source from Becton Dickinson, NJ, USA.

RNA isolation and quality control

RNA was isolated from all samples using a blinded, randomized distribution of all samples into batches of 18 to avoid batch effects and the potential influence of slight differences in RNA isolation. RNA was isolated in pre-determined batches (designed to eliminate batch effect) from each of the following T-cell subsets for all donors included in the study: CD4+ Naïve (CD4+N), CD4+ Central Memory (CD4+CM), CD4+ Effector Memory (CD4+EM), CD8+ Naïve (CD8+N), CD8+ Central Memory (CD8+CM) and CD8+ Effector Memory (CD8+EM). Each sample was then evaluated for quality control. Randomization was performed by an un-blinded collaborator who was not performing initial analyses (JB). All cell types from each donor were isolated concurrently (total of 6) and group size was 3, with each group containing either one healthy donor, one ES or VC and one CP or two HDs and one of either ES/VC or CP. Thawed samples were processed for total RNA isolation using the miRVana miRNA isolation kit (Ambion) and following the manufacturer's protocol, with final elution in 100 uL of RNAase free water. RNA concentration was measured by Qubit RNA HS according to manufacturer's specifications (Cat # Q32855) Concentration and RNA profile were also measured by Agilent BioAnalyzer 2100 using the Agilent Small RNA Kit (Catalog #5067- 1548). Subsequently, verification of RNA presence was performed by measuring the expression of several small RNAs, including miR-125b, cel-miR-39 and miR-16, with individual TaqMan miRNA assays, using a uniform input of 2 μL RNA (Applied Biosystems/Life Technologies, Carlsbad, California, USA).

TaqMan OpenArray

Custom Human TaqMan® OpenArray® Human MicroRNA chips were prepared for cell and plasma profiling. The panel was designed to detect 96 unique miRNA sequences that have been found in the cells of interest and, in several cases, have been reported in association with HIV infection and disease. All assays were previously validated with artificial miRNA templates by the manufacturer. 2 μL of RNA was used as the input for reverse transcription using MegaPlex stem-loop primer pools, following the Life Technologies OpenArray® protocol modification for low-concentration samples. Pre-amplification was done with MegaPlex pre-amp primer pools. Diluted pre-amp products were loaded onto the OpenArray chips by Accufill robot, following the standard protocols (Life Technologies part number 4461306 Rev. B). Real time quantitative PCR was performed with a QuantStudio 12K Flex Real-Time PCR System (Johns Hopkins DNA Analysis Facility), and data were collected with the manufacturer's SDS software. RQ Manager software (Applied Biosystems) was used to process the array data. The technical manual of the source code for the TaqMan OpenArray MicroRNA Panels are available at: https://tools.thermofisher.com/content/sfs/manuals/cms_092509.pdf

Individual RT-qPCR Assays

TaqMan miRNA assays (Applied Biosystems/Life Technologies) were performed according to the manufacturer's protocol and as previously described [215] with either reverse-transcribed or reverse-transcribed and pre-amplified samples. The small RNAs assayed were cel-mir-39, miRs -16, and -125b.

Data analysis and statistical methods

We removed 9 out of 288 samples run across all chips, those of which had fewer than 60 miRNAs detected in the OpenArray run. Then, we removed any samples that were not a part of this study but were run at the same time. This generated one cohesive data set that included data from all CD4+ Central Memory, CD4+ Effector Memory, CD4+ Naïve, CD8+ Central Memory, CD8+ Effector Memory, CD8+ Naïve cells and an RNA cell control sample, which was a pool of RNA derived from CD4+ Naïve cells from 7 different HDs. The RNA control sample aided in visualizing any potential batch effect. Next, the data was filtered to keep the 85 miRNAs that had an AmpScore ≥ 1.2 and at least 60% of amplifications present. Then, the cycle threshold (Ct) score was set to 40, if the Ct score for any miRNA in any sample was "Undetermined," the AmpScore was < 1.2, or if the Ct score was > 37. Subsequently, these missing data points (Ct = 40) were imputed (Bioconductor package "Non-detects") including the control sample, which had been run on each chip. Finally, delta-delta Ct ($\Delta\Delta$Ct) analysis was performed, with normalization to a set of 4 stable miRNAs: hsa-miR-103, hsa-miR-25, mmu-miR-93 and hsa-miR-142-5p. The stable miRNAs were selected using a consensus between the top 10 most stable miRNAs ranked by NormFinder and geNorm, as implemented in Bioconductor package NormqPCR. Differential expression analysis was performed by applying a Student's t-test to the normalized Ct values and the p-values were adjusted for multiple testing by controlling the false discovery rate (FDR) according to the method of Benjamini and Hochberg. A miRNA was considered to be differentially expressed if the adjusted p-value was ≤ 0.1 Results were not dependent on this normalization method, as established by investigations of alternative normalization methods, including geometric

mean, and quantile normalization. Figures and tables were prepared using Microsoft Excel and Word, GraphPad Prism, MultiExperiment Viewer, Adobe Photoshop and Illustrator, and FlowJo.

Ethics Statement

Approval for all studies was granted by the Johns Hopkins Institutional Review Board. All study participants provided informed consent in writing.

Results

A novel combinatorial method to isolate specific T-cell subsets from whole PBMC and study cohort demographics

While the primary goal of our study was to identify miRNA signatures of elite suppression in different T-cell subsets, an added benefit was the ability to identify miRNA signatures of specific T-cells in healthy individuals. To do this, whole blood was obtained from a total for 37 unique individuals, for 39 total samples: eighteen total samples from sixteen unique healthy individuals, eight samples from known elite suppressors (ES), ten from chronic progressors (CP), and three from viremic controllers (VC). Demographics of the study cohort are shown in Table 1. To evaluate miRNA expression in the relevant T-cell subsets, we first needed to ensure that we could conduct downstream RT-qPCR by determining the lowest number of starting cells detectable by quality control (QC) methods prior to RNA isolation. We determined the limit to be approximately 20,000 cells (Figure 2A, B). We then used a novel combinatorial method of T-cell subset isolation, involving negative immunomagnetic separation to isolate

CD4+ and CD8+ T-cells, followed by FACS using a negatively-based gating strategy, as outlined in Figure 3A and 3B and in the methods section. For all CD4+ subsets, cell count medians were significantly lower across all patients, while total CD8+ lymphocyte count was increased (Figure 4B, C). Final cell counts for each cell type, separated by healthy and infected were obtained following sorting (Figure 5). Isolating cells using this strategy allowed for very precise acquisition of the different subsets with generating as little stimulation as possible, ensuring the downstream data were as close to in vivo expression levels as feasible. Some RNA levels of some samples were below the level of detection by both Qubit and BioAnalyzer, however. We tested whether performing downstream assay by volume input rather than RNA input would influence expression data. Starting cell count correlated with RNA concentration determined by Qubit but not by BioAnalyzer (Figure 6A, B). In addition, no correlation between starting cell count and raw Ct value or pre-amplified RT product was appreciated when comparing Ct values via OpenArray for either miR-125b or miR-16 (Figure 6C). These results provided satisfactory data to confirm the viability of our novel combinatiorial approach to T-cell subset isolation and thus to proceed with OpenArray profiling assessment.

OpenArray miRNA profiling distinguishes Naïve and Individual Memory Cell subsets from each other in healthy individuals

Many recent studies, including from our own lab, have examined the sensitivity and specificity of different miRNA quantitation platforms. The OpenArray system has the sensitivity required to detect inadvertent sample swapping during processing [215,223]. The OpenArray platform employs reverse transcription, pre-amplification, and

quantitative real-time polymerase chain reaction (qPCR) using extremely low amounts of pre-amplified material to quantitate even low-abundance miRNAs with high sensitivity. For this study, we designed a custom chip that allowed us to profile almost 100 different features, which were carefully selected miRNA species based on previous ES profiling done in our lab and others, as well as based on previous studies indicating miRNA species importance in T-cell proliferation.

After normalizing the data against the consensus most stable miRNAs, hsa-miR-103, hsa-miR-25, mmu-miR-93 and hsa-miR-142-5p, we examined all healthy samples from all cell types separately from infected samples. This separation allowed us to examine the T-cell specific miRnome across all miRNAs. Rather than the expected hierarchical clustering by CD4+ or CD8+ phenotype, our data show that miRNA profiles are extremely similar between all Naïve cells as well as each of the Effector and Central Memory subsets (Figure 7). This trend was even more apparent when clustering only the significantly differentially expressed miRNA (Figure 8). In addition, we found that many miRNAs are differentially expressed in specific subsets relative to others.

For the purposes of this analysis, we only included miRNAs whose expression level was at least one full deltaCt different from others, because this difference represents one full qPCR cycle. Naïve cells, regardless of CD4+ or CD8+ phenotype, showed the most instances of differential expression relative to memory cells, with miR-328, miR-193b, miR-20a and miR-31, miR-342-3p, miR-125b and miR-181a being downregulated (Figure 9A), and miR-24, miR-146a, miR-21 and miR-27a being upregulated (Figure 9B). Both Central Memory and Effector Memory cells had much fewer instances that

separated them from the other memory cell type and Naïve cells. miR-196b and miR-126 appeared upregulated relative to both Effector Memory and Naïve cells (Figure 10A), while miR-150 was upregulated in Effector Memory cells relative to Central Memory and Naïve cells. These results not only represent the first T-cell subset-specific miRNA profiling but also demonstrate a surprising and novel miRNA phenotype that differentiates readily between Naïve and Memory cells in healthy individuals.

OpenArray miRNA profiling reveals cell-type specific differential expression of miRNAs distinguishing between Healthy and Infected individuals

Having evaluated the miRNA expression profiles of the T-cells in healthy individuals, we next evaluated expression difference within cell types between our healthy controls and all infected individuals. To accomplish this, we performed downstream analysis on the same normalized OpenArray data. Many miRNAs were differentially downregulated or upregulated within in each cell type. For Naïve cells, miR-9 was upregulated three-to-four-fold in CD4+ and CD8+ cells from the infected cohort relative to the healthy donors , while miR-155 was upregulated two-fold in CD8+ Naïve cells (Figure 11A, B).

Interestingly, in CD4+ Central Memory cells, no miRs were upregulated and only miR-196b was downregulated, at more than two-fold (Figure 12A). In contrast, in CD8+ Central Memory cells, miR-196b was upregulated almost two-fold in infected samples, while miR-28-3p was upregulated almost four-fold (Figure 7B). miR-23a and miR-21 were also significantly upregulated in the infected cohort, but at a rate of about 1.5-fold, equivalent to less than one qPCR cycle on average.

Finally, in Effector Memory cells, all miRNAs were downregulated in both CD4+ and CD8+ cells (Figure 13). miR-193b was significantly downregulated by almost four-fold in both types, while miR-363, -125b, -31 and 196b were downregulated in CD4+ cells (Figure 12A). miR-363 had the largest relative difference, at approximately 40-fold. miR-146b-3p was also downregulated at a rate of four-fold in CD8+ EM T-cells (Figure 13B).

OpenArray miRNA profiling reveals cell-type specific differential expression of miRNAs distinguishing between Healthy, ES, and CP individuals

To determine if the changes observed between the healthy and infected populations were more global or primarily driven by mechanisms found in ES or CP individuals, we examined the normalized data by comparing the relative expression of each population.

The greatest number of differentially expressed miRNAs, contrary to the pattern in the healthy versus infected comparison, was observed in the Naïve cells. Differentially expressed miRNAs in ES individuals relative to healthy controls were upregulated exclusively in CD4+ and CD8+ Naïve cells (Figure 14A, 15A), with miR-9 and miR-21 upregulated more than two-fold in both cell types, with miR-9 showing the greats upregulation of almost 10-fold in CD4+ cells. In CD8+ Naïve T-cells, other species were differentially upregulated in ES individuals compared to healthy controls as well, including miR-132 (3.4-fold), -15a (2-fold), -155 (2.1-fold), and -23a (1.9-fold) (Figure 15A). miR-155 and miR-23a were also similarly upregulated in CP individuals compared to healthy controls. miR-335 and 146b-5p were downregulated 2.2- and 1.8-fold,

respectively (15B). miR-197 was the lone downregulated miRNA in CD4+ Naïve T-cells, but notably in CP relative to the control.

As for the Central Memory cells, fewer differentially expressed species were found than in the Naïve cell comparison. Additionally, more differences in miRNA expression in CP versus control individuals and CP versus ES individuals were present. Importantly, miR-196b, was almost 3-fold downregulated in CP individuals compared to controls in CD4+ CM (Figure 16B). This result was especially striking when compared to the 2-fold upregulation between healthy and all infected samples. However, mir-196b was still upregulated by approximately 2-fold in CD8+ CM from ES individuals (Figure 16C). miR-186 was also downregulated in CD4+ CM T-cells in CP relative to control, but the change was only about 1.5-fold. (Figure 16B). miR-19a, -23a were almost 2-fold upregulated in CP relative to control in CD8+ CM T-cells, while let-7b was upregulated in CP relative to both control and ES (Figure 16D). Finally, miRNA species which were significantly upregulated in ES compared to healthy controls but less than 2-fold were miR-103, miR-125a-5p, while let-7g and miR-320 were upregulated relative to CP (Figure 16A).

Finally, in the Effector Memory cells, most changes were observed either in CP individuals relative to the healthy controls or between CP and ES individuals. All miRNA that were differentially expressed in CD4+ EM were downregulated, with significant downregulation calculated in miR-363, -31, -31*, -193b, and --196b and -146b-3p (Figure 17A). The largest relative differences were observed in miR-363, at almost 50-fold downregulation. For CD8+ EM, miR-19a, -16 and -195 were all approximately 2-fold higher in ES than CP individuals, although no significant differences were

appreciated between healthy controls and ES individuals (Figure 17B). miR-193b and -146b-3p were downregulated almost 4-fold, with -193b also downregulated in ES individuals relative to the healthy controls (Figure 17C).

Discussion

We present here a comprehensive examination of the miRNA profile in T-cell subsets in multiple contexts. We show, for the first time, a miRNA profile for CD4+ and CD8+ Naïve, Central Memory, and Effector Memory T-cells in a cohort of healthy individuals. Using a novel combinatorial isolation strategy, we were able to isolate sufficient quantities of each cell type for downstream assessment of miRNA expression. The profiling data demonstrate that miRNA expression in healthy individuals appears to be driven primarily by cell sub-type – i.e., Central Memory, Effector Memory, or Naïve, rather than the CD4+ or CD8+ phenotype designation. Importantly, several miRNA known to be involved in T-cell activation or modulation or involved in HIV-1 latency were here differentially upregulated or downregulated in Naïve cells: miR-181a [224,225], -31 [215,226,227], 125b, -21 [228,229], -24 [230], -146a [194,231,232] and -20a [233–235]. The clustering of these miRNA revealed unique miRNA profiles for Memory and Naïve cells.

Of these differentially expressed species in healthy populations, several were also differentially expressed when comparing healthy individuals to infected individuals: mir-196b, -193b, -31, 125b, and -21, but some of the expression differences occurred in different cell types. For example, in our intra-cell type comparison in healthy individuals, miR-125b and -193b were downregulated in CD4+ Naïve cells in healthy patients, but

these two miRNAs were specifically downregulated in CD4+ Effector Memory cells in infected individuals compared to healthy individuals. This finding improves confidence in our data, demonstrating that more general findings are not driven by huge differences in other components of the data.

One miRNA of potential importance is miR-9, which was significantly upregulated in Naïve cells across all infected individuals, a phenotype subsequently shown to be driven by ES individuals. miR-9 has previously been shown to be upregulated in viremic individuals and to have a significant role in enhancing IL-2 production in Naïve T-cells [236,237], but it is more commonly associated with upregulated in the basal ganglial cells in SIV-infected macaques. In addition, miR-9 was recently shown to mediate microglial migration when associated with extracellular vesicles secreted from cells simulated by HIV Tat [238]. There are two potential implications of miR-9 enriched expression in Naïve cells of ES individuals: 1) without a true viremic population for comparison (although the VCs included were on par or slightly lower in expression), it may be that the cytokine stimulation induced by miR-9 is beneficial in ES individuals, and 2) miR-9 upregulation may have anti-HIV-1 properties that outweigh any negative effects that occur as a result of increased inflammatory cytokine release. Further work to characterize the potential anti-HIV-1 properties of miR-9 is warranted, and could provide insight into the elite suppression mechanism.

Observed downregulation of miR-193b and -196b in Memory Cells of ES individuals is an important addition to the canon of miRNAs differentially expressed in ES individuals. A recent study by Wang et al highlighted the importance of miR-196b *in vitro* as a potential latency activator, and increased expression of miR-193b has now been

shown to be associated with liver damage in HIV-1 infected individuals [205,239]. These findings warrant further investigation into their precise mechanism and involvement in HIV-1 infection.

Another important aspect of a profiling study, such as this one, is the ability to compare miRNA species differential expression relative to other similarly designed studies. While this study is the first of its kind to look at miRNA profiles of specific T-cell subsets in ES individuals, many of the differentially expressed species are not unique. For example, in previous work from our laboratory, miR-155 was upregulated in ES individuals — this study confirms that finding but attributes the change specifically to CD8+ Naïve cells. We also saw changes in miR-155, miR-31, miR-21 and the let-7 family, which were all found on the PBMC level. Obtaining confirmation of differential expression of the same miRNAs in completely different populations also lends significant credibility to the profiling data.

Finally, as mentioned in the introduction, several miRNA, such as miR-21, -155, -28, and -29a are important co-regulators of pathways involving FOXO3a, STAT5 and Wnt, which have been shown to be involved in resisting cell death in ES individuals or influencing latency. That they are shown to be upregulated in Naïve and Effector memory cells, reveals potential cell specific roles in the modulation of different pathways involved in cellular resistance to HIV-1 infection.

One of the key limitations of this study is the lack of access to a viremic population, because these individuals are increasingly rare in the general population. Because most CP individuals receive ART treatment regularly, it is not surprising to see a dearth of differentially expressed miRNA between CP and controls. However, the

inclusion of this population in the study does allow for greater appreciation of differences between ES and control individuals. Also, in some instances, any differences between ES and CP individuals might be explained by direct role of ART in cellular processes in the face of HIV-1 infection, such as mir-16 or miR-19a in CD8+ EM or miR-103 in CD4+ CM.

This profiling study highlights numerous miRNAs species that are differentially express in ES patients relative to healthy controls, some of which have potential roles in innate antiviral cellular response. Although this is not an exhaustive study, the miRNA evaluated here represent many of the most common miRNAs altered in the context of HIV-1 infection or are involved in T-cell proliferation or viability. Importantly, we highlight key expression differences of many miRNA species in healthy individuals, establishing a highly specific miRnome for these T-cell subsets. Our hope is that these data, in combination with the results showing up and downregulation of miRNAs in ES relative to our control individuals will continue to fuel investigations into biomarker development and evaluation of combinatorial small RNA-based alternative therapies for controlling HIV-1 infections.

IV Figures:

A

Cell Type	% of P2	% of CD4 or CD8	Approximate # expected cells present based on total PBMC screening
CD8+CD45RA+ (Naive) (% of GP, P)	12.93%	51.1%	13639357
CD8+ CD45RO+CCR7+ (Central Memory) (% of GP)	0.42%	1.66%	443079
CD8+ CD45RO+CCR7- (Effector Memory) (% of GP)	5.52%	17.2%	5826063
Total CD8+ of total Lymphocytes (% of P)	25.30%		26691500
Total CD8+ Relative Percentage	32.11%		
CD4+CD45RA+ (Naive) (% of GP, P)	22.90%	42.8%	24157390
CD4+ CD45RO+CCR7+ (Central Memory) (% of GP)	7.70%	14.4%	8127720
CD4+ CD45RO+CCR7- (Effector Memory) (% of GP)	5.62%	10.5%	5926463
Total CD4+ of total Lymphocytes (% of P)	53.50%		38211573
Total CD4+ Relative Percentage	67.89%		
Total Starting # Cells	105500000		
Percentage of CD4+/CD8+ cells of interest of total lymphocytes	79%		
Number of PBMC needed for rate limiting cell type (CD8 Central Mem)	89289966		
Percentage of PBMC cells needed of total PBMC solution for CD8 selection	85%		
Initial Resuspension Volume	2.110		
CD8 Volume for sorting (mL)	1.786		
CD4 Volume for sorting (mL)	0.324		

B

POST STEM CELL SEPARATION		POST FLOW SORTING		
			Naive	Memory
Approximate Expected CD8 Count post separation	22590361			
Theoretical #CD8 Naive in CD8 selected population	11543675	Theoretical #CD8 Naive in CD8 selected population	1923946	9619729
Theoretical #CD8 Central Memory (CCR7+) in CD8 selected population	375000	Theoretical #CD8 Central Memory (CCR7+) in CD8 selected population	62500	312500
Theoretical #CD8 Effector Memory (CCR7-) in CD8 selected population	3885542	Theoretical #CD8 Effector Memory (CCR7-) in CD8 selected population	647590	3237952
Total CD8 cells of interest	15804217	Total CD8 cells of interest	2634036	13170181
Approximate Expected CD4 Count post separation	5871193			
CD4 Naive percentage of selected cells	2512871	CD4 Naive percentage of selected cells	628218	1884653
Theoretical #CD4 Central Memory (CCR7+) in CD4 selected population	845452	Theoretical #CD4 Central Memory (CCR7+) in CD8 selected population	211363	634089
Theoretical #CD4 Effector Memory (CCR7-) in CD4 selected population	616475	Theoretical #CD4 Effector Memory (CCR7-) in CD8 selected population	154119	462356
Total CD4 cells of interest	3974798	Total CD4 cells of interest	993699	2981098
Desired #CD8 Central Memory (CCR7+) in CD8 selected population	375000			
Starting PBMC needed to yield # desired memory cells	89289966			

Figure 1. **Example table for determining the appropriate volume for separating whole, FACS profiled, PBMC for downstream immunomagnetic isolation and FACS sorting.** (A) allows for input of the percentages as calculated by initial FACS analysis of whole PBMC (Orange boxes), while (B) outputs the theoretical number of each desired T-cell subset based on the initial approximate count of total PBMC isolated by Ficoll separation. The Green boxes in A are the final volumes needed prior to the immunomagnetic isolation step.

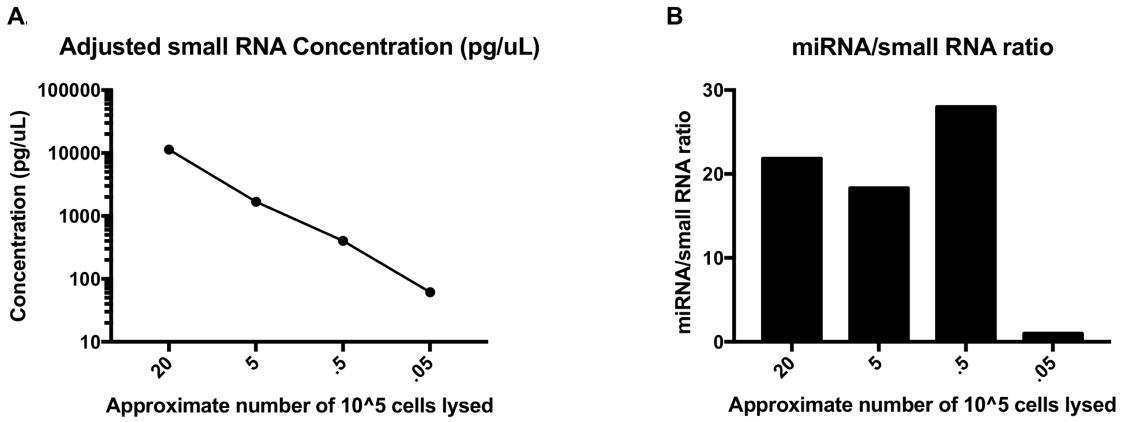

Figure 2. **The threshold of detection of RNA in a sample is compromised at 5000 starting cells.** (A) Use of the readout from the Agilent Bioanalyzer 2100 demonstrates a linear relationship between the measured small RNA concentration corresponding to the number of starting cells used for analysis. (B) when the miRNA to small RNA ratio is calculated, apparent miRNA species become undetectable at 5000 cells, although they are still highly detectable at 50000 cells.

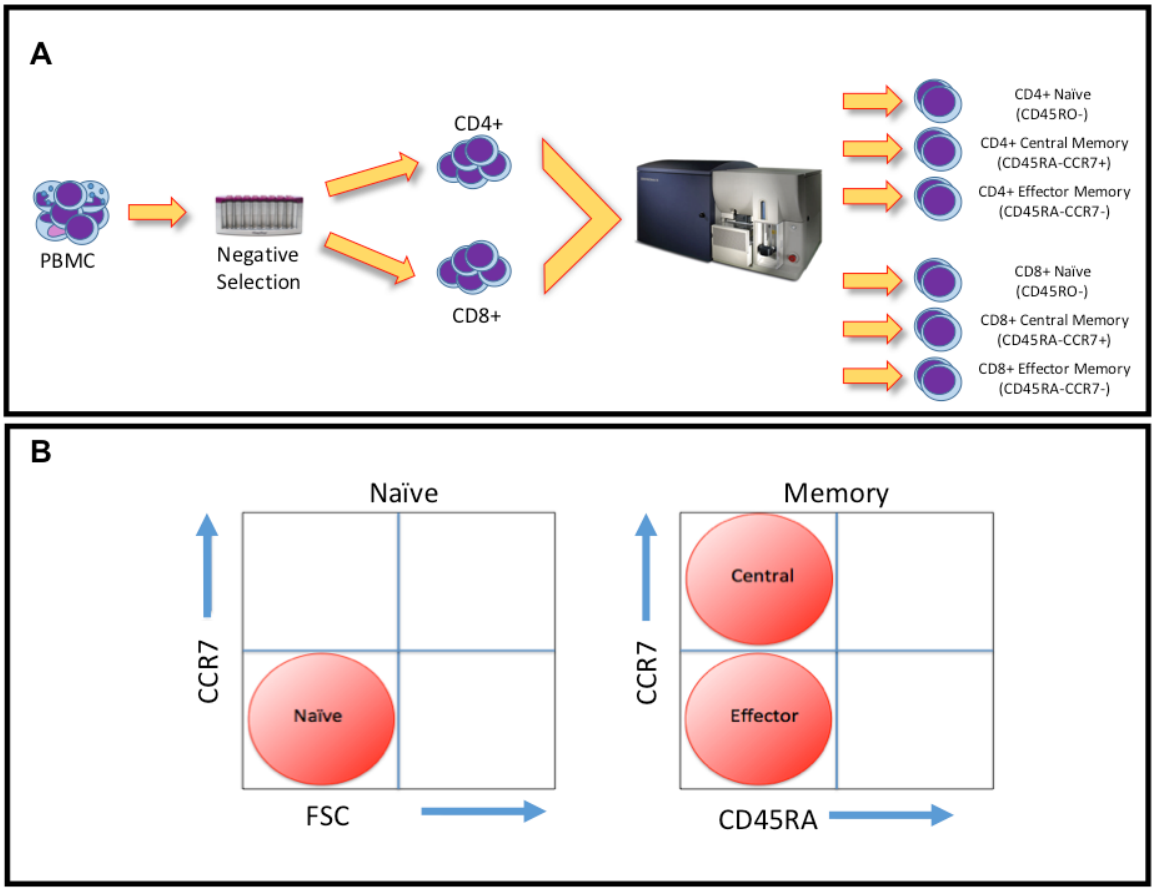

Figure 3. Experimental design and FACS sorting gating strategy. Using a combinatorial approach, PBMC are first separated into CD4+ and CD8+ populations using immunomagnetic negative isolation, then are separated into pertinent T-cell subsets using a negative staining approach in combination with FACS sorting (A). FACS gating strategy for already immunomagnetic purified populations of CD4+ and CD8+ T-cells is outlined in (B).

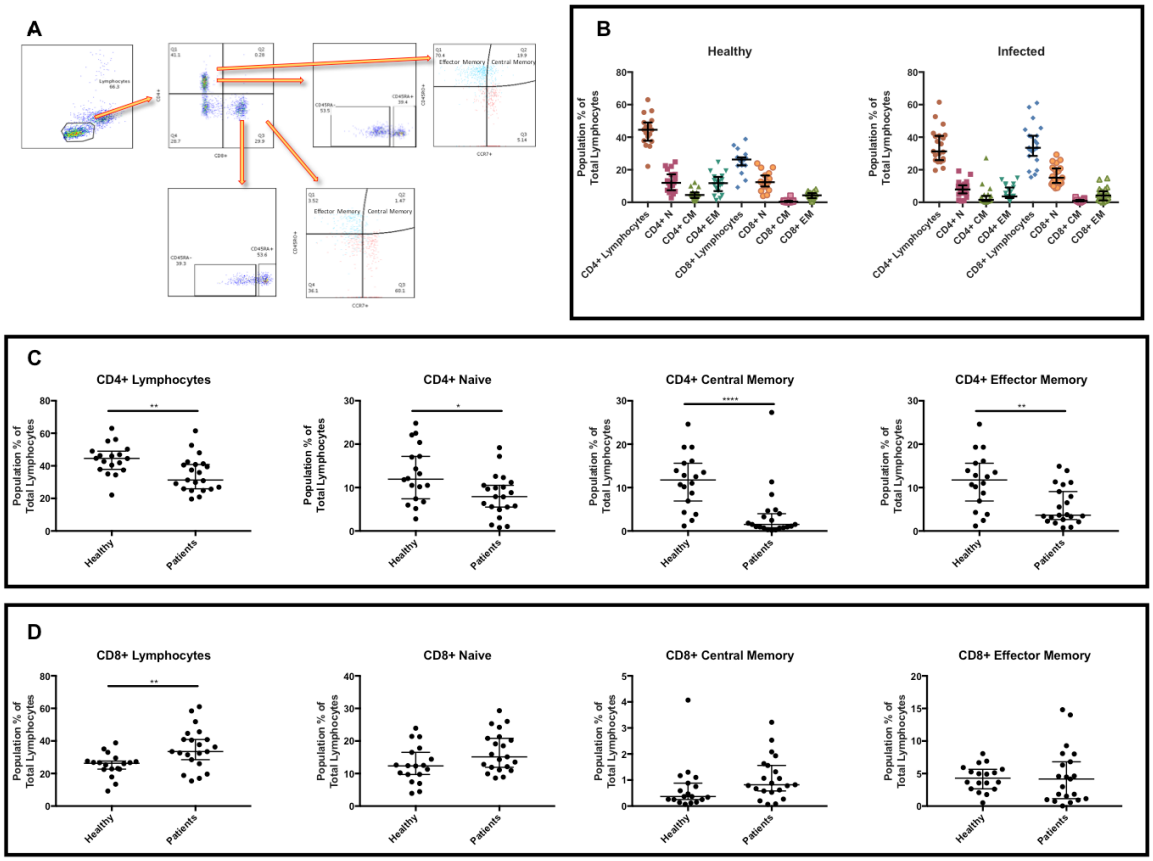

Figure 4. **Population frequencies of total CD4+ and CD8+ Lymphocytes as well as all CD4+ T-cell subsets are altered in infected donors relative to healthy controls.** (A) Schematic for FACS analysis of relative lymphocyte subset abundance. (B) Relative abundance of different T-cell subsets is consistent between healthy and infected individuals, with CD8+ Central Memory cells the lowest in population percentage (Median less than 1% of all lymphocytes in both populations). (C) When relative percentages of all CD4+ lymphocytes and each of the three studied subsets are compared between groups, there is a significant decrease in patients for all cell types. CD8+ Lymphocytes are more abundant in patient samples. Significance in (B) was assessed by a Mann-Whitney t-test. Asterisks represent p-values: * = $p < 0.05$; ** = $p < 0.01$, **** = $p < 0.0001$

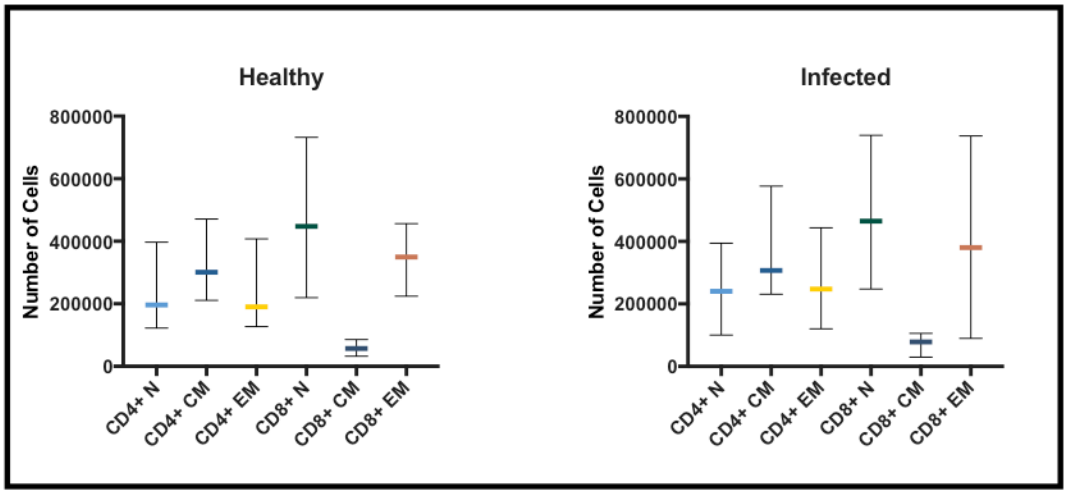

Figure 5. **Cell yields for each T-cell subset included in the study.** The median cell yield for each T-cell subset is represented by the colored bar, with 57,000 cells for healthy individuals and 78,000 for infected patients in CD8+ Central Memory cells, well below the median of any other cell. Error bars represent the 95% confidence interval.

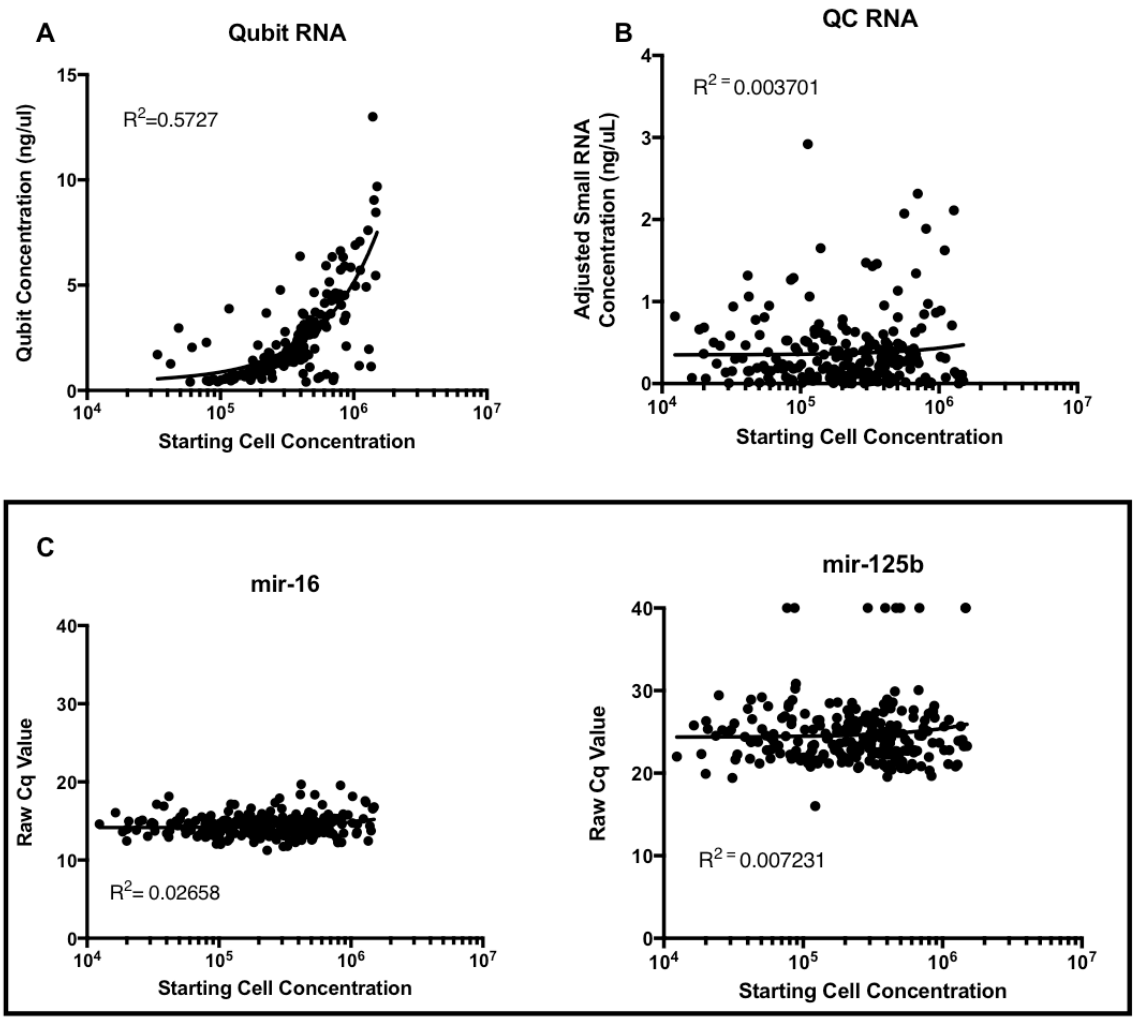

Figure 6. **Cell Concentration prior to RNA isolation correlates with RNA concentrated measured by Qubit but does not impact OpenArray readout data.** There is a correlation between cell number in samples prior to RNA isolation to measured RNA concentration by Qubit (A), but the correlation is not apparent on BioAnalyzer evaluation (B). When pre-amplified material initial loaded by volume (2uL) for the Reverse Trasncription step is measured on the OpenArray qPCR platform (C), no correlation is appreciated in either miR-16 or miR-125b.

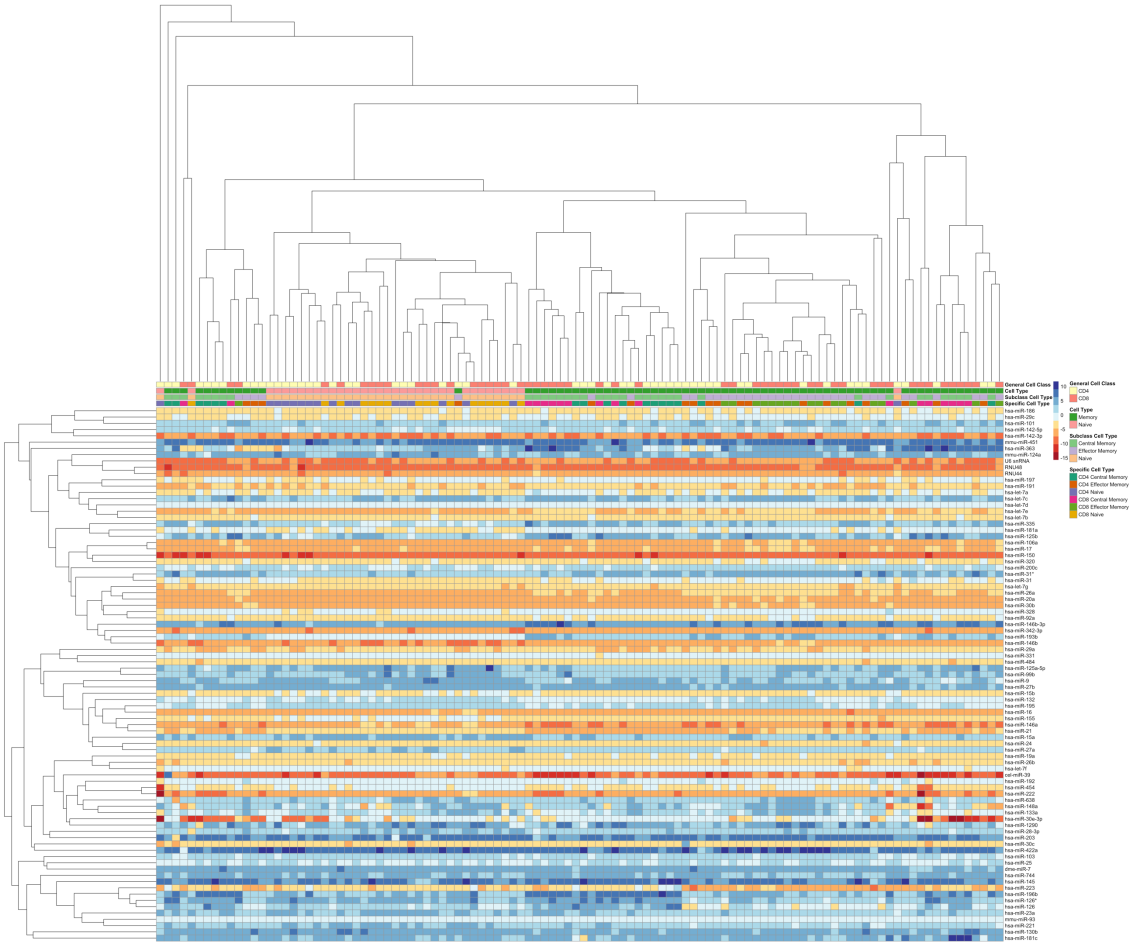

Figure 7. **Hierarchical Clustering of OpenArray data: all normalized data inhealthy individuals.** Targeted miRNA profiles were determined using the OpenArray platform. Hierarchical clustering of samples and features (Pearson correlation, average linkage) of data, normalized by approach as described in the methods. Abundance scale: red (high) to low (blue).

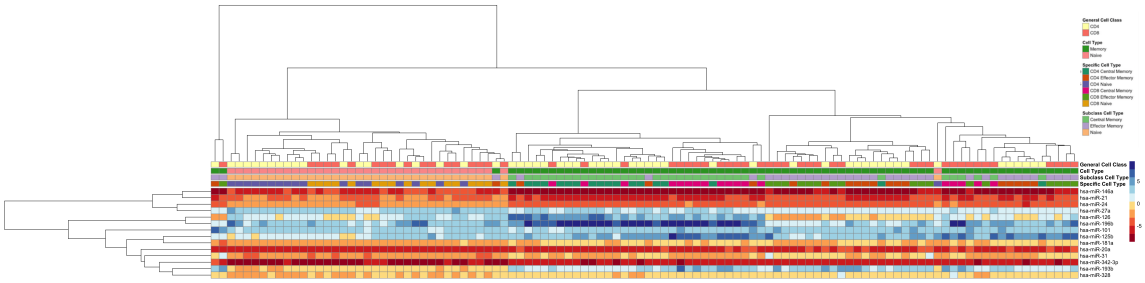

Figure 8. **Hierarchical Clustering of OpenArray data: significant differentially expressed miRNA by cell type in healthy individuals.** Targeted miRNA profiles were determined using the OpenArray platform. Hierarchical clustering of samples and features (Pearson correlation, average linkage) of data, normalized by approach as described in the methods. Significance was assessed by Kruskal Wallis test followed by Dunn's multiple comparison test, using the absolute distance of normalized expression values from the control mean. Scale: red (high) to low (blue).

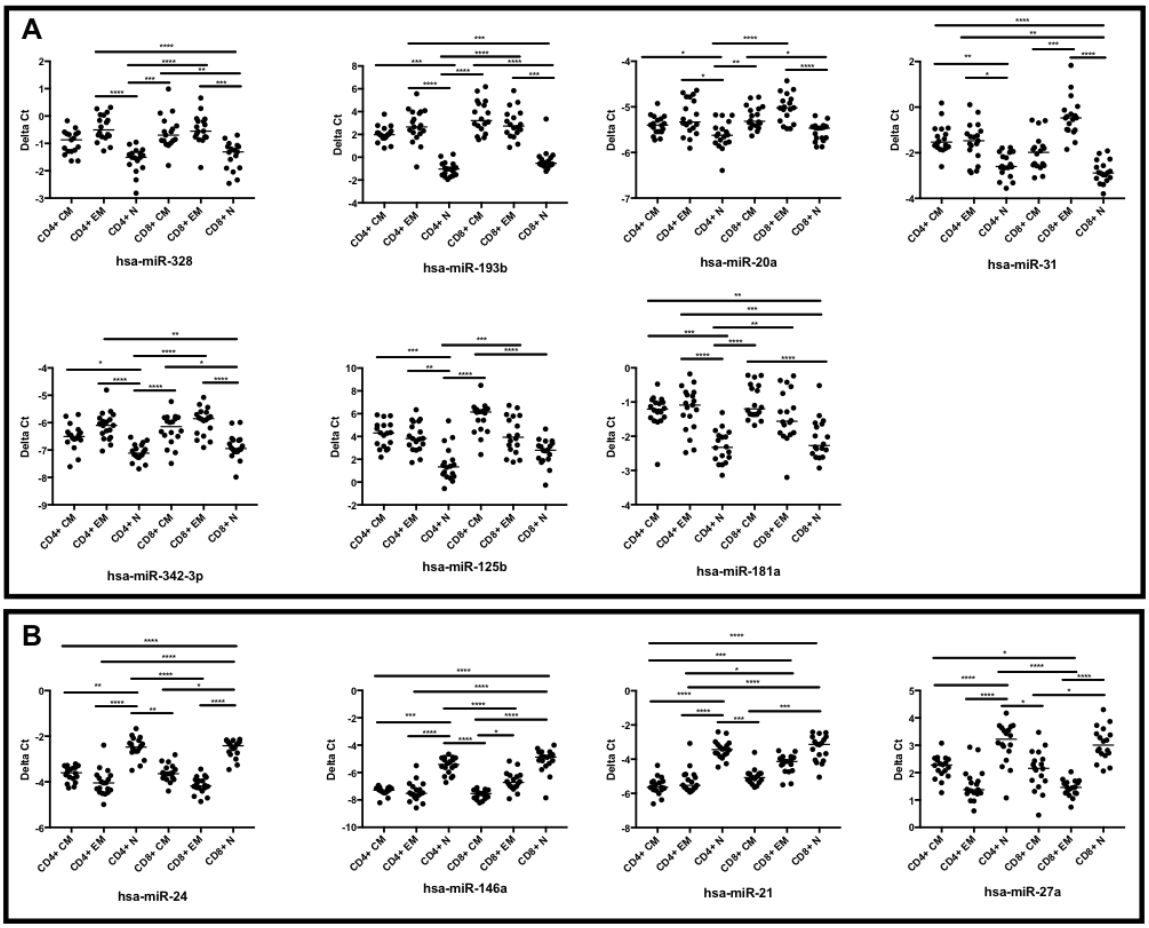

Figure 9. **Individual miRNA OpenArray profiling results in healthy individuals: Naïve cells.** The predominant number of miRNAs with differential expression occurred in Naïve cells relative to both types of memory cells. Downregulated (A) and upregulated (B) miRNAs in Naïve cells were identified from the deltaCt normalized data. Only miRNA for which the deltaCt was greater than 1 were included as significance. Significance was assessed by Dunn's multiple comparison test, using the absolute distance of one cell type's mean expression value from another. Bar represents median expression value. Asterisks represent p values: * = $p < 0.05$; ** = $p < 0.01$, *** = $p < 0.001$, **** = $p < 0.0001$.

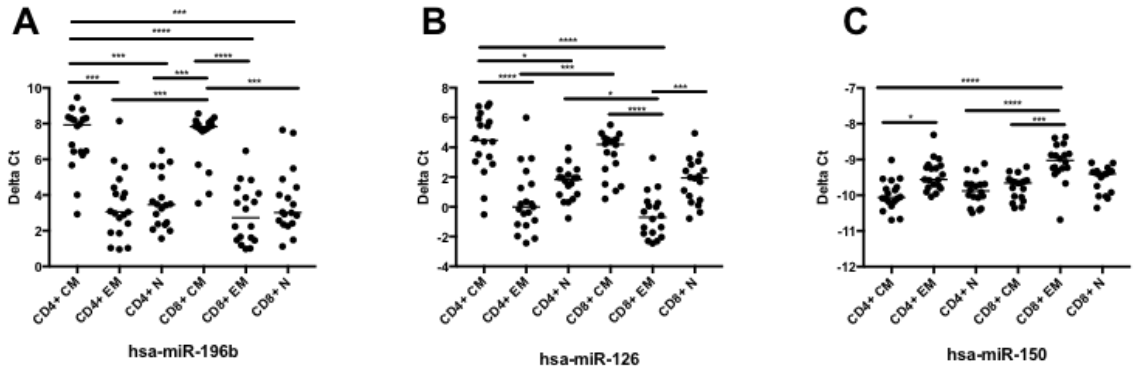

Figure 10. **Individual miRNA OpenArray profiling results in healthy individuals: other cell types.** Upregulated miRNAs (A) and (B) were observed in Central Memory cells relative to the other cell types. Single instances of downregulation (B) and upregulation (C) were observed in Effector Memory cells. Only miRNA for which the deltaCt was greater than 1 were included as significance. Significance was assessed by Dunn's multiple comparison test, using the absolute distance of one cell type's mean expression value from another. Bar represents median expression value. Asterisks represent p values: * = $p < 0.05$; ** = $p < 0.01$, *** = $p < 0.001$, **** = $p < 0.0001$.

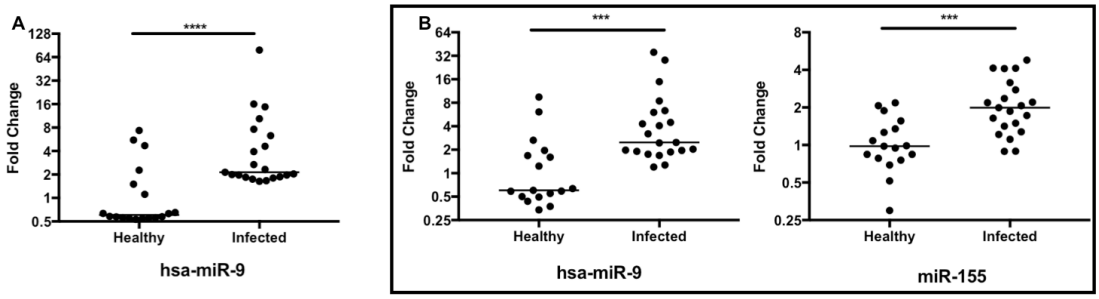

Figure 11. **OpenArray profiling results in Naïve cells comparing healthy donor to infected donor samples.** hsa-miR-9 is upregulated in infected individuals more than 3 fold in both CD4+ (A) and CD8+ (B) Naïve T-cells, while miR-155 was 2-fold upregulated in CD8+ Naive T-cells. No miRNA species were downregulated in infected individuals relative to healthy controls. Fold difference is relative to global expression of the 4 stable miRNAs as outlined in the methods section. X-axis scale is shown in log(2). Bar represents median expression value. Significance was assessed by a Mann-Whitney t-test. Asterisks represent p-values: *** = $p < 0.001$, **** = $p < 0.0001$

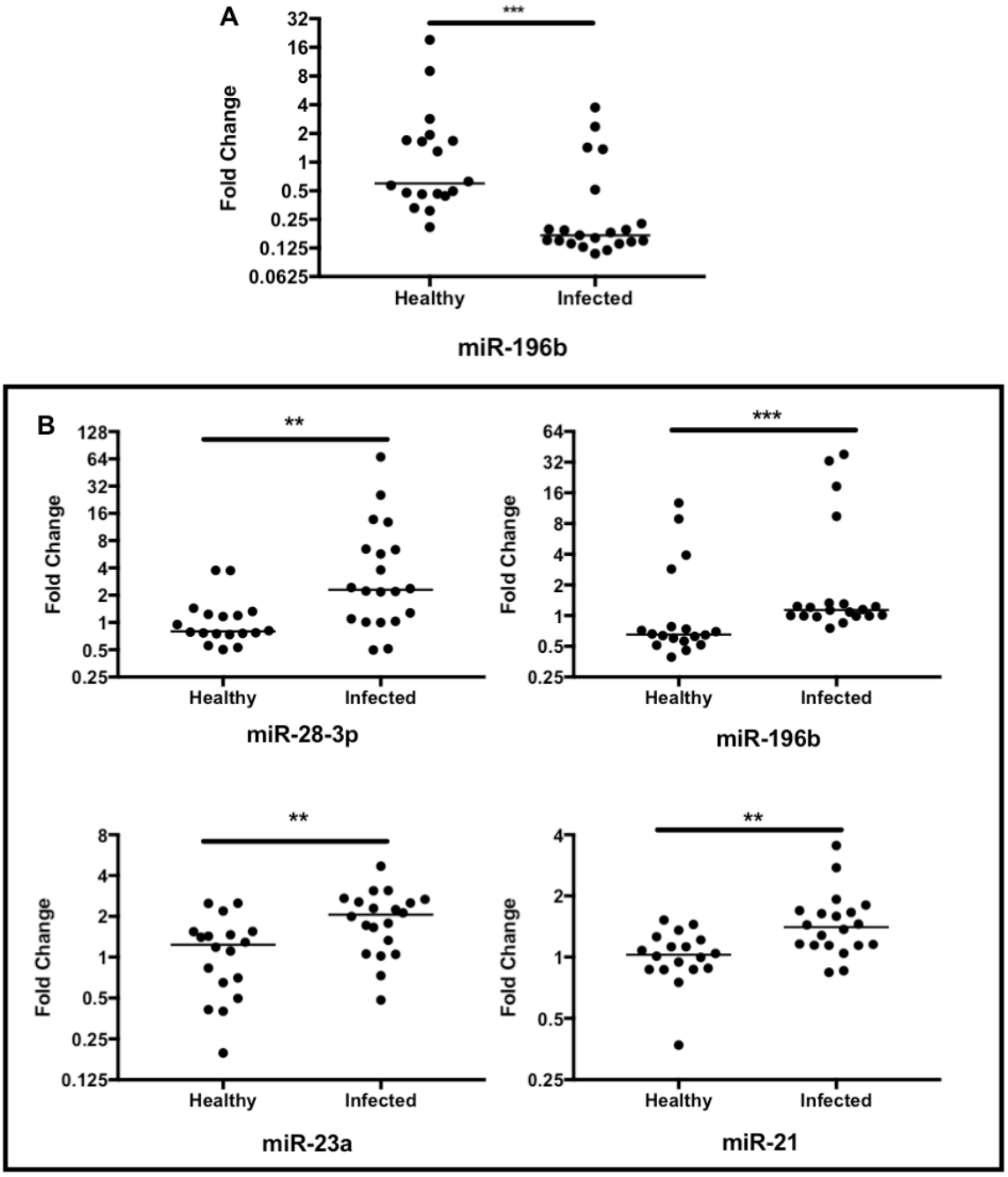

Figure 12. OpenArray profiling results in Central Memory cells comparing healthy donor to infected donor samples. hsa-miR-196 is downregulated in infected individuals more than 3 fold in CD4+ (A) CM T-cells, but upregulated almost 2-fold in CD8+ T-cells. miR–28-3p (almost 4-fold), -23a and -21 are about 2-fold upregulated in infected individual. Relative expression is relative to global expression of the 4 stable miRNAs as outlined in the methods section. X-axis scale is shown in log(2). Bar represents median expression value. Significance was assessed by a Mann-Whitney t-test. Asterisks represent p-values: ** = $p < 0.01$, *** = $p < 0.001$

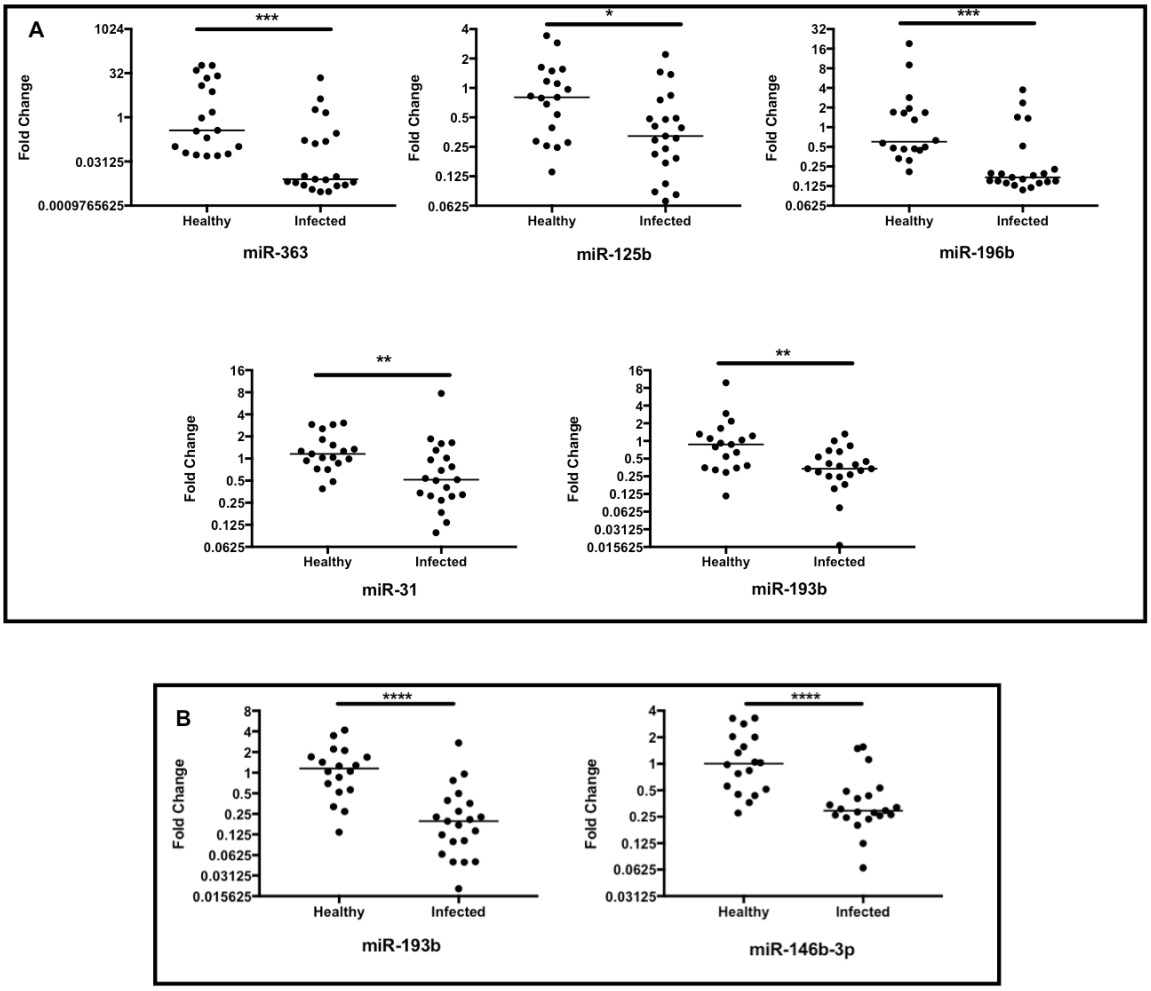

Figure 13 OpenArray profiling results in Effector Memory cells comparing healthy donor to infected donor samples. hsa-miR-193b is downregulated in infected individuals more than 2-fold in both CD4+ (A) and CD8+ (B) EM T-cells. Additionally, miRs-363, -125b, -196b, and -31 are all downregulated about 2-fold in infected individuals in CD4+ (A) cells, while miR-146b-3p is also downregulated in CD8+ cells (B). Fold change is relative to global expression of the 4 stable miRNAs as outlined in the methods section. X-axis scale is shown in log(2). Bar represents median expression value. Significance was assessed by a Mann-Whitney t-test. Asterisks represent p-values: * = $p < 0.05$, ** = $p < 0.01$, *** = $p < 0.001$, **** = $p < 0.0001$

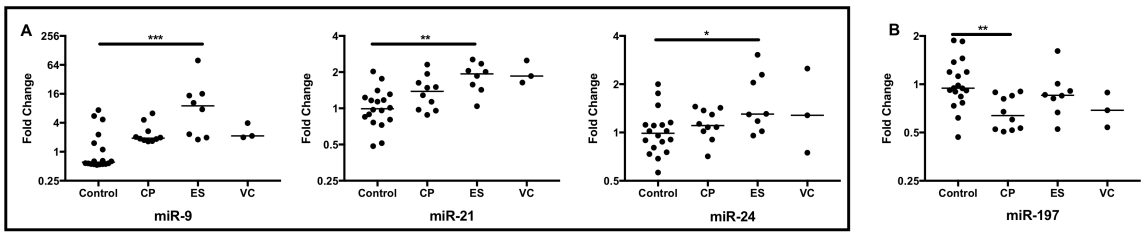

Figure 14. OpenArray profiling results in CD4+ Naïve cells comparing healthy donor to Elite Suppressor and Chronic Progressor donor samples. Most differentially expressed miRNAs are upregulated in CD4+ (A) Naive T-cells of ES. Naive cells from CPs showed downregulated differential expression in miR-197 (B). Fold change is relative to global expression of the 4 stable miRNAs as outlined in the methods section. X-axis scale is shown in log(2). Significance was assessed by Kruskal-Wallis test followed by Dunn's multiple comparison test, using the absolute distance of one cell type's normalized mean expression value from another. Bar represents median expression value. VC are shown for comparison and not included in statistical calculations. Asterisks represent p-values: * = $p < 0.05$, ** = $p < 0.01$, *** = $p < 0.001$

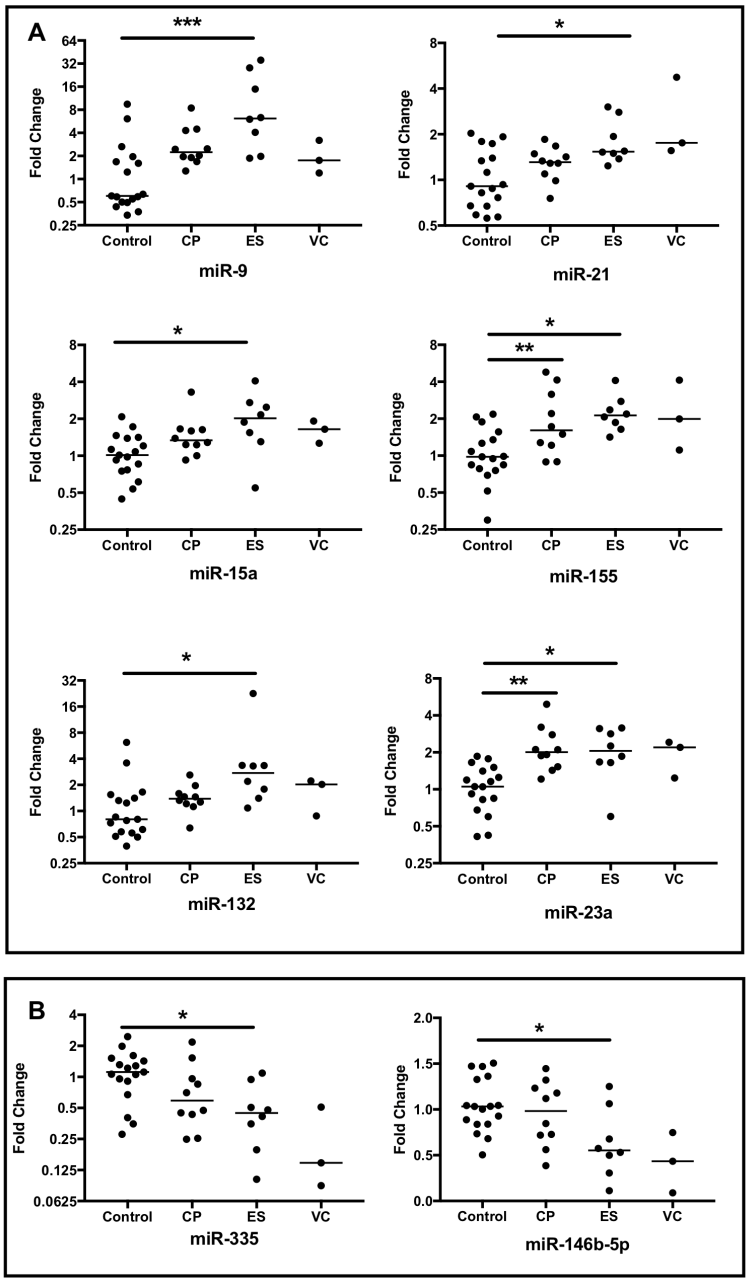

Figure 15. OpenArray profiling results in CD8+ Naïve T-cells comparing healthy donor to Elite Suppressor and Chronic Progressor donor samples. Most differentially expressed miRNAs are upregulated in CD8+ (A) Naive T-cells of ES. Naive cells from CPs showed differential expression in miR-155 and -23a (upregulated) in CD8+ Naive T-cells (A). Both mir-335 and miR-146b–3p were downregulated (B). Fold change is relative to global expression of the 4 stable miRNAs as outlined in the methods section. X-axis scale is shown in log(2). Significance was assessed by Kruskal-Wallis test followed by Dunn's multiple comparison test, using the absolute distance of one cell type's normalized mean expression value from another. Bar represents median expression value. VC are shown for comparison and not included in statistical calculations. Asterisks represent p-values: * = $p < 0.05$, ** = $p < 0.01$, *** = $p < 0.001$

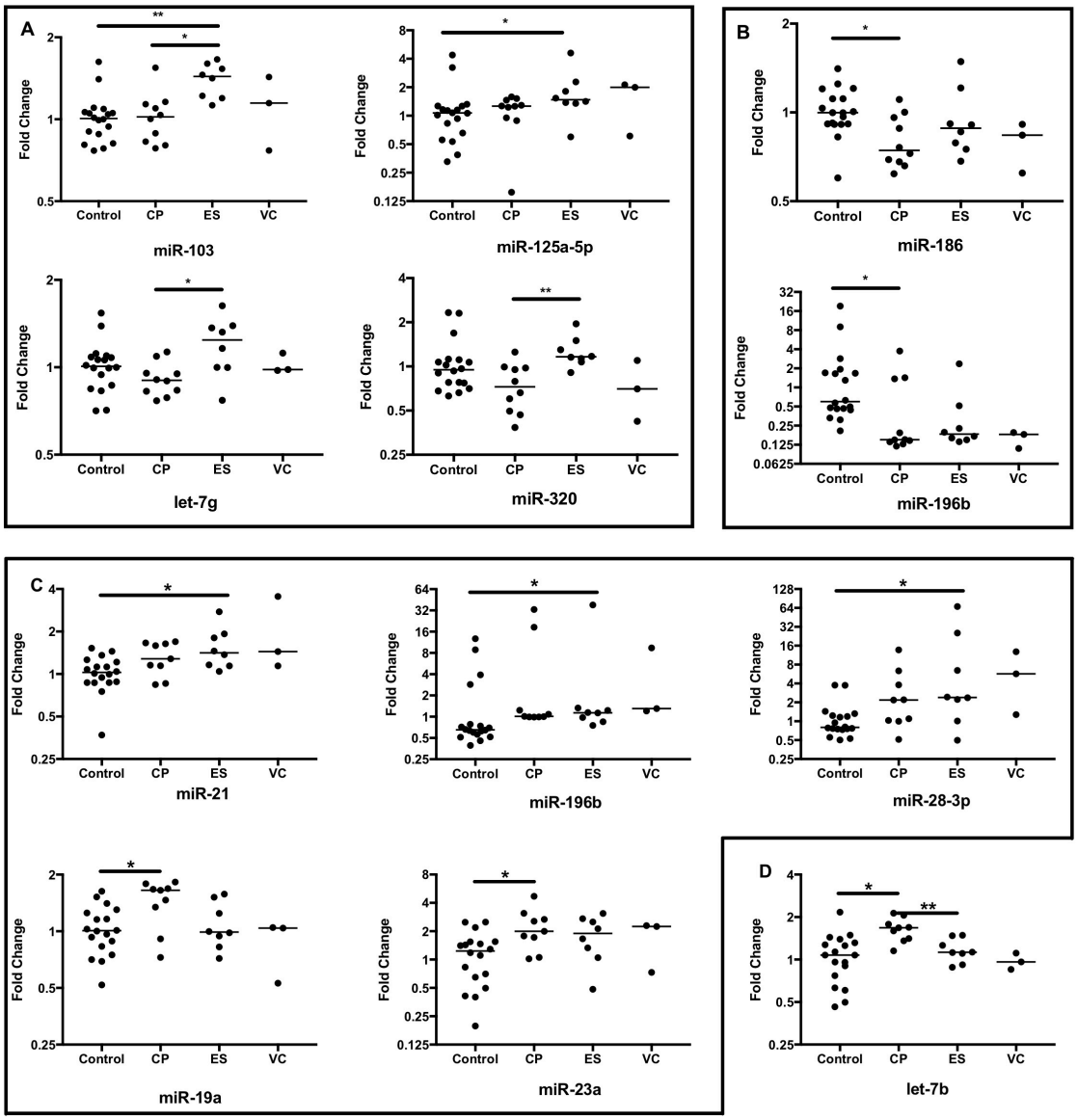

Figure 16. OpenArray profiling results in Central Memory cells comparing healthy donor to Elite Suppressor and Chronic Progressor donor samples. Most differentially expressed miRNAs are upregulated in both CD4+ (A) and CD8+ (C) CM T-cells of ES relative to controls. miR-186 and miR-196b were downregulated in CD4+ EM T-cells in CP relative to control (B). miR-19a, -23a were upregulated in CP relative to control and ES in CD8+ CM T-cells, while let-7b was upregulated in CP relative to both control and ES (D). Fold change is relative to global expression of the 4 stable miRNAs as outlined in the methods section. X-axis scale is shown in log(2). Significance was assessed by Kruskal-Wallis test followed by Dunn's multiple comparison test, using the absolute distance of one cell type's normalized mean expression value from another. Bar represents median expression value. VC are shown for comparison and not included in statistical calculations. Asterisks represent p-values: * = $p < 0.05$, ** = $p < 0.01$

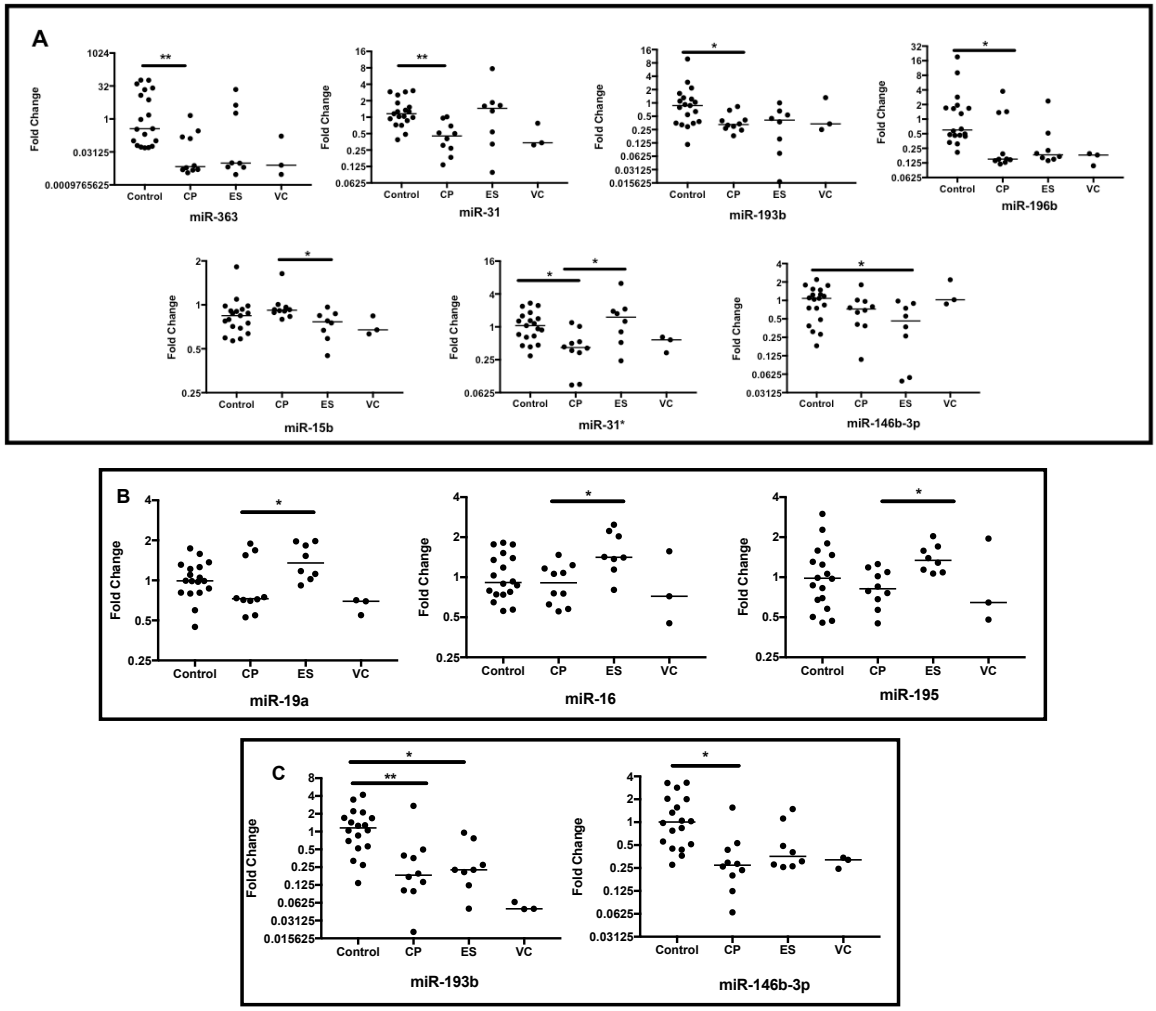

Figure 17. OpenArray profiling results in Effector Memory cells comparing healthy donor to Elite Suppressor and Chronic Progressor donor samples. All differentially expressed miRNAs are downregulated in both CD4+ (A) EMT-cells of ES reltaive to controls, with miR-31 downregulated in CP relative to control and ES. miR-19a, miR-16 and miR-195 were upregulated in EM cells from ES relative to CP in CD8+ EM (B). miR-193b and miR-146-3p were downregulated in CP relative to control in CD8+ EM (C), with 193b also downregulated in ES relative to control. Fold change is relative to global expression of the 4 stable miRNAs as outlined in the methods section. X-axis scale is shown in log(2). Significance was assessed by Kruskal-Wallis test followed by Dunn's multiple comparison test, using the absolute distance of one cell type's normalized mean expression value from another. Bar represents median expression value. VC are shown for comparison and not included in statistical calculationsAsterisks represent p-values: * = $p < 0.05$, ** = $p < 0.01$

A

Donor ID	Sex
20130904	Male
20131003	Female
20131006	Male
20131103	NA
20140701	Male
20150201	NA
20150601	NA
20150602	Female
20150604	Female
20150607	Female
20150701	Female
20150803	Male
20150806	Male
20151201	NA
20160201	NA
20160406	Female

B

Subject Number	Infection Status	Sex	Viral Load (copies/mL)	CD4+ T-cell Count	CD4+ T-cell %	ART Regimen	BMI	BMI Classification	Age	Age Range
1	ES	Female	<50	554	48.8	Untreated	17.6	Underweight	59	55-59
2	CP	Female	<50	766	26.9	TDF,FTC, RAL	27.8	Overweight	53	50-54
3	CP	Male	<50	737	34.5	EFV, ATV/r	25	Normal	53	50-54
4	CP	Male	<50	415	44.8	EFV, TDF, 3TC	25.2	Overweight	32	30-34
5	CP	Male	<50	948	24.8	ABC,3TC, FPV/r	34.5	Obese	47	45-49
6	CP	Male	<50	860	35.8	3TC, EFV, RAL	25.8	Overweight	52	50-54
7	ES	Female	<50	676	39	Untreated	35.1	Obese	64	60-64
9	CP	Male	<50	722	40	DTG, DRV/r	29.4	Overweight	49	45-49
10	CP	Male	<50	885	38.5	TDF,FTC,ELV/c	31.5	Obese	47	45-49
11	ES	Male	<50	1414	54.5	Untreated	NA	NA	54	50-54
12	ES	Female	<50	1149	47.1	Untreated	39	Obese	63	60-64
14	VC	Male	748	856	35.5	Untreated	30	Obese	60	60-64
16	ES	Male	<50	597	42.4	Untreated	20.4	Normal	49	45-49
17	CP	Male	<50	1109	41	ABC,3TC,DTG	23.5	Normal	62	60-64
18	ES	Female	<50	711	39.6	Untreated	39.2	Obese	66	65 and older
20	CP	Male	<50	642	NA	ABC, 3TC, RAL	27.7	Overweight	47	45-49
21	ES	Male	<50	447	19.1	Untreated	20.2	Normal	64	60-64
22	CP	Male	<50	995	32.5	ABC,3TC,DTG	29.9	Overweight	54	50-54
23	VC	Female	98	1101	30.3	Untreated	44.2	Obese	45	45-49
24	VC	Male	<50	719	26.2	Untreated	28.3	Overweight	60	60-64
25	CP	Male	<50	433	20.1	ETV,RAL,DRV/r	31.3	Obese	71	65 and older

Table 1. **ID numbers and characteristics of 37 unique donors.** (A) Healthy donors, (B) Patient Donors. Abbreviations for ART Regimen: TDF: tenofovir ; FTC: emtricitabine; RAL: raltegravir; EFV: efavirenz; ATV/r: atazanavir/low dose ritonavir ; 3TC: ; FPV/r: fosamprenavir/low dose ritonavir; DTG: dolutegravir; ABC: abacavir ;ELV/c:elviteagravir/cobicistat; ETV: etravirine; DRV/r: darunavir/low dose ritonavir.

V

Summary and Conclusions

Despite decades of research dedicated to understanding the complexities of HIV-1 interactions with the human immune system, a cure remains elusive. For this reason, scientists continue to learn as much as they can about the virus and how it affects all parts of the body. For our part, we utilized human disease models and *in vitro* culture to explore the interplay between HIV-1, EVs, and miRNA, ultimately leading to several insights into the complex relationship between host and retrovirus.

As described in Chapter two, we explored the potential of EVs as biomarkers of viral suppression in the cervicovaginal compartment. We observed a decrease in EV numbers in reproductive tract disease (endometriosis) and in SIV-infected macaques. We performed functional studies in human macrophages after discovering that miR-186 was more abundant in the EVs obtained from the secretions of infected animals, and found evidence for its role as an HIV-1 restriction factor. Our hope is that by dedicating some of our efforts to studying SIV and EVs in the reproductive system, which happens to be a primary location of disease transmission in people, that we will lay the groundwork for others to further explore its complex immune capacity and perhaps discover vital biomarkers or restriction factors that may help in the development of new treatment strategies.

Chapter three of this dissertation addresses EVs and HIV-1 infection through a series of *in vitro* studies using EV-depleted serum in cell culture. Work by Eitan et al using EV-depleted serum in cell culture demonstrated variable amounts of cell growth retardation and reduced viability of numerous cell lines including U87 glioblastoma, HEK-293T, HeLa, SY5Y human neuroblastoma, and N2a mouse neuroblastoma cell. Coupled with varying reports on the involvement of EVs in facilitating or hampering

HIV-1 infection [39,40,166,240], we felt it prudent to evaluate the impact of serum-derived vesicles on *in vitro* HIV-1 infection. We described and presented data demonstrating that the depletion of EVs from cell culture conditions exacerbates primary HIV-1 infection, reactivates latent, integrated virus, and creates a more infectious virus. We were able to reverse this phenotype by adding back EVs derived from serum at various concentrations. The changes observed appear to be driven primarily by lipid pathways, though elucidation of the exact mechanism is needed. Furthermore, we added to a growing canon of literature suggesting that EVs in circulation protect against HIV-1 infection. In future studies, we will perform add-back experiments using EVs derived from different cell lines to evaluate the impact of endogenous EVs on HIV infection. Although the miRNA data generated in this study showed minimal involvement of miRNAs, the panel examined was not exhaustive. We plan to investigate the entire small RNA response in this context through next-generation sequencing. It is not likely that there is a single silver bullet in the fight against HIV, but deciphering small pieces of the complex relationship may ultimately result in breakthroughs.

Finally, in chapter four, guided by previous studies of miRNA expression in PBMCs of ES and viremic individuals, we studied T-cell subsets with roles in combating HIV-1 infection. miRNA expression profiles of healthy controls, CP and ES, revealed robust clustering of Naïve, Central Memory and Effector Memory T-cells regardless of CD4+ or CD8+ phenotype or HIV-1 infection status. Perhaps the most intriguing observations, though, were the cell-specific expression differences we observed between the three cohorts – in Naïve cells almost all expression differences were elevated in ES relative to controls. In Memory cells, the differences were more variable as to whether

they were in CP or ES, and were variable in whether they were upregulated or downregulated. Specific miRNA like miR-9, -21, -31, and -155 were associated with specific T-cell types, and had previously been associated with ES at the PBMC level. Thus, by comparing miRNA expression in these same T-cells but instead evaluating for upregulation or downregulation of miRs between ES, CP and healthy individuals, we were able to build on ours and others work that indicates that miRNA play a significant role in the manifestation of HIV-1 suppression. We collected matched plasma from these individuals to study total and EV miRNA expression in ES relative to CP and HC. We hope that the miRNA profiles presented here will be helpful to others who study HIV-1 elite suppression.

The work included in this dissertation only scratches at the surface of the complex relationship between EVs and miRNA in the context of HIV-1 or SIV infection. It is our hope that the findings discussed here lay the groundwork for further studies in all areas explored here, both in our own lab and in others, that may eventually result in the discovery of novel therapies or permanent suppression or eradication of HIV-1 infection.

References

1 Korber B, Muldoon M, Theiler J, Gao F, Gupta R, Lapedes A, *et al.* Timing the ancestor of the HIV-1 pandemic strains. *Science* 2000; **288**:1789–96.

2 Gonda MA, Wong-Staal F, Gallo RC, Clements JE, Narayan O, Gilden R V. Sequence homology and morphologic similarity of HTLV-III and visna virus, a pathogenic lentivirus. *Science* 1985; **227**:173–7.

3 Unaids. Fact sheet - Latest global and regional statistics on the status of the AIDS epidemic. http://www.unaids.org/sites/default/files/media_asset/UNAIDS_FactSheet_en.pdf (accessed 9 Jun2018).

4 UNAIDS. UNAIDS DATA 2017 | UNAIDS. http://www.unaids.org/en/resources/documents/2017/2017_data_book (accessed 20 Jul2018).

5 González-Scarano F, Martín-García J. The neuropathogenesis of AIDS. *Nat Rev Immunol* 2005; **5**:69–81.

6 Saylor D, Dickens AM, Sacktor N, Haughey N, Slusher B, Pletnikov M, *et al.* HIV-associated neurocognitive disorder--pathogenesis and prospects for treatment. *Nat Rev Neurol* 2016; **12**:234–48.

7 Shen L, Siliciano RF. Viral reservoirs, residual viremia, and the potential of highly active antiretroviral therapy to eradicate HIV infection. *J Allergy Clin Immunol* 2008; **122**:22–28.

8 Richman DD, Margolis DM, Delaney M, Greene WC, Hazuda D, Pomerantz RJ. The Challenge of Finding a Cure for HIV Infection. *Science (80-)* 2009; **323**:1304–1307.

9 Finzi D, Hermankova M, Pierson T, Carruth LM, Buck C, Chaisson RE, *et al.* Identification of a reservoir for HIV-1 in patients on highly active antiretroviral therapy. *Science* 1997; **278**:1295–1300.

10 Whitney JB, Israel B, Lim S-Y, Wainberg MA. Evolutionary Mechanisms of Retroviral Persistence. Published Online First: 2014.https://www.researchgate.net/publication/51695474 (accessed 9 Jun2018).

11 Finzi D, Blankson J, Siliciano JD, Margolick JB, Chadwick K, Pierson T, *et al.* Latent infection of CD4+ T cells provides a mechanism for lifelong persistence of HIV-1, even in patients on effective combination therapy. *Nat Med* 1999; **5**:512–517.

12 Alexaki A, Liu Y, Wigdahl B. Cellular reservoirs of HIV-1 and their role in viral persistence. *Curr HIV Res* 2008; **6**:388–400.

13 Schnittman SM, Lane HC, Greenhouse J, Justement JS, Baseler M, Fauci AS. Preferential infection of CD4+ memory T cells by human immunodeficiency virus type 1: evidence for a role in the selective T-cell functional defects observed in infected individuals. *Proc Natl Acad Sci U S A* 1990; **87**:6058–62.

14 Morita E, Sandrin V, Mccullough J, Katsuyama A, Hamilton IB, Sundquist WI. ESCRT-III Protein Requirements for HIV-1 Budding. *Cell Host Microbe* 2011; **9**:235–242.

15 Kieffer C, Skalicky JJ, Morita E, De Domenico I, Ward DM, Kaplan J, *et al.* Two Distinct Modes of ESCRT-III Recognition Are Required for VPS4 Functions in Lysosomal Protein Targeting and HIV-1 Budding. *Dev Cell* 2008; **15**:62–73.

16 Sundquist WI, Krausslich H-G. HIV-1 Assembly, Budding, and Maturation. *Cold Spring Harb Perspect Med* 2012; **2**:a006924–a006924.
17 András IE, Leda A, Contreras MG, Bertrand L, Park M, Skowronska M, *et al.* Extracellular vesicles of the blood-brain barrier: Role in the HIV-1 associated amyloid beta pathology. *Mol Cell Neurosci* 2017; **79**:12–22.
18 CHARGAFF E, WEST R. The Biological Significance of the Thromboplastic Protein of Blood. *J Biol Chem* 1946; **166**:189–197.
19 Wolf P. The Nature and Significance of Platelet Products in Human Plasma. *Br J Haematol* 1967; **13**:269–288.
20 Bonucci E, Gherardi G. Histochemical and electron microscopy investigations on medullary bone. *Cell Tissue Res* 1975; **163**:81–97.
21 Raposo G, Nijman HW, Stoorvogel W, Leijendekker R, Harding C V, Melief CJM, *et al.* B lymphocytes secrete antigen-presenting vesicles. *J Exp Med* 1996; **183**:1161–1172.
22 Théry C, Amigorena S. The cell biology of antigen presentation in dendritic cells. *Curr Opin Immunol* 2001; **13**:45–51.
23 Lotvall J, Valadi H, Lötvall J, Valadi H, Lotvall J, Valadi H. Cell to cell signalling via exosomes through esRNA. *Cell Adhes & Migr* 2007; **1**:156–158.
24 Ratajczak J, Miekus K, Kucia M, Zhang J, Reca R, Dvorak P, *et al.* Embryonic stem cell-derived microvesicles reprogram hematopoietic progenitors: evidence for horizontal transfer of mRNA and protein delivery. *Leukemia* 2006; **20**:847–856.
25 Chevillet JR, Kang Q, Ruf IK, Briggs HA, Vojtech LN, Hughes SM, *et al.* Quantitative and stoichiometric analysis of the microRNA content of exosomes. *Proc Natl Acad Sci U S A* 2014; **111**:14888–14893.
26 Guermonprez P, Valladeau J, Zitvogel L, Théry C, Amigorena S. Antigen presentation and T cell stimulation by dendritic cells. *Annu Rev Immunol* 2002; **20**:621–667.
27 Van Niel G, D'Angelo G, Raposo G. Shedding light on the cell biology of extracellular vesicles. *Nat Rev Mol Cell Biol* 2018; **19**:213–228.
28 Théry C, Ostrowski M, Segura E. Membrane vesicles as conveyors of immune responses. *Nat Rev Immunol* 2009; **9**:581–593.
29 Gould SJ, Booth AM, Hildreth JEK. The Trojan Exosome Hypothesis. *Proc Natl Acad Sci U S A* 2003; **100**:10592–10597.
30 Raposo G, Stoorvogel W. Extracellular vesicles: Exosomes, microvesicles, and friends. J. Cell Biol. 2013; **200**:373–383.
31 Hildreth JEK. HIV As Trojan Exosome: Immunological Paradox Explained? *Front Immunol* 2017; **8**:1715.
32 Ramakrishnaiah V, Thumann C, Fofana I, Habersetzer F, Pan Q, de Ruiter PE, *et al.* Exosome-mediated transmission of hepatitis C virus between human hepatoma Huh7.5 cells. *Proc Natl Acad Sci* 2013; **110**:13109–13113.
33 Chivero ET, Bhattarai N, Rydze RT, Winters MA, Holodniy M, Stapleton JT. Human pegivirus RNA is found in multiple blood mononuclear cells in vivo and serum-derived viral RNA-containing particles are infectious in vitro. *J Gen Virol* 2014; **95**:1307–1319.
34 Narayanan A, Iordanskiy S, Das R, Van Duyne R, Santos S, Jaworski E, *et al.* Exosomes derived from HIV-1-infected cells contain trans-activation response

element RNA. *J Biol Chem* 2013; **288**:20014–20033.
35 Fang Y, Wu N, Gan X, Yan W, Morrell JC, Gould SJ. Higher-order oligomerization targets plasma membrane proteins and HIV gag to exosomes. *PLoS Biol* 2007; **5**:e158.
36 Lenassi M, Cagney G, Liao M, Vaupotic T, Bartholomeeusen K, Cheng Y, *et al.* HIV Nef is Secreted in Exosomes and Triggers Apoptosis in Bystander CD4(+) T Cells. *Traffic* 2010; **11**:110–122.
37 McNamara RP, Costantini LM, Myers TA, Schouest B, Maness NJ, Griffith JD, *et al.* Nef Secretion into Extracellular Vesicles or Exosomes Is Conserved across Human and Simian Immunodeficiency Viruses. *MBio* 2018; **9**:e02344-17.
38 Park I-W, He JJ. HIV-1 is budded from CD4+T lymphocytes independently of exosomes. *Virol J* 2010; **7**:234.
39 Arenaccio C, Chiozzini C, Columba-Cabezas S, Manfredi F, Affabris E, Baur A, *et al.* Exosomes from Human Immunodeficiency Virus Type 1 (HIV-1)-Infected Cells License Quiescent CD4(+) T Lymphocytes To Replicate HIV-1 through a Nef- and ADAM17-Dependent Mechanism. *J Virol* 2014; **88**:11529–11539.
40 Mercier SK, Donaghy H, Botting RA, Turville SG, Harman AN, Nasr N, *et al.* The microvesicle component of HIV-1 inocula modulates dendritic cell infection and maturation and enhances adhesion to and activation of T lymphocytes. *PLoS Pathog* 2013; **9**:e1003700.
41 de Carvalho J V, de Castro RO, da Silva EZM, Silveira PP, da Silva-Januario ME, Arruda E, *et al.* Nef neutralizes the ability of exosomes from CD4+ T cells to act as decoys during HIV-1 infection. *PLoS One* 2014; **9**:e113691.
42 Campos JH, Soares RP, Ribeiro K, Andrade AC, Batista WL, Torrecilhas AC. Extracellular Vesicles: Role in Inflammatory Responses and Potential Uses in Vaccination in Cancer and Infectious Diseases. *J Immunol Res* 2015; **2015**:832057.
43 Schorey JS, Harding C V. Extracellular vesicles and infectious diseases: new complexity to an old story. *J Clin Invest* 2016; **126**:1181–9.
44 Brody I, Ronquist G, Gottfries A. Ultrastructural localization of the prostasome - an organelle in human seminal plasma. *Ups J Med Sci* 1983; **88**:63–80.
45 Caby M-P, Lankar D, Vincendeau-Scherrer C, Raposo G, Bonnerot C. Exosomal-like vesicles are present in human blood plasma. *Int Immunol* 2005; **17**:879–887.
46 Pisitkun T, Shen R-F, Knepper MA. Identification and proteomic profiling of exosomes in human urine. *Proc Natl Acad Sci* 2004; **101**:13368–13373.
47 Gravett MG, Thomas A, Schneider KA, Reddy AP, Dasari S, Jacob T, *et al.* Proteomic Analysis of Cervical{\textminus}Vaginal Fluid:~ Identification of Novel Biomarkers for Detection of Intra-amniotic Infection. *J Proteome Res* 2007; **6**:89–96.
48 Smith JA, Daniel R. Human vaginal fluid contains exosomes that have an inhibitory effect on an early step of the HIV-1 life cycle. *AIDS* 2016; :1.
49 Lee RC, Feinbaum RL, Ambros V. The C. elegans heterochronic gene lin-4 encodes small RNAs with antisense complementarity to lin-14. *Cell* 1993; **75**:843–54.
50 Bartel DP. MicroRNAs: genomics, biogenesis, mechanism, and function. *Cell* 2004; **116**:281–97.

51 Lee Y, Kim M, Han J, Yeom K-H, Lee S, Baek SH, *et al.* MicroRNA genes are transcribed by RNA polymerase II. *EMBO J* 2004; **23**:4051–60.
52 Han J, Lee Y, Yeom K-H, Kim Y-K, Jin H, Kim VN. The Drosha-DGCR8 complex in primary microRNA processing. *Genes Dev* 2004; **18**:3016–3027.
53 Yi R, Qin Y, Macara IG, Cullen BR. Exportin-5 mediates the nuclear export of pre-microRNAs and short hairpin RNAs. *Genes Dev* 2003; **17**:3011–3016.
54 Hannon GJ. RNA interference. *Nature* 2002; **418**:244–251.
55 Rivas F V, Tolia NH, Song J-J, Aragon JP, Liu J, Hannon GJ, *et al.* Purified Argonaute2 and an siRNA form recombinant human RISC. *Nat Struct Mol Biol* 2005; **12**:340–349.
56 Kota J, Chivukula RR, O'Donnell KA, Wentzel EA, Montgomery CL, Hwang H-W, *et al.* Therapeutic microRNA Delivery Suppresses Tumorigenesis in a Murine Liver Cancer Model. *Cell* 2009; **137**:1005–1017.
57 Janssen HLA, Reesink HW, Lawitz EJ, Zeuzem S, Rodriguez-Torres M, Patel K, *et al.* Treatment of HCV Infection by Targeting MicroRNA. *N Engl J Med* 2013; **368**:1685–1694.
58 Sisk JM, Clements JE, Witwer KW. miRNA Profiles of Monocyte-Lineage Cells Are Consistent with Complicated Roles in HIV-1 Restriction. *Viruses* 2012; **4**:1844–1864.
59 Triboulet R, Mari B, Lin Y-LL, Chable-Bessia C, Bennasser Y, Lebrigand K, *et al.* Suppression of microRNA-silencing pathway by HIV-1 during virus replication. *Science* 2007; **315**:1579–1582.
60 Huang J, Wang F, Argyris E, Chen K, Liang Z, Tian H, *et al.* Cellular microRNAs contribute to HIV-1 latency in resting primary CD4+ T lymphocytes. *Nat Med* 2007; **13**:1241–1247.
61 Witwer KW, Watson AK, Blankson JN, Clements JE. Relationships of PBMC microRNA expression, plasma viral load, and CD4+ T-cell count in HIV-1-infected elite suppressors and viremic patients. *Retrovirology* 2012; **9**:5.
62 Eskenazi B, Warner ML. Epidemiology of endometriosis. *Obs Gynecol Clin North Am* 1997; **24**:235–258.
63 Clement PB. The pathology of endometriosis: a survey of the many faces of a common disease emphasizing diagnostic pitfalls and unusual and newly appreciated aspects. *Adv Anat Pathol* 2007; **14**:241–260.
64 Verkauf BS. Incidence, symptoms, and signs of endometriosis in fertile and infertile women. *J Fla Med Assoc* 1987; **74**:671–675.
65 Braundmeier AG, Fazleabas AT. The non-human primate model of endometriosis: research and implications for fecundity. *Mol Hum Reprod* 2009; **15**:577–586.
66 Sinaii N, Cleary SD, Ballweg ML, Nieman LK, Stratton P. High rates of autoimmune and endocrine disorders, fibromyalgia, chronic fatigue syndrome and atopic diseases among women with endometriosis: a survey analysis. *Hum Reprod* 2002; **17**:2715–2724.
67 Burney RO. Biomarker development in endometriosis. *Scand J Clin Lab Invest Suppl* 2014; **244**:75–81; discussion 80.
68 Santos TM, Pereira AM, Lopes RG, Depes Dde B. Lag time between onset of symptoms and diagnosis of endometriosis. *Einstein (Sao Paulo)* 2012; **10**:39–43.
69 Greene EH. Endometriosis: the urgency for early diagnosis and treatment. *J Med*

Assoc Ga 1950; **39**:283–286.
70 Rizner TL. Noninvasive biomarkers of endometriosis: myth or reality? *Expert Rev Mol Diagn* 2014; **14**:365–385.
71 Fassbender A, Vodolazkaia A, Saunders P, Lebovic D, Waelkens E, De Moor B, *et al.* Biomarkers of endometriosis. *Fertil Steril* 2013; **99**:1135–1145.
72 Borrelli GM, Abrao MS, Mechsner S. Can chemokines be used as biomarkers for endometriosis? A systematic review. *Hum Reprod* 2014; **29**:253–266.
73 Brosens J, Timmerman D, Starzinski-Powitz A, Brosens I. Noninvasive diagnosis of endometriosis: the role of imaging and markers. *Obs Gynecol Clin North Am* 2003; **30**:95–114, viii–ix.
74 Brosens I, Puttemans P, Campo R, Gordts S, Brosens J. Non-invasive methods of diagnosis of endometriosis. *Curr Opin Obs Gynecol* 2003; **15**:519–522.
75 Itsekson A, Shepshelovich D, Kanevsky A, Seidman DS. Measurement of electrical resistance of dermal-visceral zones as a diagnostic tool for gynecologic disorders. *Isr Med Assoc J* 2010; **12**:334–337.
76 Hull ML, Nisenblat V. Tissue and circulating microRNA influence reproductive function in endometrial disease. *Reprod Biomed Online* 2013; **27**:515–529.
77 Wang Z, Zhang J, Luo H, Ye Y, Yan J, Hou Y. Screening and confirmation of microRNA markers for forensic body fluid identification. *Forensic Sci Int Genet* 2013; **7**:116–123.
78 Suryawanshi S, Vlad AM, Lin HM, Mantia-Smaldone G, Laskey R, Lee M, *et al.* Plasma microRNAs as novel biomarkers for endometriosis and endometriosis-associated ovarian cancer. *Clin Cancer Res* 2013; **19**:1213–1224.
79 Jia SZ, Yang Y, Lang J, Sun P, Leng J. Plasma miR-17-5p, miR-20a and miR-22 are down-regulated in women with endometriosis. *Hum Reprod* 2013; **28**:322–330.
80 Qiu H. Plasma microRNAs in ovarian cancer--letter. *Clin Cancer Res* 2013; **19**:3325.
81 Leidner RS, Li L, Thompson CL. Dampening enthusiasm for circulating microRNA in breast cancer. *PLoS One* 2013; **8**:e57841.
82 Witwer KW. Circulating MicroRNA biomarker studies: Pitfalls and potential solutions. Clin. Chem. 2015; **61**:56–63.
83 Haider BA, Baras AS, McCall MN, Hertel JA, Cornish TC, Halushka MK, *et al.* A Critical Evaluation of microRNA Biomarkers in Non-Neoplastic Disease. *PLoS One* 2014; **9**.http://dx.plos.org/10.1371/journal.pone.0089565
84 Arroyo JD, Chevillet JR, Kroh EM, Ruf IK, Pritchard CC, Gibson DF, *et al.* Argonaute2 complexes carry a population of circulating microRNAs independent of vesicles in human plasma. *Proc Natl Acad Sci U S A* 2011; **108**:5003–5008.
85 Turchinovich A, Weiz L, Langheinz A, Burwinkel B. Characterization of extracellular circulating microRNA. *Nucleic Acids Res* 2011; **39**:7223–7233.
86 Taylor DD, Gercel-Taylor C. MicroRNA signatures of tumor-derived exosomes as diagnostic biomarkers of ovarian cancer. *Gynecol Oncol* 2008; **110**:13–21.
87 Knobil E, Neill JD, Plant TM. *Knobil and Neill's physiology of reproduction*. 3rd ed. Amsterdam ; Boston: Elsevier; 2006.
88 McLennan CE, Rydell AH. Extent of endometrial shedding during normal menstruation. *Obstet Gynecol* 1965; **26**:605–621.
89 Brenner RM, Nayak NR, Slayden OD, Critchley HOD, Kelly RW. Premenstrual

and menstrual changes in the macaque and human endometrium: relevance to endometriosis. *Ann N Y Acad Sci* 2002; **955**:60–406.

90 Van Deun J, Mestdagh P, Sormunen R, Cocquyt V, Vermaelen K, Vandesompele J, *et al.* The impact of disparate isolation methods for extracellular vesicles on downstream RNA profiling. *J Extracell Vesicles* Published Online First: 2014. doi:10.3402/jev.v3.24858

91 Gyorgy B, Modos K, Pallinger E, Paloczi K, Pasztoi M, Misjak P, *et al.* Detection and isolation of cell-derived microparticles are compromised by protein complexes resulting from shared biophysical parameters. *Blood* 2011; **117**:e39-48.

92 Webber J, Clayton A. How pure are your vesicles? *J Extracell Vesicles* 2013; **2**. doi:10.3402/jev.v2i0.1986119861 [pii]

93 Lotvall J, Hill AF, Hochberg F, Buzas EI, Di Vizio D, Gardiner C, *et al.* Minimal experimental requirements for definition of extracellular vesicles and their functions: a position statement from the International Society for Extracellular Vesicles. *J Extracell Vesicles* 2014; **3**:26913.

94 Witwer KW, Buzas EI, Bemis LT, Bora A, Lasser C, Lotvall J, *et al.* Standardization of sample collection, isolation and analysis methods in extracellular vesicle research: An ISEV position paper. *J Extracell Vesicles* 2013; **2**:20360.

95 Hadzic S V, Wang X, Dufour J, Doyle L, Marx PA, Lackner AA, *et al.* Comparison of the vaginal environment of Macaca mulatta and Macaca nemestrina throughout the menstrual cycle. *Am J Reprod Immunol* 2014; **71**:322–329.

96 Heffron R, Donnell D, Rees H, Celum C, Mugo N, Were E, *et al.* Use of hormonal contraceptives and risk of HIV-1 transmission: a prospective cohort study. *Lancet Infect Dis* 2012; **12**:19–26.

97 Hanson EK, Ballantyne J. Highly specific mRNA biomarkers for the identification of vaginal secretions in sexual assault investigations. *Sci Justice* 2013; **53**:14–22.

98 Jakubowska J, MacIejewska A, Pawłowski R, Bielawski KP. MRNA profiling for vaginal fluid and menstrual blood identification. *Forensic Sci Int Genet* 2013; **7**:272–278.

99 Park JL, Kwon OH, Kim JH, Yoo HS, Lee HC, Woo KM, *et al.* Identification of body fluid-specific DNA methylation markers for use in forensic science. *Forensic Sci Int Genet* 2014; **13**:147–153.

100 Hanson EK, Lubenow H, Ballantyne J. Identification of forensically relevant body fluids using a panel of differentially expressed microRNAs. *Anal Biochem* 2009; **387**:303–314.

101 Liu J, Sun H, Wang X, Yu Q, Li S, Yu X, *et al.* Increased Exosomal MicroRNA-21 and MicroRNA-146a Levels in the Cervicovaginal Lavage Specimens of Patients with Cervical Cancer. *Int J Mol Sci* 2014; **15**:758–773.

102 Burgener A, Boutilier J, Wachihi C, Kimani J, Carpenter M, Westmacott G, *et al.* Identification of differentially expressed proteins in the cervical mucosa of HIV-1-resistant sex workers. *J Proteome Res* 2008; **7**:4446–4454.

103 Zevin AS, Xie IY, Birse K, Arnold K, Romas L, Westmacott G, *et al.* Microbiome Composition and Function Drives Wound-Healing Impairment in the Female Genital Tract. *PLoS Pathog* 2016; **12**:e1005889.

104 Boggiano C, Littman DR. HIV's Vagina Travelogue. ; 2007.

105 Patel M V., Ghosh M, Fahey J V., Ochsenbauer C, Rossoll RM, Wira CR. Innate Immunity in the Vagina (Part II): Anti-HIV Activity and Antiviral Content of Human Vaginal Secretions. *Am J Reprod Immunol* 2014; **72**:22–33.
106 Benki S, Mostad SB, Richardson BA, Mandaliya K, Kreiss JK, Overbaugh J. Increased levels of HIV-1-infected cells in endocervical secretions after the luteinizing hormone surge. *J Acquir Immune Defic Syndr* 2008; **47**:529–34.
107 Zara F, Nappi RE, Brerra R, Migliavacca R, Maserati R, Spinillo A. Markers of local immunity in cervico-vaginal secretions of HIV infected women: implications for HIV shedding. *Sex Transm Infect* 2004; **80**:108–112.
108 Gardella B, Roccio M, Maccabruni A, Mariani B, Panzeri L, Zara F, *et al.* HIV shedding in cervico-vaginal secretions in pregnant women. *Curr HIV Res* 2011; **9**:313–20.
109 Seaton KE, Ballweber L, Lan A, Donathan M, Hughes S, Vojtech L, *et al.* HIV-1 specific IgA detected in vaginal secretions of HIV uninfected women participating in a microbicide trial in Southern Africa are primarily directed toward gp120 and gp140 specificities. *PLoS One* 2014; **9**. doi:10.1371/journal.pone.0101863
110 Ghosh M, Fahey J V., Shen Z, Lahey T, Cu-Uvin S, Wu Z, *et al.* Anti-HIV activity in cervical-vaginal secretions from HIV-Positive and -Negative women correlate with innate antimicrobial levels and IgG antibodies. *PLoS One* 2010; **5**. doi:10.1371/journal.pone.0011366
111 Clemetson DB, Moss GB, Willerford DM, Hensel M, Emonyi W, Holmes KK, *et al.* Detection of HIV DNA in cervical and vaginal secretions. Prevalence and correlates among women in Nairobi, Kenya. *Jama* 1993; **269**:2860–2864.
112 Rahman S, Rabbani R, Wachihi C, Kimani J, Plummer FA, Ball TB, *et al.* Mucosal serpin A1 and A3 levels in HIV highly exposed sero-negative women are affected by the menstrual cycle and hormonal contraceptives but are independent of epidemiological confounders. *Am J Reprod Immunol* 2013; **69**:64–72.
113 Yáñez-Mó M, Siljander PR-M, Andreu Z, Zavec AB, Borràs FE, Buzas EI, *et al.* Biological properties of extracellular vesicles and their physiological functions. *J Extracell vesicles* 2015; **4**:27066.
114 Gould SJ, Raposo G. As we wait: coping with an imperfect nomenclature for extracellular vesicles. *J Extracell Vesicles* 2013; **2**. doi:10.3402/jev.v2i0.2038920389 [pii]
115 Meehan B, Rak J, Di Vizio D. Oncosomes - large and small: what are they, where they came from? *J Extracell vesicles* 2016; **5**:33109.
116 György B, Hung ME, Breakefield XO, Leonard JN. Therapeutic applications of extracellular vesicles: clinical promise and open questions. *Annu Rev Pharmacol Toxicol* 2015; **55**:439–64.
117 Witwer KW, Buzás EI, Bemis LT, Bora A, Lässer C, Lötvall J, *et al.* Standardization of sample collection, isolation and analysis methods in extracellular vesicle research. *J Extracell Vesicles* 2013; **2**:18389.
118 Muth DC, McAlexander MA, Ostrenga LJ, Pate NM, Izzi JM, Adams RJ, *et al.* Potential role of cervicovaginal extracellular particles in diagnosis of endometriosis. *BMC Vet Res* 2015; **11**:187.
119 Sergeeva AM, Pinzon Restrepo N, Seitz H. Quantitative aspects of RNA silencing in metazoans. *Biochem* 2013; **78**:613–626.

120 Bartel DP. MicroRNAs: target recognition and regulatory functions. *Cell* 2009; **136**:215–233.
121 Arroyo JD, Chevillet JR, Kroh EM, Ruf IK, Pritchard CC, Gibson DF, *et al.* Argonaute2 complexes carry a population of circulating microRNAs independent of vesicles in human plasma. *Proc Natl Acad Sci U S A* 2011; **108**:5003–5008.
122 Witwer KW, Sarbanes SL, Liu J, Clements JE. A plasma microRNA signature of acute lentiviral infection: biomarkers of CNS disease. *AIDS* 2011; **204**:1104–1114.
123 Zubakov D, Boersma AW, Choi Y, van Kuijk PF, Wiemer EA, Kayser M. MicroRNA markers for forensic body fluid identification obtained from microarray screening and quantitative RT-PCR confirmation. *Int J Leg Med* 2010; **124**:217–226.
124 Seashols-Williams S, Lewis C, Calloway C, Peace N, Harrison A, Hayes-Nash C, *et al.* High-throughput miRNA sequencing and identification of biomarkers for forensically relevant biological fluids. *Electrophoresis* Published Online First: August 2016. doi:10.1002/elps.201600258
125 Muth DC, McAlexander MA, Ostrenga LJ, Pate NM, Izzi JM, Adams RJ, *et al.* Potential role of cervicovaginal extracellular particles in diagnosis of endometriosis. *BMC Vet Res* 2015; **11**:187.
126 Thery C, Amigorena S, Raposo G, Clayton A. Isolation and characterization of exosomes from cell culture supernatants and biological fluids. *Curr Protoc Cell Biol* 2006; **Chapter 3**:Unit 3 22.
127 McAlexander MA, Phillips MJ, Witwer KW, McAlexander MA, Phillips MJ. Comparison of Methods for miRNA Extraction from Plasma and Quantitative Recovery of RNA from Cerebrospinal Fluid. *Front Genet* 2013; **4**:83.
128 Chen C, Ridzon DA, Broomer AJ, Zhou Z, Lee DH, Nguyen JT, *et al.* Real-time quantification of microRNAs by stem-loop RT-PCR. *Nucleic Acids Res* 2005; **33**:e179.
129 Clements JE, Witwer KW, Liu J, Sarbanes SL, Liu J, Clements JE. A plasma microRNA signature of acute lentiviral infection: biomarkers of central nervous system disease. *AIDS* 2011; **25**:2057–2067.
130 Clough E, Barrett T. The Gene Expression Omnibus Database. *Methods Mol Biol* 2016; **1418**:93–110.
131 Witwer KW, Soekmadji C, Hill AF, Wauben MH, Buzás EI, Di Vizio D, *et al.* Updating the MISEV minimal requirements for extracellular vesicle studies: building bridges to reproducibility. *J Extracell Vesicles* 2017; **6**:1396823.
132 Consortium E-T, Van Deun J, Mestdagh P, Agostinis P, Akay O, Anand S, *et al.* EV-TRACK: transparent reporting and centralizing knowledge in extracellular vesicle research. *Nat Meth* 2017; **14**:228–232.
133 Nguyen HPT, Simpson RJ, Salamonsen LA, Greening DW. Extracellular Vesicles in the Intrauterine Environment: Challenges and Potential Functions. *Biol Reprod* 2016; **95**:109–109.
134 Campoy I, Lanau L, Altadill T, Sequeiros T, Cabrera S, Cubo-Abert M, *et al.* Exosome-like vesicles in uterine aspirates: a comparison of ultracentrifugation-based isolation protocols. *J Transl Med* 2016; **14**:180.
135 Zegels G, Aa G, Raemdonck V, Coen EP, Tjalma WA, Wm X, *et al.* Comprehensive proteomic analysis of human cervical-vaginal fluid using

colposcopy samples. *Proteome Sci* 2009; **7**. doi:10.1186/1477-5956-7-17
136 Arroyo JD, Chevillet JR, Kroh EM, Ruf IK, Pritchard CC, Gibson DF, *et al.* Argonaute2 complexes carry a population of circulating microRNAs independent of vesicles in human plasma. *Proc Natl Acad Sci U S A* 2011; **108**:5003–5008.
137 Pritchard CC, Kroh E, Wood B, Arroyo JD, Dougherty KJ, Miyaji MM, *et al.* Blood cell origin of circulating microRNAs: a cautionary note for cancer biomarker studies. *Cancer Prev Res* 2012; **5**:492–497.
138 Akhter A, Patel JL, Farooq F, Qureshi A, Taher-Rad M-S, Elyamany G, *et al.* De Novo Acute Myeloid Leukemia in Adults: Suppression of MicroRNA-223 is Independent of LMO2 Protein Expression BUT Associate With Adverse Cytogenetic Profile and Undifferentiated Blast Morphology. *Appl Immunohistochem Mol Morphol*; **23**:733–9.
139 Tombak A, Ay OI, Erdal ME, Sungur MA, Ucar MA, Akdeniz A, *et al.* MicroRNA Expression Analysis in Patients with Primary Myelofibrosis, Polycythemia vera and Essential Thrombocythemia. *Indian J Hematol Blood Transfus* 2015; **31**:416–25.
140 Giray BG, Emekdas G, Tezcan S, Ulger M, Serin MS, Sezgin O, *et al.* Profiles of serum microRNAs; miR-125b-5p and miR223-3p serve as novel biomarkers for HBV-positive hepatocellular carcinoma. *Mol Biol Rep* 2014; **41**:4513–9.
141 Bertoli G, Cava C, Castiglioni I. MicroRNAs: New Biomarkers for Diagnosis, Prognosis, Therapy Prediction and Therapeutic Tools for Breast Cancer. *Theranostics* 2015; **5**:1122–43.
142 Wang S, Zhang R, Claret FX, Yang H. Involvement of microRNA-24 and DNA methylation in resistance of nasopharyngeal carcinoma to ionizing radiation. *Mol Cancer Ther* 2014; **13**:3163–74.
143 Li J, Hu L, Tian C, Lu F, Wu J, Liu L. microRNA-150 promotes cervical cancer cell growth and survival by targeting FOXO4. *BMC Mol Biol* 2015; **16**:24.
144 Swaminathan S, Murray DD, Kelleher AD. miRNAs and HIV: unforeseen determinants of host-pathogen interaction. *Immunol Rev* 2013; **254**:265–280.
145 Sisk JM, Witwer KW, Tarwater PM, Clements JE. SIV replication is directly downregulated by four antiviral miRNAs. *Retrovirology* 2013; **10**:95.
146 Wang X, Ye L, Zhou Y, Liu MQ, Zhou DJ, Ho WZ. Inhibition of anti-HIV microRNA expression: a mechanism for opioid-mediated enhancement of HIV infection of monocytes. *Am J Pathol* 2011; **178**:41–47.
147 Swaminathan S, Suzuki K, Seddiki N, Kaplan W, Cowley MJ, Hood CL, *et al.* Differential regulation of the Let-7 family of microRNAs in CD4+ T cells alters IL-10 expression. *J Immunol* 2012; **188**:6238–6246.
148 Klase Z, Kale P, Winograd R, Gupta M V, Heydarian M, Berro R, *et al.* HIV-1 TAR element is processed by Dicer to yield a viral micro-RNA involved in chromatin remodeling of the viral LTR. *BMC Mol Biol* 2007; **8**:63.
149 Wagschal A, Rousset E, Basavarajaiah P, Contreras X, Harwig A, Laurent-Chabalier S, *et al.* Microprocessor, Setx, Xrn2, and Rrp6 co-operate to induce premature termination of transcription by RNAPII. *Cell* 2012; **150**:1147–1157.
150 Whisnant AW, Bogerd HP, Flores O, Ho P, Powers JG, Sharova N, *et al.* In-Depth Analysis of the Interaction of HIV-1 with Cellular microRNA Biogenesis and Effector Mechanisms. *MBio* 2013; **4**. doi:10.1128/mBio.00193-13e00193-13

[pii]mBio.00193-13 [pii]
151 Sung TL, Rice AP. miR-198 inhibits HIV-1 gene expression and replication in monocytes and its mechanism of action appears to involve repression of cyclin T1. *PLoS Pathog* 2009; **5**:e1000263.
152 Gardiner C, Vizio D Di, Sahoo S, Théry C, Witwer KW, Wauben M, *et al.* Techniques used for the isolation and characterization of extracellular vesicles: results of a worldwide survey. *J Extracell Vesicles* 2016; **5**. doi:10.3402/jev.v5.32945
153 Witwer KW, Halushka MK. Towards the Promise of microRNAs - Enhancing reproducibility and rigor in microRNA research. *RNA Biol* 2016; :0.
154 La Rocca G, Olejniczak SH, Gonzalez AJ, Briskin D, Vidigal JA, Spraggon L, *et al.* In vivo, Argonaute-bound microRNAs exist predominantly in a reservoir of low molecular weight complexes not associated with mRNA. *Proc Natl Acad Sci U S A* 2015; **112**:767–772.
155 György B, Szabó TG, Pásztói M, Pál Z, Misják P, Aradi B, *et al.* Membrane vesicles, current state-of-the-art: emerging role of extracellular vesicles. *Cell Mol Life Sci* 2011; **68**:2667–88.
156 Ramakrishnaiah V, Thumann C, Fofana I, Habersetzer F, Pan Q, de Ruiter PE, *et al.* Exosome-mediated transmission of hepatitis C virus between human hepatoma Huh7.5 cells. *Proc Natl Acad Sci U S A* 2013; **110**:13109–13113.
157 Chivero ET, Bhattarai N, Rydze RT, Winters MA, Holodniy M, Stapleton JT. Human pegivirus RNA is found in multiple blood mononuclear cells in vivo and serum-derived viral RNA-containing particles are infectious in vitro. *J Gen Virol* 2014; **95**:1307–1319.
158 Sampey GC, Saifuddin M, Schwab A, Barclay R, Punya S, Chung M-C, *et al.* Exosomes from HIV-1-infected Cells Stimulate Production of Pro-inflammatory Cytokines through Trans-activating Response (TAR) RNA. *J Biol Chem* 2016; **291**:1251–1266.
159 Lenassi M, Cagney G, Liao M, Vaupotic T, Bartholomeeusen K, Cheng Y, *et al.* HIV Nef is Secreted in Exosomes and Triggers Apoptosis in Bystander CD4(+) T Cells. *Traffic* 2010; **11**:110–122.
160 Luo X, Fan Y, Park I-W, He JJ. Exosomes are unlikely involved in intercellular Nef transfer. *PLoS One* 2015; **10**:e0124436.
161 Hubert A, Subra C, Jenabian M-A, Tremblay Labrecque P-F, Tremblay C, Laffont B, *et al.* Elevated Abundance, Size, and MicroRNA Content of Plasma Extracellular Vesicles in Viremic HIV-1+ Patients: Correlations With Known Markers of Disease Progression. *J Acquir Immune Defic Syndr* 2015; **70**:219–27.
162 Konadu KA, Chu J, Huang MB, Amancha PK, Armstrong W, Powell MD, *et al.* Association of Cytokines With Exosomes in the Plasma of HIV-1-Seropositive Individuals. *J Infect Dis* 2015; **211**:1712–1716.
163 Mayne E, Funderburg NT, Sieg SF, Asaad R, Kalinowska M, Rodriguez B, *et al.* Increased platelet and microparticle activation in HIV infection: upregulation of P-selectin and tissue factor expression. *J Acquir Immune Defic Syndr* 2012; **59**:340–346.
164 Khan MB, Lang MJ, Huang M-B, Raymond A, Bond VC, Shiramizu B, *et al.* Nef exosomes isolated from the plasma of individuals with HIV-associated dementia

(HAD) can induce Aβ1-42 secretion in SH-SY5Y neural cells. *J Neurovirol* Published Online First: September 2015. doi:10.1007/s13365-015-0383-6
165 Hu G, Yao H, Chaudhuri AD, Duan M, Yelamanchili S V, Wen H, *et al.* Exosome-mediated shuttling of microRNA-29 regulates HIV Tat and morphine-mediated neuronal dysfunction. *Cell Death Dis* 2012; **3**:e381.
166 Kadiu I, Narayanasamy P, Dash PK, Zhang W, Gendelman HE. Biochemical and biologic characterization of exosomes and microvesicles as facilitators of HIV-1 infection in macrophages. *J Immunol* 2012; **189**:744–754.
167 Arenaccio C, Chiozzini C, Columba-Cabezas S, Manfredi F, Federico M. Cell activation and HIV-1 replication in unstimulated CD4+ T lymphocytes ingesting exosomes from cells expressing defective HIV-1. *Retrovirology* 2014; **11**:46.
168 Arenaccio C, Anticoli S, Manfredi F, Chiozzini C, Olivetta E, Federico M. Latent HIV-1 is activated by exosomes from cells infected with either replication-competent or defective HIV-1. *Retrovirology* 2015; **12**:87.
169 Madison MN, Jones PH, Okeoma CM. Exosomes in human semen restrict HIV-1 transmission by vaginal cells and block intravaginal replication of LP-BM5 murine AIDS virus complex. *Virology* 2015; **482**:189–201.
170 Madison MN, Roller RJ, Okeoma CM. Human semen contains exosomes with potent anti-HIV-1 activity. *Retrovirology* 2014; **11**:102.
171 Eitan E, Zhang S, Witwer KW, Mattson MP. Extracellular vesicle-depleted fetal bovine and human sera have reduced capacity to support cell growth. *J Extracell Vesicles* 2015; **4**:26373.
172 Shelke GV, Lässer C, Gho YS, Lötvall J. Importance of exosome depletion protocols to eliminate functional and RNA-containing extracellular vesicles from fetal bovine serum. *J Extracell vesicles* 2014; **3**. doi:10.3402/jev.v3.24783
173 Beninson LA, Fleshner M. Exosomes in fetal bovine serum dampen primary macrophage IL-1β response to lipopolysaccharide (LPS) challenge. *Immunol Lett* 2015; **163**:187–92.
174 Sisk JM, Clements JE, Witwer KW. miRNA Profiles of Monocyte-Lineage Cells Are Consistent with Complicated Roles in HIV-1 Restriction. *Viruses* 2012; **4**:1844–1864.
175 Saeed AI, Bhagabati NK, Braisted JC, Liang W, Sharov V, Howe EA, *et al.* TM4 microarray software suite. *Methods Enzym* 2006; **411**:134–193.
176 Ferrick DA, Neilson A, Beeson C. Advances in measuring cellular bioenergetics using extracellular flux. *Drug Discov Today* 2008; **13**:268–74.
177 Linares R, Tan S, Gounou C, Arraud N, Brisson AR. High-speed centrifugation induces aggregation of extracellular vesicles. *J Extracell vesicles* 2015; **4**:29509.
178 Boing AN, van der Pol E, Grootemaat AE, Coumans FA, Sturk A, Nieuwland R. Single-step isolation of extracellular vesicles by size-exclusion chromatography. *J Extracell Vesicles* 2014; **3**. doi:10.3402/jev.v3.2343023430 [pii]
179 Duelli DM, Hearn S, Myers MP, Lazebnik Y. A primate virus generates transformed human cells by fusion. *J Cell Biol* 2005; **171**:493–503.
180 Wei Z, Batagov AO, Carter DRF, Krichevsky AM. Fetal Bovine Serum RNA Interferes with the Cell Culture derived Extracellular RNA. *Sci Rep* 2016; **6**:31175.
181 Kadiu I, Narayanasamy P, Dash PK, Zhang W, Gendelman HE. Biochemical and

biologic characterization of exosomes and microvesicles as facilitators of HIV-1 infection in macrophages. *J Immunol* 2012; **189**:744–754.
182 Sódar BW, Kittel Á, Pálóczi K, Vukman K V, Osteikoetxea X, Szabó-Taylor K, *et al.* Low-density lipoprotein mimics blood plasma-derived exosomes and microvesicles during isolation and detection. *Sci Rep* 2016; **6**:24316.
183 O'Connell KA, Bailey JR, Blankson JN. Elucidating the elite: mechanisms of control in HIV-1 infection. *Trends Pharmacol Sci* 2009; **30**:631–637.
184 Deeks SG, Walker BD. Human immunodeficiency virus controllers: mechanisms of durable virus control in the absence of antiretroviral therapy. *Immunity* 2007; **27**:406–416.
185 Brennan CA, Ibarrondo FJ, Sugar CA, Hausner MA, Shih R, Ng HL, *et al.* Early HLA-B*57-Restricted CD8(+) T Lymphocyte Responses Predict HIV-1 Disease Progression. *J Virol* 2012; **86**:10505–10516.
186 Samson M, Libert F, Doranz BJ, Rucker J, Liesnard C, Farber C-M, *et al.* Resistance to HIV-1 infection in Caucasian individuals bearing mutant alleles of the CCR-5 chemokine receptor gene. *Nature* 1996; **382**:722–725.
187 Paxton WA, Martin SR, Tse D, OBrien TR, Skurnick J, VanDevanter NL, *et al.* Relative resistance to HIV-1 infection of CD4 lymphocytes from persons who remain uninfected despite multiple high-risk sexual exposures. *Nat Med* 1996; **2**:412–417.
188 Liu R, Paxton WA, Choe S, Ceradini D, Martin SR, Horuk R, *et al.* Homozygous defect in HIV-1 coreceptor accounts for resistance of some multiply-exposed individuals to HIV-1 infection. *Cell* 1996; **86**:367–77.
189 Dominguez-Molina B, Tarancon-Diez L, Hua S, Abad-Molina C, Rodriguez-Gallego E, Machmach K, *et al.* HLA-B*57 and IFNL4-related polymorphisms are associated with protection against HIV-1 disease progression in controllers. *Clin Infect Dis* 2017; **64**:621–628.
190 Altfeld M, Addo MM, Rosenberg ES, Hecht FM, Lee PK, Vogel M, *et al.* Influence of HLA-B57 on clinical presentation and viral control during acute HIV-1 infection. *AIDS* 2003; **17**:2581–91.
191 Kane M, Yadav SS, Bitzegeio J, Kutluay SB, Zang T, Wilson SJ, *et al.* MX2 is an interferon-induced inhibitor of HIV-1 infection. *Nature* 2013; **502**:563–566.
192 Ambrose Z, Aiken C. HIV-1 uncoating: connection to nuclear entry and regulation by host proteins. *Virology* 2014; **454**–**455**:371–9.
193 Chen C-Z, Schaffert S, Fragoso R, Loh C. Regulation of immune responses and tolerance: the microRNA perspective. *Immunol Rev* 2013; **253**:112–128.
194 Tsitsiou E, Lindsay MA. microRNAs and the immune response. Curr. Opin. Pharmacol. 2009; **9**:514–520.
195 Bartel DP. MicroRNAs: Target Recognition and Regulatory Functions. *Cell* 2009; **136**:215–233.
196 Norman KL, Sarnow P. Modulation of hepatitis C virus RNA abundance and the isoprenoid biosynthesis pathway by microRNA miR-122 involves distinct mechanisms. *J Virol* 2010; **84**:666–670.
197 Gupta A, Swaminathan G, Martin-Garcia J, Navas-Martin S. MicroRNAs, Hepatitis C Virus, and HCV/HIV-1 Co-Infection: New Insights in Pathogenesis and Therapy. *Viruses* 2012; **4**:2485–2513.

198 Lanford RE, Hildebrandt-Eriksen ES, Petri A, Persson R, Lindow M, Munk ME, *et al.* Therapeutic silencing of microRNA-122 in primates with chronic hepatitis C virus infection. *Science* 2010; **327**:198–201.
199 Gebert LFR, Rebhan MAE, Crivelli SEM, My Denzler R, Stoffel M, Hall J. Miravirsen (SPC3649) can inhibit the biogenesis of miR-122. doi:10.1093/nar/gkt852
200 Yeung ML, Bennasser Y, Myers TG, Jiang G, Benkirane M, Jeang KT. Changes in microRNA expression profiles in HIV-1-transfected human cells. *Retrovirology* 2005; **2**:81.
201 Ruelas DS, Chan JK, Oh E, Heidersbach AJ, Hebbeler AM, Chavez L, *et al.* MicroRNA-155 Reinforces HIV Latency * □ S. Published Online First: 2015. doi:10.1074/jbc.M115.641837
202 Rosca A, Anton G, Botezatu A, Temereanca A, Ene L, Achim C, *et al.* miR-29a associates with viro-immunological markers of HIV infection in treatment experienced patients. *J Med Virol* 2016; **88**:2132–2137.
203 Barbosa F, Lix Lombard-Vadnais F, Ancuta P, Tremblay MJ, Cohen Correspondence RA. Host MicroRNAs-221 and -222 Inhibit HIV-1 Entry in Macrophages by Targeting the CD4 Viral Receptor. Published Online First: 2017. doi:10.1016/j.celrep.2017.09.030
204 Egaña-Gorroño L, Guardo AC, Bargalló ME, Planet E, Vilaplana E, Escribà T, *et al.* MicroRNA Profile in CD8+ T-Lymphocytes from HIV-Infected Individuals: Relationship with Antiviral Immune Response and Disease Progression. *PLoS One* 2016; **11**:e0155245.
205 Wang P, Qu X, Zhou X, Shen Y, Ji H, Fu Z, *et al.* Two cellular microRNAs, miR-196b and miR-1290, contribute to HIV-1 latency. *Virology* 2015; **486**:228–238.
206 Houzet L, Klase Z, Yeung ML, Wu A, Le SY, Quinones M, *et al.* The extent of sequence complementarity correlates with the potency of cellular miRNA-mediated restriction of HIV-1. *Nucleic Acids Res* 2012; **40**:11684–11696.
207 Bennasser Y, Le S-Y, Yeung M, Jeang K-T. HIV-1 encoded candidate micro-RNAs and their cellular targets. *Retrovirology* 2004; **1**:43.
208 Zhang Y, Fan M, Geng G, Liu B, Huang Z, Luo H, *et al.* A novel HIV-1-encoded microRNA enhances its viral replication by targeting the TATA box region. *Retrovirology* 2014; **11**:1–15.
209 Reynoso R, Laufer N, Hackl M, Skalicky S, Monteforte R, Turk G, *et al.* MicroRNAs differentially present in the plasma of HIV elite controllers reduce HIV infection in vitro. *Sci Rep* 2014; **4**:5915.
210 Wells AC, Daniels KA, Angelou CC, Fagerberg E, Burnside AS, Markstein M, *et al.* Modulation of let-7 miRNAs controls the differentiation of effector CD8 T cells. *Elife* 2017; **6**. doi:10.7554/eLife.26398
211 Lu X, Yang J, Wu H, Yang Z, Jin C, Wang J, *et al.* High-throughput sequencing identifies HIV-1-replication- and latency-related miRNAs in CD4(+) T cell lines. *Arch Virol* 2017; **162**:1933–1942.
212 Pagani M, Rossetti G, Panzeri I, de Candia P, Bonnal RJP, Rossi RL, *et al.* Role of microRNAs and long-non-coding RNAs in CD4(+) T-cell differentiation. *Immunol Rev* 2013; **253**:82–96.
213 Rossi RL, Rossetti G, Wenandy L, Curti S, Ripamonti A, Bonnal RJP, *et al.*

Distinct microRNA signatures in human lymphocyte subsets and enforcement of the naive state in CD4+ T cells by the microRNA miR-125b. *Nat Immunol* 2011; **12**:796–803.
214 Chiang K, Liu H, Rice AP, Chiang K, Liu H, Rice AP, *et al.* miR-132 enhances HIV-1 replication. *Virology* 2013; **438**:1–4.
215 Witwer KW, Watson AK, Blankson JN, Clements JE. Relationships of PBMC microRNA expression, plasma viral load, and CD4+ T-cell count in HIV-1-infected elite suppressors and viremic patients. *Retrovirology* 2012; **9**:5.
216 Schwarz EC, Backes C, Knoerck A, Ludwig N, Leidinger P, Hoxha C, *et al.* Deep characterization of blood cell miRNomes by NGS. *Cell Mol Life Sci* 2016; **73**:3169–3181.
217 López M, Soriano V, Peris-Pertusa A, Rallón N, Restrepo C, Benito JM. Elite Controllers Display Higher Activation on Central Memory CD8 T Cells Than HIV Patients Successfully on HAART. *AIDS Res Hum Retroviruses* 2011; **27**:157–165.
218 van Grevenynghe J, Procopio FA, He Z, Chomont N, Riou C, Zhang Y, *et al.* Transcription factor FOXO3a controls the persistence of memory CD4+ T cells during HIV infection. *Nat Med* 2008; **14**:266–274.
219 Ndhlovu ZM, Proudfoot J, Cesa K, Alvino DM, Mcmullen A, Vine S, *et al.* Elite Controllers with Low to Absent Effector CD8 ⁺ T Cell Responses Maintain Highly Functional, Broadly Directed Central Memory Responses. doi:10.1128/JVI.00531-12
220 Fonseca SG, Procopio FA, Goulet J-P, Yassine-Diab B, Ancuta P, Sékaly R-P. Unique features of memory T cells in HIV elite controllers: a systems biology perspective. *Curr Opin HIV AIDS* 2011; **6**:188–196.
221 Edgar R, Domrachev M, Lash AE. Gene Expression Omnibus: NCBI gene expression and hybridization array data repository. *Nucleic Acids Res* 2002; **30**:207–210.
222 Barrett T, Wilhite SE, Ledoux P, Evangelista C, Kim IF, Tomashevsky M, *et al.* NCBI GEO: archive for functional genomics data sets—update. *Nucleic Acids Res* 2012; **41**:D991–D995.
223 McCall MN, Baras AS, Crits-Christoph A, Ingersoll R, McAlexander MA, Witwer KW, *et al.* A benchmark for microRNA quantification algorithms using the OpenArray platform. *BMC Bioinformatics* 2016; **17**:138.
224 Palin AC, Ramachandran V, Acharya S, Lewis DB. Human neonatal naive CD4+ T cells have enhanced activation-dependent signaling regulated by the microRNA miR-181a. *J Immunol* 2013; **190**:2682–2691.
225 Li Q-J, Chau J, Ebert PJR, Sylvester G, Min H, Liu G, *et al.* miR-181a Is an Intrinsic Modulator of T Cell Sensitivity and Selection. *Cell* 2007; **129**:147–161.
226 Aprelikova O, Yu X, Palla J, Wei B-R, John S, Yi M, *et al.* The role of miR-31 and its target gene SATB2 in cancer-associated fibroblasts. *Cell Cycle* 2010; **9**:4387–4398.
227 Dudaronek JM, Barber SA, Clements JE. CUGBP1 Is Required for IFNβ-Mediated Induction of Dominant-Negative CEBPβ and Suppression of SIV Replication in Macrophages. *J Immunol* 2007; **179**:7262 LP-7269.
228 Smigielska-Czepiel K, van den Berg A, Jellema P, Slezak-Prochazka I, Maat H, van den Bos H, *et al.* Dual role of miR-21 in CD4+ T-cells: activation-induced

miR-21 supports survival of memory T-cells and regulates CCR7 expression in naive T-cells. *PLoS One* 2013; **8**:e76217.

229 Parikh VN, Park J, Nikolic I, Channick R, Yu PB, De Marco T, *et al.* Coordinated modulation of circulating miR-21 in HIV, HIV- associated pulmonary arterial hypertension, and HIV/HCV co- infection HHS Public Access. *J Acquir Immune Defic Syndr Novemb* 2015; **1**:236–241.

230 Liu J, Wu C-P, Lu B-F, Jiang J-T. Mechanism of T cell regulation by microRNAs. *Cancer Biol Med* 2013; **10**:131–137.

231 Schmolka N, Papotto PH, Romero PV, Amado T, Enguita FJ, Amorim A, *et al.* MicroRNA-146a controls functional plasticity in γδ T cells by targeting NOD1. *Sci Immunol* 2018; **3**.http://immunology.sciencemag.org/content/3/23/eaao1392.abstract

232 Sheppard HM, Verdon D, Brooks AES, Feisst V, Ho Y-YJ, Lorenz N, *et al.* MicroRNA regulation in human CD8+ T cell subsets--cytokine exposure alone drives miR-146a expression. *J Transl Med* 2014; **12**:292.

233 Jeker LT, Bluestone JA. microRNA regulation of T-cell differentiation and function. *Immunol Rev* 2013; **253**:65–81.

234 Qian C, Wang H, Fan H, Gu M, Ren C, Deng A, *et al.* [MicroRNA profiling in T cells of peripheral blood mononuclear cell from patients with primary biliary cirrhosis]. *Zhonghua Yi Xue Za Zhi* 2012; **92**:2265–2267.

235 Reddycherla A V, Meinert I, Reinhold A, Reinhold D, Schraven B, Simeoni L. miR-20a inhibits TCR-mediated signaling and cytokine production in human naive CD4+ T cells. *PLoS One* 2015; **10**:e0125311.

236 Swaminathan S, Kelleher AD. MicroRNA modulation of key targets associated with T cell exhaustion in HIV-1 infection. *Curr Opin HIV AIDS* 2014; **9**:464–471.

237 Stefanie T, Jürgen W, Hans-Martin J, Andreas P. miR-9 enhances IL-2 production in activated human CD4+ T cells by repressing Blimp-1. *Eur J Immunol* 2012; **42**:2100–2108.

238 Yang L, Niu F, Yao H, Liao K, Chen X, Kook Y, *et al.* Exosomal miR-9 Released from HIV Tat Stimulated Astrocytes Mediates Microglial Migration. *J Neuroimmune Pharmacol* Published Online First: 2018. doi:10.1007/s11481-018-9779-4

239 Franco S, Buccione D, Pluvinet R, Mothe B, Ruiz L, Nevot M, *et al.* Large-scale screening of circulating microRNAs in individuals with HIV-1 mono-infections reveals specific liver damage signatures. *Antiviral Res* 2018; **155**:106–114.

240 Madison MN, Roller RJ, Okeoma CM. Human semen contains exosomes with potent anti-HIV-1 activity. *Retrovirology* 2014; **11**:102.

Dillon C. Muth

Born: New York City, NY, June 30, 1986

EDUCATION

December 2018	**Doctor of Philosophy (PhD)** Department of Molecular and Comparative Pathobiology, Graduate Program in Cellular and Molecular Medicine, Johns Hopkins University, School of Medicine, Baltimore, Maryland
June 2016	**Residency in Anatomic Pathology,** Johns Hopkins University, School of Medicine, Department of Molecular and Comparative Pathobiology**,** Baltimore, Maryland
June 2012	**Doctor of Veterinary Medicine (DVM)** College of Veterinary Medicine, The Ohio State University, College of Veterinary Medicine, Columbus, Ohio
June 2008	**Bachelor of Arts (BA),** *cum laude,* Double Major in Biology and Philosophy, Carleton College**,** Northfield, Minnesota

WORK EXPERIENCE

2009-2010	T32 Summer Research Fellow	Department of Veterinary Biosciences The Ohio State University, College of Veterinary Medicine Advisor: Tracey Papenfuss
2010	Summer Research Fellow	Department of Molecular and Comparative Pathobiology Johns Hopkins University, School of Medicine Supervisor: Christine Zink
2012-2016	Anatomic Pathology Fellow	Department of Molecular and Comparative Pathobiology Johns Hopkins University School of Medicine Advisor: Cory Brayton
2013-Present	Postdoctoral Graduate Researcher	Department of Molecular and Comparative Pathobiology Johns Hopkins University School of Medicine Advisor: Kenneth Witwer

EDUCATIONAL ACTIVITIES

Leadership, mentoring, and teaching

2014-Present — Assisted in day-to-day work of five rotation student projects, supervised one undergraduate project over three and half years and provided assistance to more than six other undergraduates; Advised numerous graduate students within the entire collaborative lab group; Trained technicians and supervised their contributions to multiple projects/collaborations; Assisted with in-person interviews as needed for various lab positions

2012-Present	Attended and contributed to weekly pathology rounds, gave numerous lectures/talks on various topics for veterinary pathology residents, including but not limited to: comparative anatomy, general principles of disease, system-specific disease

RESEARCH ACTIVITIES

PEER-REVIEWED PUBLICATIONS

Muth, D. C., Powell, B. H, Lu, Y, Halushka M, Blankson, JN & Witwer, K. W. miRNA expression in T-cell subsets in health and HIV-1 Elite Suppression. In preparation.

Muth, D. C., Paulaitis, M, Witwer, K. W**.** Size and concentration analyses of extracellular vesicles: A comparison of common NTA platforms. In preparation.

Liao, Z., Martin-Jaular, L., Soueidi, E., **Muth DC,** *et al*.. Acetylcholineterase activity is not a generic marker of EVs. In preparation.

Muth, D. C.*, Powell, B. H.*, Zhao, Z. & Witwer, K. W. miRNAs in platelet-poor blood plasma and purified RNA are highly stable: a confirmatory study. BMC Research Notes 2018 May 4; 11:273 doi.org:10.1186/s13104-018-3378-6

Zhao, Z*., **Muth, D.C*** *et al.* miRNA profiling of primate cervicovaginal lavage and extracellular vesicles reveals miR-186-5p as a potential retroviral restriction factor in macrophages. *bioRxiv* (2018). doi:10.1101/263947

Mangus, L. M. *et al,*. including **Muth, D.C**. Lymphocyte-Dominant Encephalitis and Meningitis in Simian Immunodeficiency Virus–Infected Macaques Receiving Antiretroviral Therapy. *The American Journal of Pathology* 188**,** 125–134 (2018).

Van Deun J. et al. including **Muth, D.C.** EV-TRACK: transparent reporting and centralizing knowledge in extracellular vesicle research. *Nature Methods* 14(3):228-232 (2017).

Liao, Z*., **Muth DC*** *et al.* Serum extracellular vesicle depletion processes affect release and infectivity of HIV-1 in culture. *Sci. Rep.* 7, (2017).

Zhao, Z., **Muth DC**, Mahairaki V., Cheng L. & Witwer KW Isolation and Characterization of Extracellular Vesicles in Stem Cell-Related Studies. *Stem Cell Technologies in Neuroscience* 205–223 (2017).

Seeley KE, Clayton LA, Hadfield CA, **Muth DC**, Mankowski JL & Kelly KM. Retrospective Review of Mortality in Giant Pacific Octopus (Enteroctopus Dofleini) *Journal of Zoo and Wildlife Medicine* 47 (1), 271-274 (2016).

Ji Diana Lee, Y, Kim V, **Muth DC,** & Witwer, KW. Validated MicroRNA Target Databases: An Evaluation. *Drug Development Research* (2015).

Muth, DC, McAlexander, MA, Ostrenga, LJ, Pate, NM, Izzi, JM, Adams, RJ, et al. Potential role of cervicovaginal extracellular particles in diagnosis of endometriosis. *BMC Veterinary Research*, *11*(1), 187 (2015).

Garrett, CM, **Muth, DC**, & Watson, J. Effects of Medicated Diet to Eradicate *Helicobacter* spp. on Growth, Pathology, and Infection Status in *Rag1–/–* and Nude Mice. *JAALAS*, 53 (3), 8 (2014).

Vangundy, ZC, Guerau-de-Arellano, M., Baker, JD, Strange, H. R., Olivo-Marston, S., **Muth, DC**, & Papenfuss, TL. Continuous retinoic acid induces the differentiation of mature regulatory monocytes but fails to induce regulatory dendritic cells. BMC Immunology, 15(1), 8 (2014).

ORAL AND POSTER PRESENTATIONS

Cigarette smoke-exposed monocyte-derived dendritic cells release EVs that elicit Th1/Th17 responses in autologous T-cells Proceedings of the ISEV conference held in Barcelona, Spain, May 2-May 6, 2018
EVs and HIV infection Extracellular Vesicle Education day and Symposium held in Baltimore, MD March 23, 2018
Extracellular Vesicles affect HIV Infection and Production Extracellular Vesicles and Infection Symposium held in Potomac, MD June 2, 2017
Cellular Survival and Response to HIV-1 Infection in the Absence of Extracellular Vesicles Proceedings of the ISEV conference held in Rotterdam, Netherlands, April 23-April 26, 2016
Extracellular particles in cervico-vaginal secretions of SIV infected and uninfected Rhesus Macaques Proceedings of the ISEV conference held in Rotterdam, Netherlands, April 23-April 26, 2016
The Diplomonad flagellate S. vortens displays impaired proliferation and heightened oxygen sensitivity in EV-depleted media Proceedings of the ISEV conference held in Bethesda, MD, April 23-April 26, 2015.
Extracellular vesicles and small RNA of the cervicovaginal compartment in Macaques. Proceedings of the ISEV conference held in Bethesda, MD, May 4- May 7, 2015
Extracellular vesicles and small RNA of the cervicovaginal compartment in Macaques Proceedings of the ACVP conference held in Minneapolis, MN, October 17-21, 2015.
Extracellular particles and RNA in SIV and HIV infection. Proceedings of the ACVP conference held in Atlanta GA, November 8-November 12, 2014.

Not Listed: Numerous Departmental Seminars, lectures in various topics of veterinary pathology

AWARDS AND HONORS

- 2013-2016: NIH T32 Postdoctoral Fellow
- 2011: American College of Veterinary Pathologists, Externship scholarship

- 2011: Ohio State College of Veterinary Medicine, Matthew Eggert scholarship for aptitude in pathology
- 2011: Ohio State College of Veterinary Medicine, General scholarship
- 2009: NIH T-35 Training Grant for summer research
- 2008: Ohio State College of Veterinary Medicine, General scholarship
- 2008: Inducted into Sigma Xi scientific research society, Associate Member
- 2007: Mote Marine Laboratory, Einar T. Anderson Scholarship
- 2004: National Merit Commended Scholar
- 2003: Collegiate School, Herzig Grant for Summer Study

PROFESSIONAL MEMBERSHIPS

- International Society for Extracellular Vesicles
- American Society for Exosomes and Microvesicles
- Sigma Xi